1-1-2014

Distinct Circuit States Enable State-dependent Flexibility in a Rhythm Generating Network

Jason Christopher Rodriguez
University of Pennsylvania, jasoncrodriguez@gmail.com

Distinct Circuit States Enable State-dependent Flexibility in a Rhythm Generating Network

Abstract
My thesis aimed to elucidate general organizing principles underlying the modulation of neural circuits. These circuits are flexible constructs that, when modulated, can occupy many distinct states and produce different output patterns. Distinct circuit states can also produce the same output pattern in some cases. However, understanding the mechanisms and consequences of this latter phenomenon is impossible to achieve without the capability to observe and manipulate the cellular and synaptic properties of all circuit neurons. This work takes advantage of our detailed, cellular-level access to the central pattern generator (CPG) circuits found in the decapod crustacean stomatogastric nervous system, a specialized extension of the CNS dedicated to internal feeding-related behaviors. As CPGs are rhythmically active networks, much of this work focuses on the ability of such circuits to produce rhythmic output patterns (i.e. rhythm generation). Using this system, I found that distinct circuit states (configured by MCN1 projection neuron stimulation and CabPK peptide application) can enable comparable rhythm generation by recruiting distinct ionic conductances with overlapping functional roles (i.e. I_{MI} and $I_{Trans\text{-}LTS}$), each being regulated by synaptic inhibition to produce phasic excitatory drive to a pivotal circuit neuron (LG). In one case (MCN1 stimulation), the conductance is activated by a modulatory peptide transmitter whose release is regulated by presynaptic feedback inhibition. In the other case (CabPK application), the conductance has a slow inactivation property that is removed by hyperpolarization caused by synaptic inhibition. I also describe the consequences of having different circuit states that produce identical outputs by assaying their responses to the same, well-defined modulatory inputs - peptide (CCAP) hormone modulation and sensory feedback (GPR neuron). I found that hormonal modulation produced opposite effects on these two circuits states even though the cellular-level hormonal action is likely the same in both states. In contrast, I found these circuits were similarly sensitive to sensory feedback, despite this feedback acting via different synapses under each condition. My work thereby provides the first mechanistic understanding of input-pathway specific rhythm generators that produce convergent output patterns and the flexibility enabled by these circuit states when responding to additional modulatory inputs.

Degree Type
Dissertation

Degree Name
Doctor of Philosophy (PhD)

Graduate Group
Neuroscience

First Advisor
Michael P. Nusbaum

Subject Categories
Neuroscience and Neurobiology

DISTINCT CIRCUIT STATES ENABLE STATE-DEPENDENT FLEXIBILITY IN A RHYTHM GENERATING NETWORK

Jason Christopher Rodriguez

A DISSERTATION

in

Neuroscience

Presented to the Faculties of the University of Pennsylvania

in

Partial Fulfillment of the Requirements for the

Degree of Doctor of Philosophy

2014

Supervisor of Dissertation

_____

Michael P. Nusbaum, Ph.D., Professor of Neuroscience

Graduate Group Chairperson

_____

Joshua I. Gold, Ph.D., Associate Professor of Neuroscience

Dissertation Committee

Minghong Ma, Ph.D., Associate Professor of Neuroscience and Thesis Committee Chair

Douglas Coulter, Ph.D., Professor of Pediatrics

Diego Contreras, Ph.D., Professor of Neuroscience

Farzan Nadim, Ph.D., Professor of Biology & Mathematics, Rutgers University, New Jersey Institute of Technology

ABSTRACT

DISTINCT CIRCUIT STATES ENABLE STATE-DEPENDENT FLEXIBILITY IN A RHYTHM GENERATING NETWORK

Jason C. Rodriguez

Michael P. Nusbaum

My thesis aimed to elucidate general organizing principles underlying the modulation of neural circuits. These circuits are flexible constructs that, when modulated, can occupy many distinct states and produce different output patterns. Distinct circuit states can also produce the same output pattern in some cases. However, understanding the mechanisms and consequences of this latter phenomenon is impossible to achieve without the capability to observe and manipulate the cellular and synaptic properties of all circuit neurons. This work takes advantage of our detailed, cellular-level access to the central pattern generator (CPG) circuits found in the decapod crustacean stomatogastric nervous system, a specialized extension of the CNS dedicated to internal feeding-related behaviors. As CPGs are rhythmically active networks, much of this work focuses on the ability of such circuits to produce rhythmic output patterns (i.e. rhythm generation). Using this system, I found that distinct circuit states (configured by MCN1 projection neuron stimulation and CabPK peptide application) can enable comparable rhythm generation by recruiting distinct ionic conductances with overlapping functional roles (i.e. I_{MI} and $I_{Trans\text{-}LTS}$), each being regulated by synaptic inhibition to produce phasic excitatory drive to a pivotal

circuit neuron (LG). In one case (MCN1 stimulation), the conductance is activated by a modulatory peptide transmitter whose release is regulated by presynaptic feedback inhibition. In the other case (CabPK application), the conductance has a slow inactivation property that is removed by hyperpolarization caused by synaptic inhibition. I also describe the consequences of having different circuit states that produce identical outputs by assaying their responses to the same, well-defined modulatory inputs – peptide (CCAP) hormone modulation and sensory feedback (GPR neuron). I found that hormonal modulation produced opposite effects on these two circuits states even though the cellular-level hormonal action is likely the same in both states. In contrast, I found these circuits were similarly sensitive to sensory feedback, despite this feedback acting via different synapses under each condition. My work thereby provides the first mechanistic understanding of input-pathway specific rhythm generators that produce convergent output patterns and the flexibility enabled by these circuit states when responding to additional modulatory inputs.

TABLE OF CONTENTS

LIST OF ILLUSTRATIONS

FIGURE **PAGE**

CHAPTER 1
Introduction

CHAPTER 2
Convergent Rhythm Generation from Divergent Cellular Mechanisms

FIGURE **PAGE**

FIGURE **PAGE**

CHAPTER 3

Convergent Rhythm Generation from Divergent Cellular Mechanisms

LIST OF ABBREVIATIONS

5HT	serotonin
AB	Anterior Burster Neuron
AM	anterior median neuron
CabPK	*Cancer borealis pyrokinin*
CabTRP	*Cancer borealis* tachykinin-related peptide
CCAP	crustacean cardio-active peptide
CoG	commissural ganglion
CPG	central pattern generator
DCC	discontinuous current clamp
DMSO	dimethylsulfoxide
DG	dorsal gastric neuron
dvn	dorsal ventricular nerve
EPSP	excitatory postsynaptic potential
GABA	γ-amino-butyric acid
GM	gastric mill neuron
GMR	gastric mill rhythm
GPR	gastropyloric receptor
IC	inferior cardiac neuron
I_{MI}	modulator-activated inward current
Int1	interneuron 1
ion	inferior oesphageal nerve
IPSP	inhibitory postsynaptic potential

LIST OF ABBREVIATIONS

$I_{Trans\text{-}LTF}$	transient low-threshold fast current
$I_{Trans\text{-}LTS}$	transient low-threshold slow current
LG	lateral gastric neuron
lgn	lateral gastric nerve
LP	lateral pyloric neuron
LPG	lateral posterior gastric neuron
lvn	lateral ventricular nerve
MCN1	modulatory commissural neuron 1
MG	medial gastric neuron
mvn	medial ventricular nerve
NMDG	N-methyl-D-glucamine
OG	oesophageal ganglion
OXO	oxotremorine
pdn	pyloric dilator neuron
PD	pyloric dilator nerve
PIR	post inhibitory rebound
PTX	picrotoxin
PY	pyloric constrictor neuron
son	superior oesophageal nerve
STG	stomatogastric ganglion
stn	stomatogastric nerve
STNS	stomatogastric nervous system

LIST OF ABBREVIATIONS

TG	thoracic ganglion
TTX	tetrodotoxin
VCN	ventral cardiac neurons
VD	ventricular dilator

CHAPTER 1

INTRODUCTION

Neural Circuit Modulation

The main goal of my thesis is to elucidate novel mechanistic insights regarding neural circuit modulation, and how different modulatory states vary in their sensitivity to hormonal inputs and sensory feedback.

Neural circuits are flexible constructs that exhibit short- and long-term changes in dynamics in response to synaptic- and paracrine/endocrine-mediated metabotropic actions (Getting, 1989; Marder, 2012). Synaptic inputs are subject to homo- or heterosynaptic influences that result in processes such as synaptic depression, facilitation and potentiation. Metabotropic (often termed modulatory) actions provide the opportunity for state-dependence, wherein different metabotropic actions configure different circuit states from the same network (Kupfermann, 1979; Getting, 1989; Doi and Ramirez, 2008; Marder, 2012; Nusbaum and Blitz, 2012). These latter inputs commonly act through intracellular signaling cascades (e.g. G-protein signaling) to produce cellular- and circuit-level changes that persist well past the initiating event, lasting for minutes, hours, or even days.

Neuromodulation is a key mechanism for achieving behavioral states in all organisms (Köhler et al., 2011; Lee and Dan, 2012; Taghert and Nitabach, 2012; Patton and Mistlberger, 2013). This state involves the coordination of cellular and network properties for the purpose of achieving some goal. For example, a collection of neuromodulatory peptides coordinates feeding behaviors in

mammals (Jobst et al., 2004). While the importance of neuromodulation is appreciated in all systems, there are still only a few systems sufficiently accessible to study the consequences of neuromodulation in a cellular and circuit context.

Central pattern generator (CPG) networks provide convenient systems for studying neuromodulation (Marder, 2012; Nusbaum and Blitz, 2012). These specialized neural circuits produce the rhythmic neuronal activity patterns that underlie rhythmic behaviors (e.g. locomotion, respiration, mastication), and they continue to generate these rhythmic activity patterns even after isolation from the rest of the nervous system. This allows researchers to have better access for recording and manipulating the network neurons and to more readily record the physiologically relevant network activity in the context of different experimental manipulations. Experimental results from small systems have provided insight into larger CPG networks, as highlighted by studies showing that CPGs in all animals, regardless of the particular rhythmic behavior, share several general operating principles (Marder and Calabrese, 1996; Marder, 2012). For instance, as indicated above, CPGs can generate at least a basic form of their *in vivo* pattern even in isolation from the rest of the CNS. Additional shared principles include CPGs generating rhythmic activity in response to non-rhythmic input, and the fact that they are multi-functional (i.e. one network generates different activity patterns in response to different modulatory inputs). Lastly, in the few cases where sufficient information is available, it appears common for CPGs to be functionally subdivided into a circuit responsible for rhythm generation and one

responsible for pattern generation (Guertin, 2009). These two functions can be served by separate or overlapping sets of neurons (Guertin, 2009).

Modulatory inputs select particular output patterns from a neural circuit (Dickinson, 2006; Briggman and Kristan, 2008; Doi and Ramirez, 2008; Harris-Warrick, 2011; Marder, 2012). They do so by altering the synaptic and ionic conductances of circuit neurons. These actions cause changes in the cellular properties and synaptic dynamics of the affected neurons, enabling generation of specific output patterns. It is appreciated in many systems that different neuromodulators can produce distinct output patterns from the same neural circuit (Fig. 1) (Getting, 1989; Stein, 2009; Marder, 2012; Nusbaum and Blitz, 2012). However, via a variety of mechanisms, different neuromodulators can also elicit the same output pattern from a particular network (Fig. 1) (Di Prisco et al., 2000; Korn and Faber, 2005; Saideman et al., 2007b; Derjean et al., 2010; Doi and Ramirez, 2010; White and Nusbaum, 2011).

As suggested above, distinct circuit states do not necessarily produce different output patterns. At the single neuron level, modulation of different sets of ionic conductances can produce similar cellular consequences (Swensen and Bean, 2005; Goaillard et al., 2009). This phenomenon also holds true at the level of neural circuits, where different combinations of ionic and synaptic conductances can produce identical output patterns (Golowasch et al., 1999; Prinz et al., 2004). Obviously, this level of understanding requires access to ionic and synaptic conductances of identified circuit neurons, the ability to selectively activate particular input pathways, and comprehensive monitoring of the resulting

circuit output. There remain few systems in which these criteria can be fulfilled. For this reason, my work was performed in a very well-defined and uniquely accessible system called the stomatogastric nervous system (STNS) of decapod crustaceans (Fig. 2) (Marder & Bucher, 2007; Stein, 2009).

The *Cancer borealis* stomatogastric nervous system

The STNS is an extension of the CNS that controls the feeding-associated behaviors of the foregut. The decapod crustacean foregut has four distinct structures, including the oesophagus (swallows food), cardiac sac (stores food), gastric mill (chews food), and pylorus (filters chewed food) (Fig. 2) (Johnson and Hooper, 1992). During feeding, swallowed food passes through the oesophagus into the cardiac sac, where it is stored. The food is then squeezed into the gastric mill compartment where it is chewed by the rhythmic movements of the paired lateral teeth and unpaired medial tooth. Once food particles are sufficiently small, they pass through the pylorus, which is continually pumping in a series of front to rearward peristaltic waves, and into the midgut for further digestion and absorption. These behaviors are coordinately executed by the CPG circuits within the STNS.

The STNS is composed of four ganglia plus their connecting and peripheral nerves (Fig. 3) (Marder and Bucher, 2007; Stein, 2009). The ganglia include the paired commissural ganglia (CoGs: in *C. borealis*, contains ~600 neurons), oesophageal ganglion (OG: in *C. borealis*, contains 14 neurons), and

stomatogastric ganglion (STG: in *C. borealis*, contains 26 neurons) (Kilman and Marder, 1996). Most CPG studies in this system focus on the STG, where the gastric mill and pyloric circuits are located (see below). The CoGs and OG contain, among other functional types of neurons, the cell bodies of projection neurons that regulate/modulate the STG neurons (Coleman et al., 1992).

The STG circuits are very accessible, such that all STG neurons are identified (Marder and Bucher, 2007). In the crab *Cancer borealis*, where my work was performed, nearly all of the STG neurons (22 of 26) contribute to the gastric mill and/or pyloric CPG. Among these 22 neurons are 13 different neuron types, with 9 of them present as single copies and 4 present as multiple, apparently equivalent copies (2-5 copies, depending on the neuron type) (Fig. 4). The neuronal cell bodies in the STG are organized in a single layer surrounding a central neuropil (Fig. 4). Once the glial sheath that covers the STG is removed, sharp electrode recordings are readily obtained from the relatively large STG neuron somata, with minimal damage to the surrounding nervous system. Aside from two STG interneurons (AB, Int1 neurons) which have relatively small diameter somata (~35 µm), the STG neuron somata range from ~50 µm to ~120 µm in diameter. Most of the STG neurons are motor neurons that project their axons through a stereotyped set of peripheral nerves to innervate the 30 muscles of the foregut (Fig. 3). Consequently, their action potentials are readily recorded extracellularly as they propagate through these peripheral nerves. Dissecting

and recording from smaller nerve branches enables the activity of individual neuron types to be recorded in isolation (e.g. Fig. 5).

The aforementioned level of accessibility has enabled an extensive characterization of this system. Not only are each of the 26 STG neurons physiologically-identified in *C. borealis* (as well as the related crab *C. pagurus* and two lobsters, *Panulirus interruptus* and *Homarus americanus*), but so are their transmitters and synapses (Marder and Bucher, 2007). Additionally, the sensitivity of individual STG neurons to various applied neuromodulators, including amines, muscarinic agonists and numerous neuropeptides, as well as several identified sensory and projection neurons are established (Dickinson, 2006; Marder, 2012; Blitz and Nusbaum, 2011; Nusbaum and Blitz, 2012).

As is the case for CPG networks in other systems, both the gastric mill and pyloric CPGs can be subdivided into core rhythm generator and pattern generator modules. In each case, the rhythm generator neurons also contribute to pattern generation. The pyloric rhythm generator is a pacemaker-driven, electrically-coupled ensemble whose core includes the AB and PD neurons (Marder and Bucher, 2007). The core gastric mill rhythm generator is network-driven, and includes the reciprocally inhibitory neurons LG and Int1 (Coleman et al., 1995; Bartos et al., 1999; Saideman et al., 2007b). A few additional, different neurons also contribute to gastric mill rhythm generation under different modulatory states. This work focuses on the gastric mill rhythm generator during two specific modulatory states, as described below.

The Gastric Mill Rhythm

All characterized gastric mill rhythms in *C. borealis* require activation of the half-center formed by reciprocal inhibitory synapses between LG and Int1 (Fig. 4) (Bartos et al., 1999; Saideman et al., 2007b; White and Nusbaum, 2011). The term “half-center” indicates pairs or populations of reciprocally inhibitory neurons which, under appropriate conditions, generate a rhythmic repeating bursting pattern during which each neuron or population is active for ~half of each cycle (Marder and Calabrese, 1996). Prior to modulation, both in vivo and in the isolated STNS, the LG/Int1 half-center is asymmetric, with LG being silent and Int1 exhibiting a pyloric-timed activity pattern (Fig. 5) (Bartos et al., 1999; Beenhakker and Nusbaum, 2004; Blitz et al., 2004; Diehl et al., 2013). Int1 activity is self-generated, enabling it to fire tonically at ~10 Hz, with this activity pattern being rhythmically interrupted by synaptic inhibition from the pyloric pacemaker neuron AB (Bartos et al., 1999; Saideman et al., 2007b). Each Int1 action potential elicits an ionotropic, glutamatergic inhibitory post-synaptic potential (IPSP) in the LG neuron. In normal saline, each pyloric-timed Int1 burst causes an LG hyperpolarization. When LG is released from each of these inhibitory events, it repolarizes to its subthreshold membrane potential.

Neuromodulators that elicit a gastric mill rhythm do so by activating LG and thereby balancing the LG/Int1 half-center (i.e. enabling them to burst rhythmically in an alternating pattern) (Bartos et al., 1999; Saideman et al.,

2007b). The rhythmic alternation of Int1 and LG activity, and their synaptic actions on the other gastric mill motor neurons, then coordinates a biphasic chewing pattern (Bartos et al., 1999; Saideman et al., 2007b). In the best characterized versions of the gastric mill rhythm, the basic operation of the activated LG-Int1 half-center involves LG acquiring the ability (from a modulatory input) to periodically escape or rebound from Int1 inhibition and fire a self-terminating burst. The gastric mill pattern is, therefore, a biphasic alternation between protraction (LG-timed) and retraction (Int1-timed) neurons, driving the rhythmically alternating protraction and retraction movements of the teeth that define chewing behavior. This work will focus on two gastric mill rhythm generating mechanisms that result from two distinct modulatory input pathways, including modulatory commissural neuron 1 (MCN1: Fig. 5) and the CabPK (*Cancer borealis* pyrokinin) peptide-containing projections neurons.

Cancer borealis **pyrokinins (CabPKs)**

The CabPKs are two bioactive peptides found in the STNS (Saideman et al., 2007a). They include CabPK I (TNFAFSPRLamide) and CabPK II (SGGFAFSPRLamide). The CabPKs are PK/PBAN peptide family members, which all contain the FXPRL amino acid sequence at their *n*-terminus (Rafaeli, 2009). Antisera raised against a shrimp PK peptide (pevpyrokinin) were used to localize the CabPKs. These peptides were thereby immunolocalized in both a

neurohemal structure, called the pericardial organ, and within the STNS (Saideman et al., 2007a).

CabPK immunoreactive (CabPK-IR) neuronal somata in the *C. borealis* STNS included 2 or 3 STG-innervating projection neurons within the CoGs (Saideman et al., 2007a). The STG-innervating CabPK-IR projection neurons project through the bilateral superior oesophageal nerve (*son*) and unpaired stomatogastric nerve (*stn*) to innervate the STG (Fig. 5). Within the STG, CabPK-IR was limited to elaborate neuropilar processes, presumably representing the axonal terminations of the CabPK projection neurons. No STG somata were CabPK-IR (Saideman et al., 2007a).

Despite being localized to the CoGs, the CabPK-projection neurons remain to be physiologically identified. Moreover, there is currently no way to selectively activate them extracellularly, because all but two of the 15-20 CoG projection neurons that innervate the STG project through the *sons* (Coleman et al., 1992). Therefore, in my experiments CabPK neuron activity is simulated by CabPK bath application. This approach has been used successfully in previous studies with other neuropeptides. For example, bath application of the neuropeptide proctolin (10^{-6} M) mimics the influence of selective stimulation of the proctolin-containing projection neuron MPN (modulatory proctolin neuron) on the *C. borealis* pyloric rhythm (Nusbaum and Marder, 1989ab). However, it is important to indicate that the actions of bath-applied neuropeptide do not always

mimic those of the neuron(s) containing that peptide (Blitz and Nusbaum, 1999; Blitz et al., 1999). There are several reasons for the latter situation, including synaptic specificity, extracellular peptidase activity, actions of cotransmitters and receptor desensitization (Wood et al., 2000; Nusbaum et al., 2001; Nusbaum, 2002; Wood and Nusbaum, 2002).

Convergent Gastric Mill Output Patterns, Divergent Mechanisms

CabPK bath-application at concentrations (≥ 10^{-7} M) that likely mimic neuronal release activate a gastric mill rhythm (Saideman et al., 2007ab). Surprisingly, CabPK application and stimulation of the CoG projection neuron MCN1 elicit the same gastric mill motor pattern, even though MCN1 neither contains CabPK nor is necessary for the CabPK-elicited gastric mill rhythm (Saideman et al., 2007ab). In contrast, other pathways that activate the gastric mill rhythm elicit distinct gastric mill motor patterns (Beenhakker and Nusbaum, 2004; Blitz et al., 2004; Christie et al., 2004; White and Nusbaum, 2011). Not only are the basic CabPK- and MCN1-elicited gastric mill rhythm parameters the same (e.g. retraction duration, protraction duration, cycle period), but so are additional details of these motor patterns (Saideman et al., 2007b). For example, the firing rates and activity patterns of all neurons measured were the same, as were most phase relationships, during the CabPK- and MCN1-elicited gastric mill patterns. Additionally, the same two gastric mill motor neurons (GM, AM) were

not activated by either CabPK or MCN1, even though they are activated by other pathways.

Given the extent of the concurrence between these two gastric mill rhythms, it was surprising that the network states and even aspects of the basic gastric mill rhythm-generating mechanism varied when CabPK was applied or MCN1 was stimulated (Fig. 6) (Saideman et al., 2007b). For example, a pivotal aspect of MCN1-driven gastric mill rhythm generation is a slow MCN1-elicited metabotropic (peptidergic) excitation of LG that is regulated by feedback inhibition from LG (Bartos et al., 1999; DeLong et al., 2009). Specifically, MCN1 excites LG through the release of *C. borealis* tachykinin-related peptide Ia (CabTRP Ia). MCN1-released CabTRP Ia causes a slow depolarization of LG by activating the voltage-dependent, modulator-activated inward current (I_{MI}) (DeLong et al., 2009). When I_{MI} becomes sufficiently large, LG overcomes the inhibition that it receives from Int1 and fires a burst. While LG is active, it presynaptically inhibits the MCN1 terminals in the STG ($MCN1_{STG}$), reducing MCN1 transmitter release and initiating a decay of I_{MI} availability which eventually terminates the LG burst. LG burst termination results in the resumption of MCN1 transmitter release and Int1 activity. Insofar as the feedback inhibition onto $MCN1_{STG}$ and its consequences for MCN1 signaling are necessary for gastric mill rhythm generation, $MCN1_{STG}$ itself is part of this version of the gastric mill rhythm generator, as well as being its activator. Additionally, the pyloric pacemaker neuron AB regulates the MCN1-gastric mill cycle period, although it is not necessary for rhythm generation (Bartos et al., 1999).

The CabPK-gastric mill rhythm generating mechanism cannot be the same as that used by MCN1 for several reasons (Saideman et al., 2007b). First, the core neurons involved in rhythm generation are different. MCN1 is not involved in the CabPK-gastric mill rhythm, nor does it release the CabPK peptide. Second, the pyloric-timed inhibitory synapse from the AB neuron onto Int1 is necessary only for CabPK-gastric mill rhythm generation. Third, the retraction motor neuron DG regulates the CabPK-gastric mill rhythm, but not the MCN1-gastric mill rhythm.

My dissertation research focused on the CabPK-gastric mill rhythm generating mechanism and its sensitivity to hormonal and sensory influences, including a comparison to the previously determined comparable conditions (and underlying mechanisms) during the MCN1-gastric mill rhythm. As presented in the following chapters, my findings establish that (1) distinct modulators can produce convergent output patterns by recruiting different ionic conductances to perform overlapping roles in rhythm generation, (2) the same ionic conductance in a single neuron can contribute to rhythm generation in a state-dependent manner, (3) circuit states that produce the same output pattern can flexibly respond to hormonal input (Fig. 7), (4) distinct circuit states can generate invariant responses to sensory feedback despite using different synaptic mechanisms (Fig. 7). As discussed in the following chapters, each of these findings provides novel insights into the degree of flexibility intrinsic to rhythmically active neuronal circuits. Based on the fact that many previous findings regarding circuit dynamics in the STNS have been subsequently

established in other model invertebrate and vertebrate systems, it is likely that the present findings will also resonate with the operation of other such networks.

REFERENCES

Bartos M, Manor Y, Nadim F, Marder E, Nusbaum MP (1999) Coordination of fast and slow rhythmic neuronal circuits. J Neurosci 19:6650–6660.

Beenhakker MP, Kirby MS, Nusbaum MP (2007) Mechanosensory gating of proprioceptor input to modulatory projection neurons. J Neurosci 27:14308–14316.

Beenhakker MP, Nusbaum MP (2004) Mechanosensory activation of a motor circuit by coactivation of two projection neurons. J Neurosci 24:6741–6750.

Blitz DM, Beenhakker MP, Nusbaum MP (2004) Different sensory systems share projection neurons but elicit distinct motor patterns. J Neurosci 24:11381–11390.

Blitz DM, Christie a E, Coleman MJ, Norris BJ, Marder E, Nusbaum MP (1999) Different proctolin neurons elicit distinct motor patterns from a multifunctional neuronal network. J Neurosci 19:5449–5463.

Briggman KL, Kristan WB (2008) Multifunctional pattern-generating circuits. Annu Rev Neurosci 31:271–294.

Christie AE, Stein W, Quinlan JE, Beenhakker MP, Marder E, Nusbaum MP (2004) Actions of a histaminergic/peptidergic projection neuron on rhythmic motor patterns in the stomatogastric nervous system of the crab Cancer borealis. J Comp Neurol 469:153–169.

Coleman MJ, Nusbaum MP, Cournil I, Claiborne BJ (1992) Distribution of modulatory inputs to the stomatogastric ganglion of the crab, Cancer borealis. J Comp Neurol 325:581–594.

DeLong ND, Beenhakker MP, Nusbaum MP (2009) Presynaptic inhibition selectively weakens peptidergic cotransmission in a small motor system. J Neurophysiol 102:3492–3504.

Derjean D, Moussaddy A, Atallah E, St-Pierre M, Auclair F, Chang S, Ren X, Zielinski B, Dubuc R (2010) A novel neural substrate for the transformation of olfactory inputs into motor output. PLoS Biol 8:e1000567.

Dickinson PS (2006) Neuromodulation of central pattern generators in invertebrates and vertebrates. Curr Opin Neurobiol 16:604–614.

Doi A, Ramirez J-M (2008) Neuromodulation and the orchestration of the respiratory rhythm. Respir Physiol Neurobiol 164:96–104.

Doi A, Ramirez J-M (2010) State-dependent interactions between excitatory neuromodulators in the neuronal control of breathing. J Neurosci 30:8251–8262.

Getting PA (1989) Emerging principles governing the operation of neural networks. Annu Rev Neurosci 12:185–204.

Goaillard J-M, Taylor AL, Schulz DJ, Marder E (2009) Functional consequences of animal-to-animal variation in circuit parameters. Nat Neurosci 12:1424–1430.

Golowasch J, Abbott LF, Marder E (1999) Activity-dependent regulation of potassium currents in an identified neuron of the stomatogastric ganglion of the crab Cancer borealis. J Neurosci 19:RC33.

Guertin P a (2009) The mammalian central pattern generator for locomotion. Brain Res Rev 62:45–56.

Harris-Warrick RM (2011) Neuromodulation and flexibility in Central Pattern Generator networks. Curr Opin Neurobiol 21:685–692.

Jobst EE, Enriori PJ, Cowley M a (2004) The electrophysiology of feeding circuits. Trends Endocrinol Metab 15:488–499.

Johnson BR, Hooper SL (1992) Johnson and Hooper (1992) Overview of STNS.pdf. In: Dynamic Biological Networks: The Stomatogastric Nervous System (Harris-Warrick RM, Marder E, Selverston AI, Moulins M, eds), pp.1–30. Cambridge, MA: MIT Press.

Kilman VL, Marder E (1996) Ultrastructure of the stomatogastric ganglion neuropil of the crab, Cancer borealis. J Comp Neurol 374:362–375.

Kirby MS, Nusbaum MP (2007) Peptide hormone modulation of a neuronally modulated motor circuit. J Neurophysiol 98:3206–3220.

Köhler CA, da Silva WC, Benetti F, Bonini JS (2011) Histaminergic mechanisms for modulation of memory systems. Neural Plast 2011:328602.

Korn H, Faber DS (2005) The Mauthner cell half a century later: a neurobiological model for decision-making? Neuron 47:13–28.

Kupfermann I (1979) Modulatory actions of neurotransmitters. Annu Rev Neurosci 2:447–465.

Lee S-H, Dan Y (2012) Neuromodulation of brain states. Neuron 76:209–222.

Marder E (2012) Neuromodulation of neuronal circuits: back to the future. Neuron 76:1–11.

Marder E, Bucher D (2007) Understanding circuit dynamics using the stomatogastric nervous system of lobsters and crabs. Annu Rev Physiol 69:291–316.

Marder E, Calabrese RL (1996) Principles of rhythmic motor pattern generation. Physiol Rev 76:687–717.

Nusbaum MP, Blitz DM (2012) Neuropeptide modulation of microcircuits. Curr Opin Neurobiol 22:592–601.

Nusbaum MP, Blitz DM, Swensen AM, Wood D, Marder E (2001) The roles of co-transmission in neural network modulation. Trends Neurosci 24:146–154.

Patton DF, Mistlberger RE (2013) Circadian adaptations to meal timing: neuroendocrine mechanisms. Front Neurosci 7:185.

Prinz AA, Bucher D, Marder E (2004) Similar network activity from disparate circuit parameters. Nat Neurosci 7:1345–1352.

Di Prisco G V, Pearlstein E, Le Ray D, Robitaille R, Dubuc R (2000) A cellular mechanism for the transformation of a sensory input into a motor command. J Neurosci 20:8169–8176.

Rafaeli A (2009) Pheromone biosynthesis activating neuropeptide (PBAN): regulatory role and mode of action. Gen Comp Endocrinol 162:69–78.

Saideman SR, Ma M, Kutz-Naber KK, Cook A, Torfs P, Schoofs L, Li L, Nusbaum MP (2007a) Modulation of rhythmic motor activity by pyrokinin peptides. J Neurophysiol 97:579–595.

Saideman SR, Blitz DM, Nusbaum MP (2007b) Convergent motor patterns from divergent circuits. J Neurosci 27:6664–6674.

Stein W (2009) Modulation of stomatogastric rhythms. J Comp Physiol A Neuroethol Sens Neural Behav Physiol 195:989–1009.

Swensen AM, Bean BP (2005) Robustness of burst firing in dissociated purkinje neurons with acute or long-term reductions in sodium conductance. J Neurosci 25:3509–3520.

Taghert PH, Nitabach MN (2012) Peptide neuromodulation in invertebrate model systems. Neuron 76:82–97.

White RS, Nusbaum MP (2011) The same core rhythm generator underlies different rhythmic motor patterns. J Neurosci 31:11484–11494.

Wood DE, Nusbaum MP (2002) Extracellular peptidase activity tunes motor pattern modulation. J Neurosci 22:4185–4195.

Wood DE, Stein W, Nusbaum MP (2000) Projection neurons with shared cotransmitters elicit different motor patterns from the same neural circuit. J Neurosci 20:8943–8953.

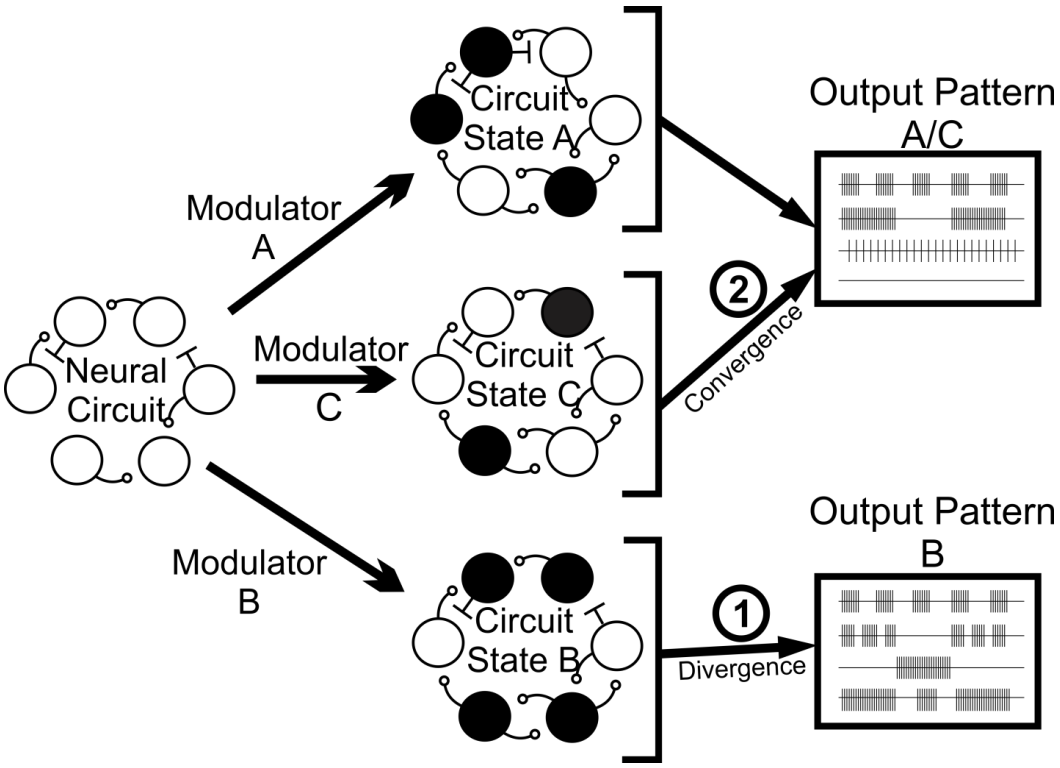

Figure 1. Neuromodulation enables flexible circuit states and output patterns. Schematic representation of the multifunctional nature of neural circuits. A neural circuit receives a variety of modulatory inputs which can produce different circuit states, as defined by each circuit neuron exhibiting different cellular and synaptic properties. These distinct circuit configurations can produce (1) divergent output patterns or (2) convergent output patterns.

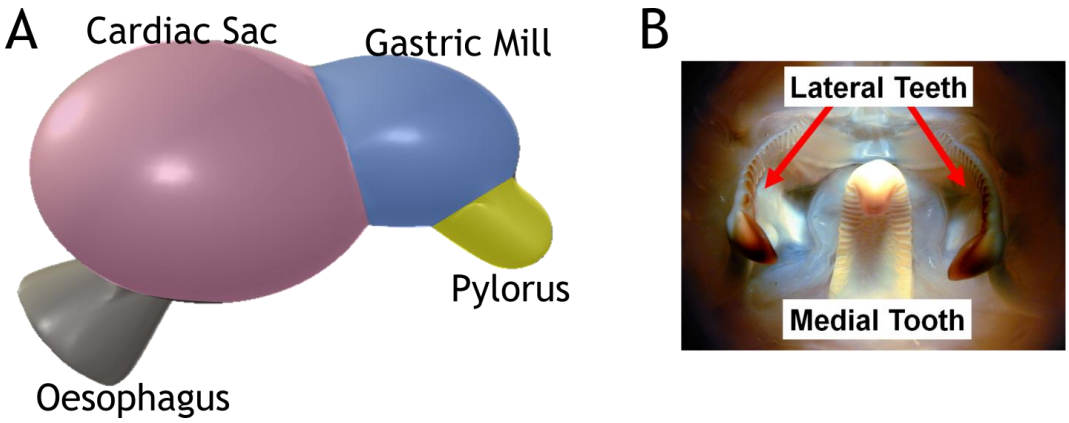

Figure 2. The feeding-related compartments and associated behaviors of the crab foregut. A, The crab foregut is composed of 4 interconnected structures with separate functional properties, including (from anterior to posterior) the (1) oesophagus (swallowing), (2) cardiac sac (storage), (3) gastric mill (chewing), and (4) pylorus (pumping and filtering). **B,** The gastric mill rhythmically chews food using a medial tooth (attached to the internal dorsal surface) and a pair of lateral teeth (attached to the internal lateral surfaces), which coordinately rhythmically protract and retract. The gastric mill network neurons control the pattern of teeth movement during mastication. Modified from Heinzel et al. (1993).

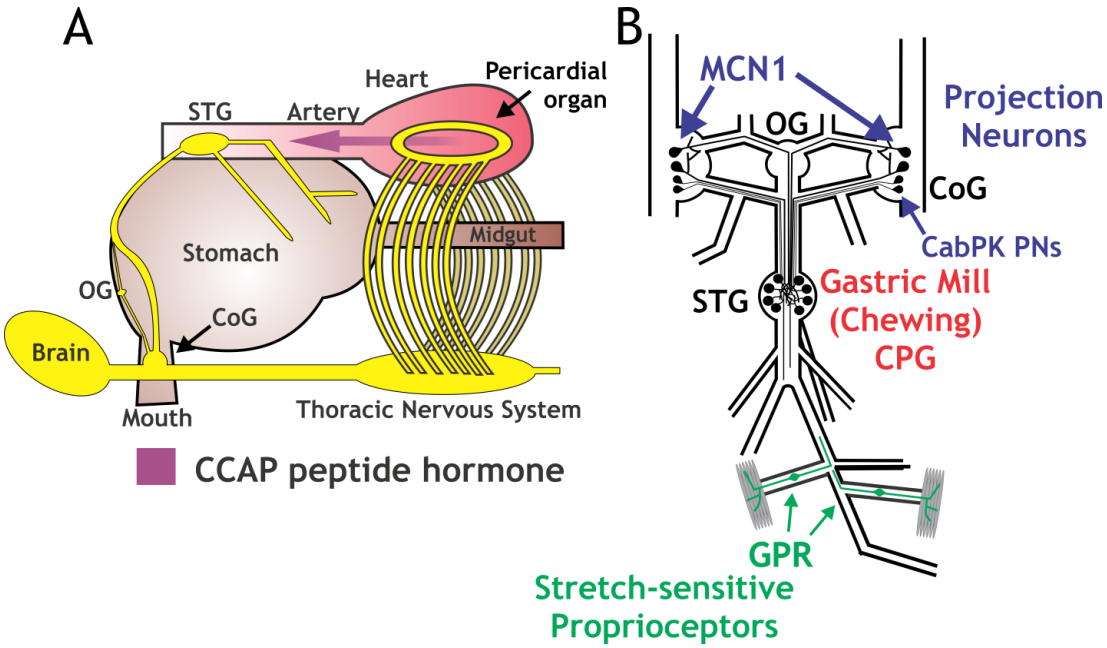

Figure 3. Neuromodulation in the crab foregut and stomatogastric nervous system. **A,** Schematic side-view of the crab foregut, including the circulatory (red) and nervous systems (yellow). Decapod crustaceans have a semi-open circulatory system which includes a major artery projecting from the heart which directs the hemolymph into the thoracic cavity, from where it collects back into vessels to reenter the heart. There is no vasculature within the STG. Instead, the STG is located within the major artery and so is continually superfused with arterial blood and the associated hormones (e.g. CCAP) that are released into the cardiac sinus by a neurohemal structure (the paired pericardial organs, POs) embedded within the heart. The neuroendocrine terminals within the POs originate from neurons within the thoracic nervous system. Modified from Marder (2012). **B,** Schematic of the STNS, including the four ganglia plus their connecting nerves and a subset of their peripheral nerves. The gastric mill and pyloric CPGs are located in the STG. The OG and CoGs contain projection

neurons (e.g. MCN1, CabPK PNs) that innervate and modulate the STG networks. GPRs are a bilaterally symmetric pair of proprioceptors that modulate the STG networks in response to changes in muscle length and tension. Abbreviations – CCAP, crustacean cardio-active peptide; CoG, commissural ganglia; CPG, central pattern generator; GPR, gastro-pyloric receptor; OG, oesophageal ganglion; STG, stomatogastric ganglion.

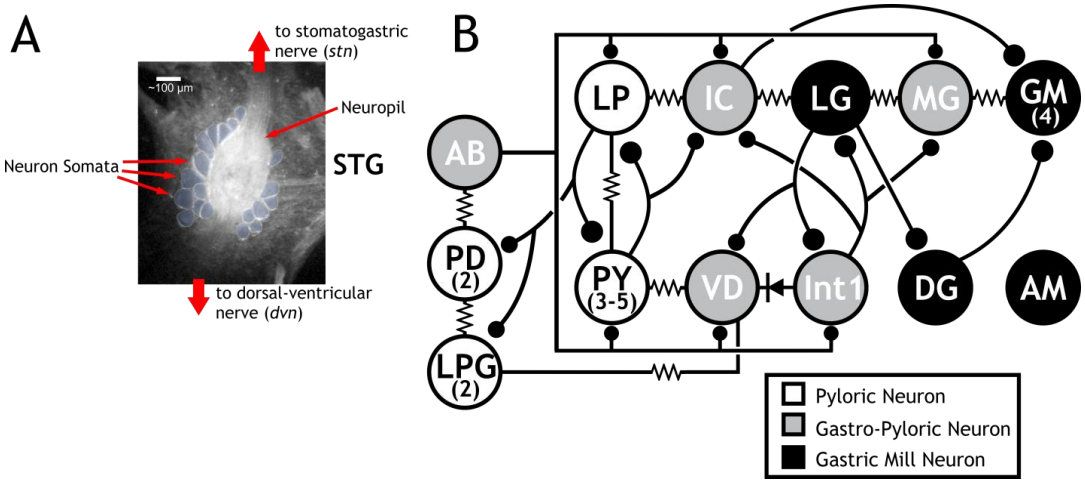

Figure 4. The gastric mill and pyloric circuits within the *C. borealis* STG are composed of 13 neuron types that include 22 of the 26 neurons in the STG. **A,** Whole-mount image of a desheathed STG photographed during illumination via a dark-field condenser. The STG neuron somata exhibit a laminar arrangement surrounding a central neuropil, with each neuron soma projecting a neurite into the neuropil where it branches extensively to make and receive synapses before extending into the appropriate nerve to reach its targets in the periphery (*dvn*: projects to muscle) or centrally (e.g. *stn*: projects to OG, CoGs and rest of CNS). Input from projection neurons projects into the STG neuropil via the *stn*. **B,** Each neuron type occurs once per STG unless labeled with a number or range (e.g. GM, 4 copies; PY, 3-5 copies). The gastric mill neurons are separated into two groups: the top row is active during protraction, while the bottom row is active during retraction. Note that the protractor neurons, shown here as serially coupled, have an unknown electrical coupling configuration. The strength of all electrical coupling is modest to weak except for that among the pyloric pacemaker group (AB, PDs, LPGs) which is sufficient strong to enable to

them to oscillate together. Abbreviations: AB, anterior burster; AM, anterior median; GM, gastric mill; IC, inferior cardiac; Int1, interneuron 1; LG, lateral gastric; LP, lateral pyloric; LPG, lateral posterior gastric; MG, medial gastric; PD, pyloric dilator; PY, pyloric; VD, ventricular dilator.

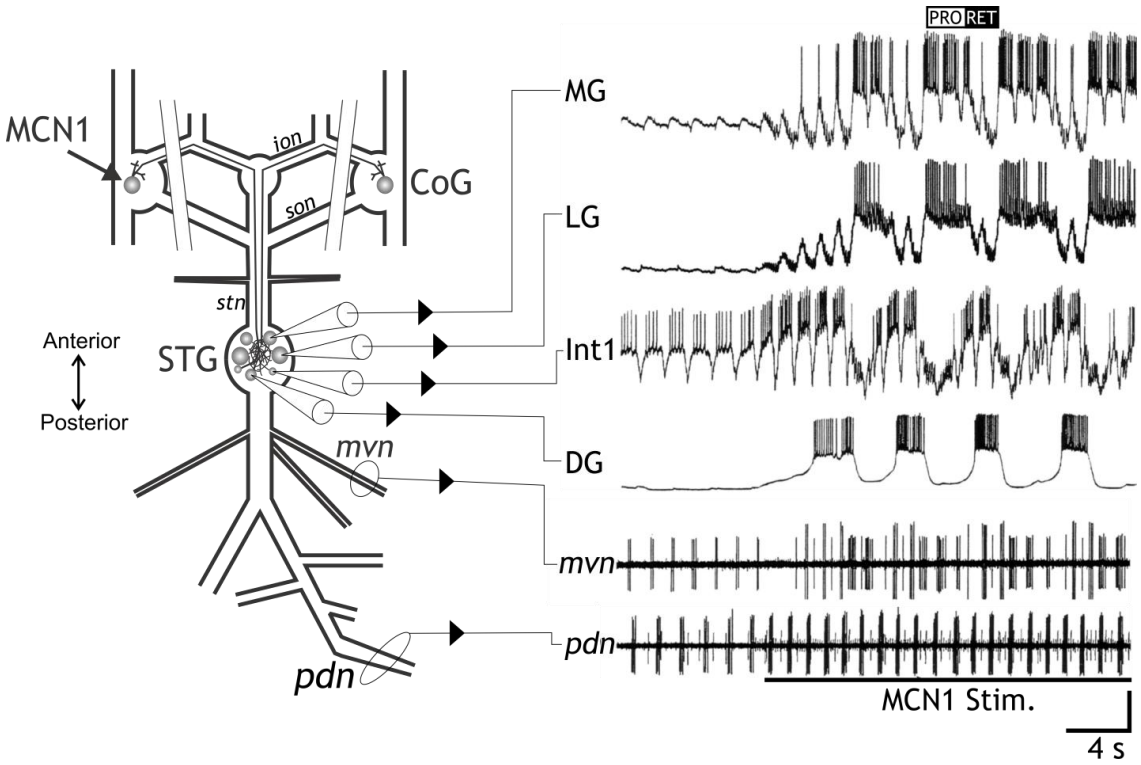

Figure 5. Gastric mill motor patterns are monitored using intracellular and extracellular recordings. Stimulation of the projection neuron, MCN1, drives a gastric mill motor pattern and strengthens the pyloric rhythm. The top four traces are sharp electrode intracellular recordings of the gastric mill protractor neurons MG and LG, plus the retractor neurons Int1 and DG. The bottom two traces are extracellular nerve recordings from the *mvn* and *pdn*. The *mvn* contains the axons of the gastro-pyloric neurons IC and VD. The *pdn* recording contains only the two PD neuron axons, thus serving as a monitor of the pyloric pacemaker kernel. Abbreviations: CoG, commissural ganglia; DG, dorsal gastric; Int1, interneuron 1; LG, lateral gastric; MCN1, modulatory commissural neuron 1; MG, medial gastric; *mvn*, medial ventricular nerve; STG, stomatogastric ganglion. Recordings from Stein et al. (2007).

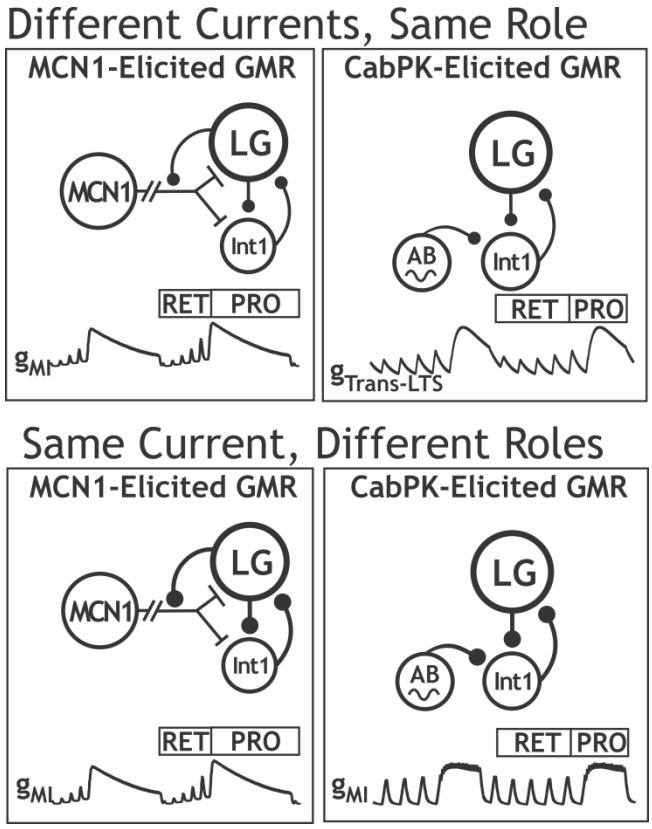

Figure 6. Core mechanisms of gastric mill rhythm generation during MCN1 stimulation and CabPK superfusion. ***A,*** During gastric mill rhythm generation, LG neuron bursting results from the rhythmic build-up and decay of (left) MCN1-activated g_{MI}, or (right) CabPK-activated $g_{Trans\text{-}LTS}$. During tonic MCN1 stimulation, g_{MI} accrues continually during retraction, while g_{MI} decay during protraction results from LG inhibition of $MCN1_{STG}$ transmitter release. During CabPK superfusion, the voltage-dependent $g_{Trans\text{-}LTS}$ accumulates deinactivation during retraction, while during protraction it first activates and then exhibits a time-dependent inactivation. ***B,*** Activation of g_{MI} in LG directly underlies LG burst generation during the MCN1-gastric mill rhythm, whereas it indirectly enables LG burst generation by facilitating activation of $I_{Trans\text{-}LTS}$ during the CabPK-gastric mill

rhythm. Note the different g_{MI} trajectories during protraction, which result from its being both voltage- and synaptic inhibition-dependent during the MCN1-gastric mill rhythm but only regulated by membrane potential during the CabPK-gastric mill rhythm. Both panels from Rodriguez et al. (2013).

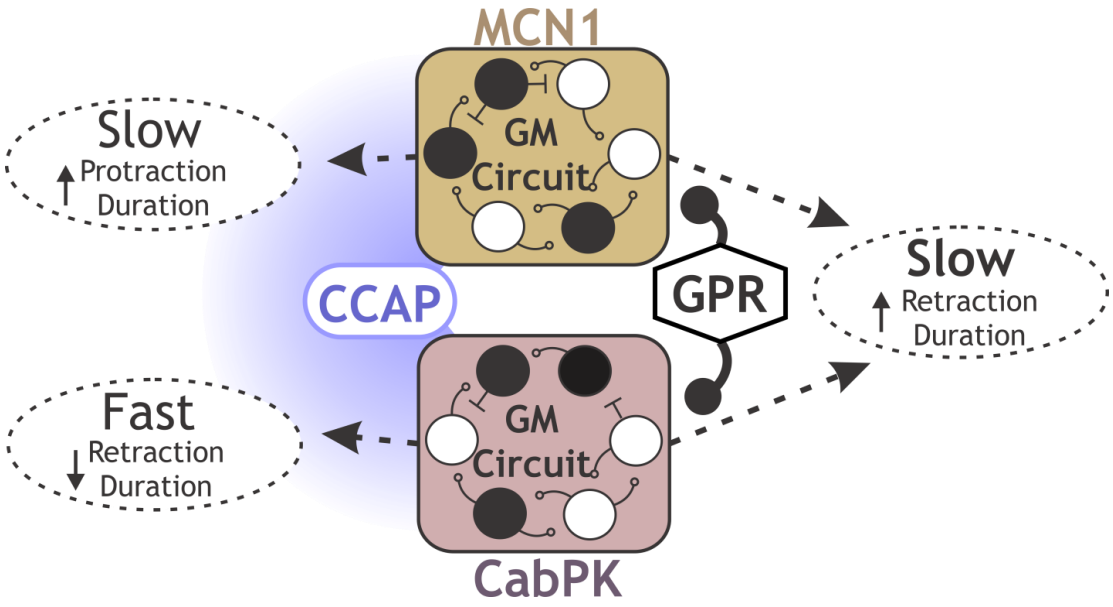

Figure 7. The MCN1- and CabPK-configured circuit states flexibly respond to additional modulation from hormones (CCAP) and sensory feedback (GPR). Left, CCAP bath application slows the MCN1-gastric mill rhythm by selectively prolonging protraction (Kirby and Nusbaum, 2007). In contrast, as shown in Chapter 3, CCAP reduces the CabPK-gastric mill cycle period by selectively reducing retraction duration. **Right,** GPR has identical actions on the MCN1- and CabPK-gastric mill rhythms. Specifically, GPR slows both rhythms by selectively prolonging the retractor phase duration (Beenhakker et al., 2007; DeLong et al., 2009; Chapter 3). Abbreviations: CabPK, *Cancer borealis* pyrokinin; CCAP, crustacean cardioactive peptide; GPR, gastro-pyloric receptor; MCN1, modulatory commissural neuron 1.

CHAPTER 2

Convergent Rhythm Generation from Divergent Cellular Mechanisms

Jason C. Rodriguez

Dawn M. Blitz

Michael P. Nusbaum

Published:

Journal of Neuroscience, 2013

46: 18047 - 18064

Sept 17, 2013

Convergent Rhythm Generation from Divergent Cellular Mechanisms

Jason C. Rodriguez

Dawn M. Blitz[1]

Michael P. Nusbaum*

Dept. of Neuroscience, 215 Stemmler Hall, Perelman School of Medicine, Univ. of Pennsylvania, Philadelphia, PA 19104

[1]Current Address: Department of Biology, Miami University, 242 Pearson Hall, Oxford, OH 45056

Running title: Rhythm generation by distinct mechanisms

Abstract:	250/250 Words
Introduction:	493/500 Words
Discussion:	1497/1500 Words
Pages:	61

Figures: 14

Tables: 2

*To whom correspondence should be addressed:

Michael P. Nusbaum, PhD

Dept. of Neuroscience

215 Stemmler Hall

Perelman School of Medicine, Univ. of Pennsylvania

Philadelphia, PA 19104-6074

Phone: (215) 898-1585

FAX: (215) 573-9050

Email: nusbaum@mail.med.upenn.edu

Acknowledgments: This work was supported by National Institute of Neurological Disorders and Stroke Grant R37-NS 29436 (M.P.N.), National Science Foundation Grant IOS-1153417 (D.M.B.), and the Behavioral and Cognitive Neurosciences Training Grant T32-MH 17168.

Keywords: Stomatogastric, Postinhibitory Rebound, Modulation, Central Pattern Generator, Reciprocal Inhibition

ABSTRACT

Different modulatory inputs commonly elicit distinct rhythmic motor patterns from a central pattern generator (CPG), but they can instead elicit the same pattern. We are determining the rhythm-generating mechanisms in this latter situation, using the gastric mill (chewing) CPG in the crab (*Cancer borealis*) stomatogastric ganglion where stimulating the projection neuron MCN1 or bath-applying CabPK peptide elicits the same gastric mill motor pattern, despite configuring different gastric mill circuits. In both cases, the core rhythm generator includes the same reciprocally inhibitory neurons (LG, Int1), but the pyloric (food filtering) circuit pacemaker neuron AB is additionally necessary only for CabPK rhythm generation. MCN1 drives this rhythm generator by activating in LG the modulator-activated inward current (I_{MI}), which waxes and wanes periodically due to phasic feedback inhibition of MCN1 transmitter release. Each buildup of I_{MI} enables LG to generate a self-terminating burst and thereby alternate with Int1 activity. Here we establish that CabPK drives gastric mill rhythm generation by activating in LG I_{MI} plus a slowly activating transient, low threshold inward current ($I_{Trans\text{-}LTS}$) that is voltage-, time- and Ca^{2+}-dependent. Unlike MCN1, CabPK maintains a steady I_{MI} activation, causing a subthreshold depolarization in LG that facilitates a periodic postinhibitory rebound (PIR) burst caused by the regular buildup and decay of availability of $I_{Trans\text{-}LTS}$. Thus, different modulatory inputs can use different rhythm generating mechanisms to drive the same neuronal rhythm. Additionally, the same ionic current (I_{MI}) can play different roles under these different conditions, while different currents (I_{MI}, $I_{Trans\text{-}LTS}$) can play the

same role.

INTRODUCTION

Different modulatory inputs enable individual neuronal networks to generate different output patterns by changing the intrinsic and synaptic properties of network neurons (Dickinson, 2006; Doi and Ramirez, 2008; Briggman and Kristan, 2008; Rauscent et al., 2009; Harris-Warrick, 2011, Marder, 2012). However, different modulatory inputs can also elicit the same activity pattern from that network (Saideman et al., 2007b). Determining how different modulatory pathways influence network activity is challenging, because these different pathways can converge onto the same direct input(s) to a network (Viana di Prisco et al., 2000; Korn and Faber, 2005; Derjean et al., 2010; White and Nusbaum, 2011), comparably modulate the same network (Doi and Ramirez, 2010), distinctly alter multiple cellular and synaptic properties in the same circuit neurons (MacLean et al., 2003; Prinz et al., 2004a; Goaillard et al., 2009; Calabrese et al., 2011; Marder, 2012) and/or configure different circuits (Saideman et al., 2007b). The cellular mechanisms underlying the last of these processes are not determined in any system.

We are determining the cellular mechanisms that enable two differently configured, network-driven central pattern generator (CPG) circuits to generate the same biphasic motor pattern, using the isolated crab stomatogastric ganglion (STG) (Marder and Bucher, 2007; Stein, 2009). These two gastric mill (chewing) circuits are configured by the projection neuron MCN1 (modulatory commissural neuron 1) and bath-applied CabPK (*Cancer borealis* pyrokinin) peptide (Saideman et al., 2007a,b).

The core rhythm generator for both gastric mill circuits includes the reciprocally inhibitory neurons LG (lateral gastric) and Int1 (interneuron 1). Rhythmic MCN1 transmitter release is also necessary for the MCN1-gastric mill rhythm, while the pyloric pacemaker neuron AB (anterior burster) is necessary for the CabPK-rhythm. The cellular and synaptic mechanisms underlying MCN1-gastric mill rhythm generation are established (Coleman et al., 1995; Bartos et al., 1999; DeLong et al., 2009a,b). A key MCN1 rhythm-generating mechanism is its activation of I_{MI} (modulator-activated, voltage-dependent inward current) in LG, which waxes and wanes periodically due to rhythmic feedback inhibition of MCN1 transmitter release by LG. These events enable LG to periodically fire a self-terminating burst and alternate with Int1 activity.

Here we identify two CabPK-activated currents in LG that are necessary and sufficient for gastric mill rhythm generation. These currents include I_{MI} and a transient, low threshold, slowly-activating inward current ($I_{Trans\text{-}LTS}$). $I_{Trans\text{-}LTS}$ exhibits voltage- and time-dependent properties. CabPK-gastric mill rhythm generation results from I_{MI} providing a constant depolarizing drive that enables periodic postinhibitory rebound (PIR) bursting, triggered by $I_{Trans\text{-}LTS}$. The rhythmic nature of the PIR burst generation results from the time- and voltage-dependent properties of $I_{Trans\text{-}LTS}$. Computational modeling and dynamic clamp manipulations of these two currents support their necessity and sufficiency for CabPK-gastric mill rhythm generation, and reveal that the pyloric rhythm (AB)-timed influence on LG is necessary for triggering each PIR burst. Thus, distinct rhythm-generating mechanisms enable distinct circuits to generate the same

rhythmic activity. Additionally, the same ionic current (I_{MI}) plays a different role under these two conditions, whereas different currents (I_{MI}, $I_{Trans\text{-}LTS}$) play a comparable role.

METHODS

Animals. Male Jonah crabs (*Cancer borealis*) were purchased from commercial suppliers (Fresh Lobster; Marine Biological Laboratory) and maintained in aerated, filtered artificial seawater at 10 – 12° C. Animals were cold anesthetized by packing in ice for at least 30 min before dissection, after which the foregut was removed, in physiological saline at ~4° C, and the STNS isolated.

Solutions. C. borealis physiological saline contained (in mM): 440 NaCl, 26 $MgCl_2$, 13 $CaCl_2$, 11 KCl, 10 Trisma base, 5 maleic acid, 5 glucose, pH 7.4 – 7.6. All preparations were superfused continuously with *C. borealis* saline (8 – 12° C). CabPK-I or CabPK-II (Saideman et al., 2007a) (Biotechnology Center, Univ. of Wisconsin, Madison, WI) was diluted from a stock solution (10^{-3} M) into physiological saline or voltage clamp saline immediately before use. Bottles containing *C. borealis* saline and CabPK saline were connected to the same switching manifold for rapid solution changes. Oxotremorine (OXO: 10^{-5} M; Sigma Chemical Co.), a muscarinic agonist, was applied in the same manner.

For voltage clamp experiments, tetrodotoxin (TTX: 10^{-7} M, Sigma), picrotoxin (PTX: 10^{-5} M, Sigma) and tetraethylammonium chloride (TEACl: 10^{-2} M, Sigma) were added to *C. borealis* saline (i.e. voltage clamp saline). These substances were used to suppress voltage-dependent Na^+ currents (TTX), glutamatergic inhibitory synaptic transmission (PTX), and a subset of K^+ currents (TEACl) (Marder and Eisen, 1984; Golowasch and Marder, 1992a). In some

experiments, the microelectrode was filled with a solution of CsCl (1 M; Sigma) and TEACl (1 M) to additionally suppress a subset of K^+ currents. To test the sensitivity of CabPK-influenced currents to extracellular Na^+, in some experiments Na^+ in the saline was replaced by $NMDG^+$ (n-methyl, d-glucamine; Fluka) (Golowasch and Marder, 1992). The $NMDG^+$ was added to the solution first and then neutralized with HCl before adding all other components. Additionally, in some experiments we used flufenamic acid (FFA: 10^{-5} M; Sigma), an inhibitor of I_{CAN} (Ca^{2+}-activated, non-specific cation current), dissolved in dimethyl sulfoxide (DMSO) and added directly to *Cancer* saline. The final DMSO concentration never exceeded 1%.

Electrophysiology. Electrophysiology experiments were performed using standard techniques for this system (Beenhakker and Nusbaum, 2004). In brief, the isolated STNS (Fig. 1*A*) was pinned into a silicone elastomer (Sylgard 184, KR Anderson)-lined Petri dish. Extracellular nerve recordings were obtained using pairs of stainless steel wire electrodes (reference and recording) whose ends were pressed into the Sylgard-coated dish. A differential AC amplifier (Model 1700: AM Systems) amplified the voltage difference between the reference wire, in the main bath compartment, and the recording wire, isolated with a section of an individual nerve from the main bath compartment by petroleum jelly (Vaseline, Lab Safety Supply). This signal was then further amplified and filtered (Model 410 Amplifier: Brownlee Precision). For extracellular nerve stimulation, the pair of wires used to record nerve activity was

placed into a stimulus isolation unit (SIU 5: Astromed/Grass Instruments) connected to a stimulator (Model S88: Astromed/Grass Instruments).

For current clamp experiments, intrasomatic recordings of STG neurons were made with sharp glass microelectrodes (15 – 30 MΩ) filled with either K_2SO_4 (0.6 M) plus KCl (10 mM) or KCl (1 M). For voltage clamp experiments, neurons were impaled with separate recording and current injection electrodes. The recording electrode, in most experiments, contained CsCl (1 M) and TEACl (1 M) to suppress additional K^+ currents. The current injection electrode was filled with KCl (2.5 M). All intracellular recordings were amplified using Axoclamp 900A amplifiers (Molecular Devices) in bridge mode or discontinuous current clamp mode (2 – 5 kHz sampling rate) and digitized at 5 kHz using a Micro 1401 data acquisition interface and Spike2 software (Cambridge Electronic Design). To facilitate intracellular recording, the desheathed STG was viewed with light transmitted through a dark-field condenser (Nikon). In all experiments, the STG was isolated from the commissural ganglia (CoGs) by bisecting the inferior (*ions*)- and superior oesophageal nerves (*sons*) (Fig. 1*A*). Individual STNS neurons were identified by their axonal pathways, activity patterns and interactions with other neurons (Weimann et al., 1991; Blitz et al., 1999; Beenhakker and Nusbaum, 2004).

During the gastric mill rhythm, the LG burst defines the protractor phase while its interburst duration, which is equivalent to the duration of Int1 activity, defines the retractor phase (Coleman et al., 1995; Bartos et al., 1999; Diehl et al. 2013). In experiments where Int1 activity was suppressed by hyperpolarizing

current injection to trigger PIR in LG, the current was usually injected into the VD (ventricular dilator) neuron instead of directly into Int1. These two neurons are electrically coupled, VD has a larger soma and therefore is easier to impale and manipulate, and VD has no direct synapse onto LG (Fig. 1*B*). Suppressing Int1 activity via this approach was routinely confirmed by the absence of unitary IPSPs in LG, insofar as Int1 is the only source of unitary IPSPs in LG in the isolated STG. The hyperpolarizing current duration used to elicit PIR was standardized at 5 s, which approximates the retraction phase (Int1 active) duration of the gastric mill rhythm (Saideman et al., 2007b). The PIR burst was defined as having a minimum of three spikes with inter-spike intervals ≤ 2 s. In the TTX experiments, the PIR response was measured as the amount of depolarization following the hyperpolarizing step relative to the baseline voltage prior to the step.

Two Electrode Voltage Clamp (TEVC). We used TEVC to record currents in the LG neuron. In these experiments, LG was impaled with designated recording and current-injecting electrodes. Recordings were used only if they exhibited a minimum input resistance (R_{input}) of 5 MΩ. The range of R_{input} was 5 MΩ – 15 MΩ**.** Protocols were developed and injected using pClamp software (Molecular Devices).

Modulator-activated currents were identified using two basic voltage clamp protocols, including ramps and steps. I_{MI} was isolated by injecting voltage ramps

into LG (-90 to 0 mV at 75 mV/s) in the presence of CabPK peptide (10^{-6} M) and saline, after which the currents recorded in control saline were subtracted from those recorded with peptide present (Swensen and Marder, 2000; DeLong et al., 2009a). In some experiments, voltage ramps were used instead to identify I_{MI} activated by OXO (10^{-5} M) application. I_{MI} was originally described by Golowasch and Marder (1992) as a proctolin-activated current and thus designated I_{proct}. However, many modulators are now known to activate this current in the STG (Swensen and Marder 2000, 2001), so it is now designated as I_{MI} (Grashow et al., 2009; DeLong et al., 2009a).

Transient currents cannot be reliably identified with ramp protocols so, to determine if any transient currents were influenced by CabPK, we also implemented a standard pre-step voltage-clamp step protocol. To characterize CabPK-influenced transient currents, we obtained estimations of their *m* and *h* parameters by independently varying the holding voltage, pre-step voltage, pre-step duration and step voltage, focusing primarily on the physiological range of LG membrane potentials (-65 mV to -30 mV). To measure the voltage-dependence of activation, LG was hyperpolarized to a pre-step voltage of -80 mV for 10 s followed by a step depolarization to a voltage between -65 to 0 mV, in 5 mV increments. To determine the voltage dependence of deinactivation of the CabPK-influenced transient currents, LG was held at -45 mV and given a hyperpolarizing pre-step to -50, -60, -70 or -80 mV for 10 s, and then stepped back to -45 mV for 6 s. To measure the time-dependence of deinactivation, LG was given a hyperpolarizing pre-step to -80 mV for a range of durations (1 – 13

s) and then depolarized to -40 mV for 6 s. Currents measured in normal saline were subtracted from those measured during CabPK bath application (10^{-6} M). In all figures, unless otherwise indicated, the subtracted currents (CabPK saline minus normal saline) are displayed. We assessed the sensitivity of the transient, low threshold slow inward current ($I_{Trans\text{-}LTS}$) to Ca^{2+} influx by replacing most of the Ca^{2+} in the saline with equimolar Mn^{2+} (0.1X Ca^{2+} saline). We also determined the sensitivity of $I_{Trans\text{-}LTS}$ to Na^{+} influx by replacing Na^{+} with an equimolar concentration of $NMDG^{+}$.

Dynamic Clamp. We used the dynamic clamp to inject artificial versions of ionic (I_{MI}, $I_{Trans\text{-}LTF}$, $I_{Trans\text{-}LTS}$) and synaptic (Int1-mediated inhibition) currents into the LG neuron (Sharp et al, 1993; Bartos et al., 1999; Prinz et al, 2004b; Beenhakker et al., 2005; DeLong et al., 2009a,b; DeLong and Nusbaum, 2010; Blitz and Nusbaum, 2012). The dynamic clamp software used the intracellularly recorded LG membrane potential to calculate and continually update an artificial, dynamic clamp current (I_{dyn}), using a predetermined reversal potential (E_{rev}) and a conductance [$g_{dyn}(t)$] that was numerically computed. The injected current was based on real time computations, updated in each time step (0.2 ms) according to the new values of recorded membrane potential, and injected back into the LG neuron. The currents were computed according to the following equations:

$$I_{dyn} = G_{\max} m^p h^q n^r \left(V_1 - E_{syn}\right)$$

$$\tau_x\left(V_2\right)\frac{dX}{dt} = X_\infty\left(V_2\right) - X; X = m, h$$

$$X_\infty\left(V\right) = \frac{1}{1+\exp\left(\frac{V - V_X}{k_X}\right)}$$

$$\tau_X\left(V\right) = \tau_{X,Lo} + \frac{\tau_{X,Hi} - \tau_{X,Lo}}{1+\exp\left(-\frac{V - V_X}{\left|k_X\right|}\right)},$$

where V_1 and V_2 both represent the membrane potential, and X represents either m or h for calculations involving activation or inactivation, respectively. The values are provided in Table 1.

We modeled our dynamic clamp I_{MI} using previously determined parameters (Table 1) (Golowasch and Marder, 1992; Swensen and Marder, 2000, 2001; DeLong et al., 2009a). Specifically, we set the half-maximum voltage of the activation curve at -42 mV, with the peak current occurring at -32 mV and the reversal potential (E_{syn}) at 0 mV. These values reflect the ones obtained from intra-neurite LG recordings within the STG neuropil (DeLong et al., 2009a). Hence, they occur at more hyperpolarized potentials than those obtained in the current study from intra-somatic recordings, which are electrotonically more distant from the site of these events within the neuropil. I_{MI} shows a voltage-dependence to its activation (Golowasch and Marder, 1992a; Swensen and Marder, 2000, 2001). Therefore, the integer power of the activation variable *m* (P) was set to a value of 1. The slope of the activation curve (K_m) was -5.0 mV, and the time constant of activation was 5.0 s^{-1}. I_{MI} does

not inactivate, so the integer power of the inactivation variable *h* (abbreviated 'q' above) was set to 0. The conductance value at maximum activation (G_{max}) varied between 50 and 200 nS. In all of our dynamic clamp experiments, the maximum current injected into the LG neuron never exceeded 3 nA (see Results). Synaptic conductances were modeled in a manner similar to intrinsic conductances, except that activation depended on the presynaptic neuron voltage and was more depolarized than the presynaptic action potential threshold. These synapses have been well documented and incorporated into previous models of gastric mill rhythm generation (Nadim et al., 1998; Bartos et al., 1999; Kintos et al., 2008; DeLong and Nusbaum, 2010; Blitz and Nusbaum, 2012), and the G_{max} could be readily scaled to match the observed physiological synapses.

Our dynamic clamp model for both of the low threshold transient currents was based on the aforementioned voltage clamp step protocol experiments. The results from activation protocols were manually fit to Hodgkin-Huxley equations using HHfit (Version 3.2) software developed by the Nadim lab (NJIT and Rutgers University, Newark, NJ; available at http://stg.rutgers.edu/software/). Occasionally, the resting V_m and action potential threshold coordinately varied between preparations, possibly due to impalement quality. Therefore, the dynamic clamp parameters were linked to the resting V_m. Table 1 contains a full parameter set for a neuron resting at -60 mV.

We used two versions of the dynamic clamp on a personal computer (PC) running Windows XP/7 and a NI PCI-6070-E data acquisition board (National

Instruments). The first version was developed in the Nadim laboratory (NJIT and Rutgers University, Newark, NJ; available at http://stg.rutgers.edu/software/). The second version was developed by E. Brady Trexler (Fishberg Dept. of Neuroscience, Mt. Sinai School of Medicine; freely available through Gotham Scientific: http://gothamsci.com/NetClamp/). Dynamic clamp current injections were performed while recording in single-electrode, DCC mode (sampling rates 2 – 5 kHz) or with separate voltage recording and current-injecting electrodes.

Data analysis. Data were collected onto a computer, with later playback onto a chart recorder (Astro-Med Everest). Acquisition onto computer (sampling rate 5 kHz) used the Spike2 data acquisition and analysis system (Cambridge Electronic Design). Some analyses, including CabPK-gastric mill rhythm parameters, were conducted on the digitized data using a custom-written Spike2 program (The Crab Analyzer: freely available at http://www.uni-ulm.de/~wstein/spike2/index.html).

Voltage-clamp data analysis was performed using PClamp (version 9: Molecular Devices), Spike2 (CED), and Igor Pro (Wavemetrics) software. For ramps, total neuron currents were determined by averaging 10 ramps in each condition and subtracting the control from the experimental condition. For pre-step protocols, the protocols were run once in each condition and the control currents were subtracted prior to analysis.

For gastric mill rhythm analyses, unless otherwise stated, each data point

in a data set was derived by determining the mean for the analyzed parameter from 10 consecutive gastric mill cycles. One gastric mill cycle was defined as extending from the onset of consecutive LG neuron action potential bursts (Beenhakker and Nusbaum, 2004; Wood et al., 2004). Thus, the gastric mill cycle period was measured as the duration (s) between the onset of two successive LG neuron bursts. The protractor phase was measured as the LG burst duration, while the retractor phase was measured as the LG interburst duration. The gastric mill rhythm-timed LG burst duration was defined as the duration (s) between the onset of the first and last action potential within an impulse burst, during which no inter-spike interval was longer than 1.5 s (approximately one pyloric cycle period during the CabPK-gastric mill rhythm and briefer than the duration of each gastric mill phase; Saideman et al., 2007b). The intraburst firing rate of LG was defined as the number of action potentials minus one, divided by the burst duration**.**

Data were plotted with Igor Pro (version 6.10A). Figures were produced using CorelDraw (version 13.0 for Windows). Statistical analyses were performed with Microsoft Excel (Microsoft) and SigmaStat 3.0 (SPSS). Comparisons were made to determine statistical significance using the paired Student's *t*-test or Analysis of Variance with Repeated Measures (RM-ANOVA) followed by the Student-Newman-Keuls (SNK) post-hoc test. In all experiments, the effect of each manipulation was reversible, and there was no significant difference between the pre- and post-manipulation groups. Data are expressed as the mean ± standard error (SE).

Gastric Mill Model. We constructed a computational model of the CabPK gastric mill rhythm generator modified from an existing conductance-based model of the MCN1-gastric mill rhythm generator (Nadim et al., 1998; Beenhakker et al., 2005; DeLong et al., 2009a,b). The previously published version modeled the LG, Int1, and MCN1 neurons as having multiple compartments separated by an axial resistance, with each compartment possessing intrinsic and/or synaptic conductances. The parameters of the CabPK-gastric mill rhythm generator model were based on both previously published voltage clamp analyses in STG neurons (including LG) and on the LG neuron voltage clamp results obtained in this paper (Golowasch and Marder, 1992a; Swensen and Marder, 2000, 2001; DeLong et al., 2009a). To mimic the effects of CabPK bath application to the biological system, we added I_{MI} to the LG neuron dendrite compartment as an intrinsic (non-synaptically activated) current (Table 2). This approach was based on the fact that CabPK excites LG by activating I_{MI} (this paper) and that CabPK was constantly present during its application. To more realistically mimic the biological system, in this version of the model we modified the CabPK-activated G_{MI} ($G_{MI\text{-}CabPK}$) in the LG dendrite compartment to include a voltage dependence (Table 2). Based on data collected in this paper, we also added a CabPK-activated $I_{Trans\text{-}LTS}$ to LG (Table 2). The time- and voltage dependence of $I_{Trans\text{-}LTS}$ were empirically determined with voltage-clamp, while a canonical reversal potential was used for I_{Ca} (E_{Ca} = 45 mV) (Zhang and Harris-Warrick, 1995).

Simulations were performed on a PC with the freely available Ubuntu Linux operating system (www.ubuntu.com). We used the Network simulation software developed in the Nadim laboratory (http://stg.rutgers.edu/software/network.htm). This included using a fourth-order Runge–Kutta numerical integration method with time steps of 0.05 and 0.01 ms. Results were visualized by plotting outputted data points using the freely available Gnuplot software package (www.gnuplot.info). In most figures showing the model output, we present conductance (g) instead of the associated current (I) to more clearly display the trajectory during the gastric mill retractor and protractor phases. The main difference between "g" and "I" is that the former lacks the fast transient changes that occur in the latter during each LG action potential (DeLong et al., 2009a). In particular, the relatively slow kinetics of the CabPK-activated conductances make them insensitive to these fast transient changes in voltage.

The presentation of currents in the model and dynamic clamp figures represent different conventions. Specifically, the model output uses the standard voltage clamp convention, whereas the dynamic clamp output uses the standard current clamp convention. For example, depolarizing current has a downward trajectory in the model output figures but has an upward trajectory in the dynamic clamp output figures.

RESULTS

In the isolated crab STG, tonic MCN1 stimulation and bath applied CabPK ($\geq 10^{-7}$ M) elicit comparable gastric mill motor patterns, despite configuring different gastric mill circuits (Fig. 1*B*) (Saideman et al., 2007b). MCN1 does not contain CabPK, and the CabPK-gastric mill rhythm can occur without MCN1 activity. CabPK is present in two or three pairs of CoG projection neurons which innervate the STG, although these neurons are not physiologically identified (Saideman et al., 2007a). However, bath-applied peptide can mimic the actions resulting from its neuronal release. For example, in the crab STG, bath application of the peptide proctolin (10^{-6} M) and direct stimulation of the modulatory proctolin neuron (MPN) elicit comparable responses from the pyloric CPG, despite the fact that MPN contains a small molecule co-transmitter (Nusbaum and Marder, 1989ab; Blitz et al., 1999).

There are also at least several additional gastric mill motor patterns in *C. borealis*, each distinct from the pattern elicited by MCN1 and CabPK and driven by a different input pathway (Beenhakker and Nusbaum, 2004; Blitz et al., 2004; Christie et al., 2004; White and Nusbaum, 2011). These different rhythms all share the same basic structure, which includes a biphasic motor pattern exhibiting rhythmic alternating bursting of protraction- and retraction-related neurons across an overlapping range of cycle periods (~5 – 20 s) (Fig. 1*C*). They differ in the relative timing, intensity, duration and pattern of activity in the component neurons. There are 7 gastric mill motor neurons, including 4 protractor motor neurons and 3 retractor motor neurons, plus a single retraction-

timed interneuron (Int1) (Fig. 1*B*). As discussed below, the pyloric CPG pacemaker neuron AB also influences these gastric mill rhythms (Fig. 1*B*). Like the gastric mill rhythm, the pyloric (filtering of chewed food) rhythm is generated in the STG (Marder and Bucher, 2007).

A core component of the rhythm generator for the MCN1- and CabPK-gastric mill rhythms is the half-center formed by the reciprocally inhibitory protraction neuron LG and retraction neuron Int1 (Saideman et al., 2007b) (Fig. 1*B*). The biphasic rhythm generated by these two neurons is then imposed on the other gastric mill neurons by synaptic actions from the rhythm generator plus the influences of MCN1 or CabPK. Under baseline conditions LG is silent (Fig. 1*C*) and Int1 is spontaneously active, exhibiting a pyloric rhythm-timed activity pattern due to inhibitory input it receives from the AB neuron (Fig. 1*B*) (Bartos et al., 1999; Saideman et al., 2007b). The pivotal event for enabling gastric mill rhythm generation is the acquisition by LG of the ability to fire rhythmic bursts.

The cellular and synaptic mechanisms underlying MCN1 activation of the gastric mill rhythm generator are known (Coleman et al., 1995; Bartos et al., 1999; DeLong et al., 2009a). In brief, during the MCN1-gastric mill rhythm, there is a rhythmic release of the MCN1 cotransmitters, which includes the peptides proctolin and CabTRP Ia (*Cancer borealis* tachykinin-related peptide Ia) plus GABA (Blitz et al., 1999). MCN1 uses only CabTRP Ia to influence LG (slow excitation) and only GABA to influence Int1 (fast excitation) (Wood et al., 2000; Stein et al., 2007). MCN1 cotransmitter release is rhythmic, even when MCN1 is tonically active, because its STG terminals ($MCN1_{STG}$) receive ionotropic synaptic

inhibition from LG (Fig. 1*B*) (Coleman and Nusbaum, 1994). Thus, during retraction, continuous MCN1 release of CabTRP Ia drives a steady buildup of I_{MI} in LG that eventually is sufficient to enable LG to fire an action potential burst (DeLong et al., 2009a). During protraction, when $MCN1_{STG}$ cotransmitter release is inhibited by LG, there is a steady decline in the amount of I_{MI} in LG until it can no longer sustain the LG burst. This rhythmic activation of I_{MI} in LG appears to be sufficient to drive the gastric mill rhythm across the physiological range of MCN1 firing frequencies (DeLong et al., 2009a,b; DeLong and Nusbaum, 2010). MCN1-driven gastric mill rhythm generation is also facilitated by the pyloric rhythm (cycle period ~1 s), because every LG burst initiates, after sufficient I_{MI} has accrued, during a pyloric-timed depolarization (i.e. disinhibition) that results from AB inhibition of Int1 (Bartos et al., 1999; DeLong et al., 2009a). These disinhibitions reduce the MCN1-gastric mill cycle period by reducing the amount of I_{MI}-mediated depolarization needed to enable LG to fire a burst. However, this rhythm does persist, with a longer cycle period, when there is no pyloric rhythm (Bartos et al., 1999).

The cellular and synaptic mechanisms underlying the CabPK-gastric mill rhythm were not known, although it was determined previously that activity in LG, Int1 and AB was necessary to enable this rhythm (Saideman et al., 2007b). Additionally, as during the MCN1-gastric mill rhythm, it appeared that direct CabPK excitation of LG was a pivotal event for rhythm generation. Thus, we identified CabPK-influenced ionic current(s) in LG.

CabPK activates three voltage-dependent inward currents in the LG neuron

CabPK application (10^{-6} M) provides a depolarizing drive to LG from its resting potential (-57.5 ± 1.5 mV; n=8). For example, under the most reduced conditions, with LG isolated from synaptic input, CabPK consistently elicited in LG a steady 5-10 mV depolarization. This depolarizing response occurred when LG was isolated by either hyperpolarizing Int1 (dep. response: 8.5 ± 1.1 mV; n=8) (Fig. 2*A*), or suppressing all glutamatergic inhibitory input to LG by bath-applying PTX (10^{-5} M; dep. response: 10.7 ± 0.54 mV; n=11). The CabPK-mediated depolarization moved the LG membrane potential closer to its spike threshold, which was not changed by CabPK (Saline: -42.4 ± 1.3 mV; n=9; CabPK: -44.5 ± 1.4 mV; n=9, p=0.15). When Int1 was active, the LG membrane potential exhibited subthreshold, pyloric-timed oscillations which exhibited a more depolarized peak in the presence of CabPK (Saline: -57.5 ± 1.4 mV; n=10; CabPK: -48.7 ± 1.7 mV; n=10, $p<0.01$) (Fig. 2*B*). These depolarized peaks remained subthreshold prior to the onset of the gastric mill rhythm, as well as during the ensuing gastric mill retraction phase. In contrast, CabPK did not alter the membrane potential at the trough of these LG oscillations (Saline: -59.8 ± 1.8 mV; n=10; CabPK: -59.1 ± 1.7 mV; n=10, p=0.4) (Fig. 2*B*; see below). Thus, the increased pyloric-timed oscillation amplitude was due to a more depolarized peak.

Based on the assumption that the sustained depolarizing drive in LG during CabPK application resulted from CabPK influence on a persistent current, we isolated CabPK-sensitive currents using a voltage ramp protocol (see

Methods) in TEVC. Difference currents between CabPK and control solutions revealed a voltage-dependent, inward net current at potentials more hyperpolarized than 0 mV (Fig. 2*C*). This inward current exhibited a small, relatively constant amplitude at membrane potentials more hyperpolarized than ~-60 mV, whereas in the depolarizing direction from ~-60 mV, the I-V plot for this current displayed a trajectory reminiscent of voltage-dependent inward currents. Specifically, it displayed a steadily increasing inward current that peaked at -8.1 ± 1.4 mV (peak amplitude: -4.4 ± 0.6 nA, n=7), after which the amplitude steadily decreased (Fig. 2*C*). It was not possible to determine its reversal potential, likely due to an inability to completely clamp the residual, relatively large K^+ currents at more depolarized potentials (DeLong et al., 2009a). This I-V relationship was comparable to that of the previously identified I_{MI}, which is activated by several different neuromodulators in crab STG neurons including the LG neuron (Golowasch and Marder, 1992; Swensen and Marder, 2000, 2001; DeLong et al., 2009a).

To further establish that the CabPK-activated, voltage-dependent inward current in the LG neuron that we identified in voltage ramp protocols was I_{MI}, we performed an occlusion experiment with a known I_{MI} activator in LG, crustacean cardioactive peptide (CCAP: DeLong et al., 2009a). CCAP application occludes the ability of the MCN1 peptide CabTRP Ia to activate I_{MI} in LG (DeLong et al., 2009a). In these experiments, CabPK (10^{-4} M) was first pressure applied onto the desheathed STG neuropil while recording LG in TEVC. CCAP (10^{-6} M) was then bath applied to activate I_{MI}, during which time CabPK (10^{-4} M) was again

puffed onto the STG neuropil. As shown in Figure 2*C*, the maximal CabPK-activated current amplitude was decreased substantially during CCAP bath application (CabPK pre-CCAP: -4.2 ± 0.6 nA; CabPK during CCAP application: -0.9 ± 0.1 nA; CabPK post-CCAP: -3.5 ± 0.9; p=0.01: CabPK pre-CCAP or CabPK post-CCAP vs CabPK during CCAP; p=0.33: CabPK pre-CCAP vs. CabPK post-CCAP; One-way RM ANOVA with SNK post-hoc test; n=3, F(2,8) = 16.8). This occlusion effect of CCAP thus supported the hypothesis that the aforementioned CabPK-activated inward current in the LG neuron was I_{MI}. In contrast to the CabPK condition, in normal saline I_{MI} was either not expressed or was present at low levels, insofar as the LG resting potential in normal saline was ~-60 mV (see above) and even modest levels of modulator-activated I_{MI} elicit a more depolarized LG membrane potential (Kirby and Nusbaum, 2007; DeLong et al., 2009a).

I_{MI} is also sensitive to changes in extracellular Ca^{2+} (Golowasch and Marder, 1992). Specifically, replacing most of the extracellular Ca^{2+} (0.1X normal Ca^{2+}) in the saline with additional Mg^{2+}, to maintain the total divalent cation concentration, linearizes the I-V curve for I_{MI} at hyperpolarized potentials. This linearization in reduced Ca^{2+}/added Mg^{2+} saline also occurred for the CabPK-sensitive current (Current measured at -90 mV: CabPK saline, -0.21 ± 0.3 nA; CabPK w/reduced Ca^{2+} saline, -5.67 ± 1.3 nA, n=3, $p<0.05$), further supporting the hypothesis that CabPK activates I_{MI} in LG.

To test the hypothesis that I_{MI} was responsible for the aforementioned, CabPK-mediated depolarization in LG, we used the dynamic clamp (DClamp) to

inject an artificial version of I_{MI} into LG in normal saline (Fig. 2*D*). Doing so using DClamp conductances comparable to those identified in voltage clamp (50-300 nS), while Int1 was silent or only weakly active, consistently depolarized the LG resting potential to the same extent as CabPK application (CabPK: 10.68 ± 0.5 mV; DClamp I_{MI}: 10.3 ± 2 mV, n=6, p=0.4) (Fig. 2*A,D*).

CabPK also activated other voltage-dependent inward currents in LG. These additional currents were not evident with our voltage ramp protocol, but they were present during a TEVC voltage step protocol. Their absence during our voltage ramp manipulations was likely due to their time-dependent inactivation (see below). We identified these other currents using a pre-step hyperpolarization (-80 mV) whose duration was similar to the gastric mill retraction phase (see Methods). Using this approach, with relatively prolonged depolarizing steps (6 s) comparable to the gastric mill protraction phase during which LG is depolarized and spiking, we identified three inward currents (Figs. 3 – 5). These currents included a (1) transient, low threshold, fast inward current ($I_{Trans\text{-}LTF}$), (2) transient, low threshold but more slowly developing inward current ($I_{Trans\text{-}LTS}$), and (3) sustained inward current. The $I_{Trans\text{-}LTF}$ was not evident in the raw current recordings obtained during CabPK superfusion (Fig, 3*A*), due to overlap with the capacitative current, but was readily evident in the difference current traces (Figs. 3*B*,4,5). In contrast, $I_{Trans\text{-}LTS}$ was identifiable in both the raw-CabPK and difference currents (Figs. 3 – 5), but was not evidently expressed under control conditions (Fig. 3*A*). Lastly, in the raw CabPK recordings the sustained inward current was evident as a smaller amplitude

outward current relative to the control recordings (Fig. 3*A*).

The CabPK-activated, sustained inward current was predominantly I_{MI}. During the last 3 s of the voltage step, we consistently observed a voltage-dependent, time-independent inward current, as anticipated from our voltage ramp experiments that identified CabPK activation of I_{MI} (Fig. 3*B*). There were three features of this sustained current in the voltage step protocols, however, that were distinct from I_{MI} measured from the voltage ramp protocol: 1) the peak amplitude was smaller (Step: -1.6 ± 0.4 nA, n=9; Ramp: -4.6 ± 0.4 nA, n=9; $p<0.01$), 2) the current exhibited less voltage-dependence at depolarized potentials (data not shown), and 3) in some recordings, particularly with steps more depolarized than -40 mV, a reduced inward current or small outward current was evident immediately following $I_{Trans\text{-}LTS}$, relative to the current amplitude at the end of the step (e.g. Figs. 3*A,B*, 4*B*, 5*B*). These features suggested that CabPK also activated a voltage- and time-dependent outward current. We did not, however, further isolate and characterize this additional component insofar as it did not appear to be necessary for the CabPK actions on gastric mill rhythm generation (see below).

The fast transient inward current exhibited a relatively rapid time to peak (32.9 ± 1.9 ms, n=16) and small peak amplitude (~0.5 nA), which occurred at ~-10 mV. It exhibited an apparent voltage threshold of ~-45 mV (range: -50 to -30 mV; n=16). Only an approximate peak current amplitude is provided for $I_{Trans\text{-}LTF}$ because we could not isolate this current from the other two CabPK-activated inward currents, and these other currents appeared to contribute substantially to

the fast transient peak. In this context, it is noteworthy that I_{MI} reaches its peak current level relatively quickly in response to a depolarizing voltage step (Fig. 5*A*). We did not further characterize $I_{Trans\text{-}LTF}$, insofar as it was not necessary for the ability of CabPK to enable gastric mill rhythm generation (see below).

$I_{Trans\text{-}LTS}$ exhibited a longer time to peak than $I_{Trans\text{-}LTF}$ (time to peak at -45 mV: 633 ± 48 ms, n=9, $p<0.01$) as well as a larger peak amplitude (-5.3 ± 0.6 nA, measured at -15 ± 3.1 mV, n=9) (Fig. 3*B,C*). It exhibited a voltage threshold of ~-55 mV (range: -60 to -50 mV, n=9) and its amplitude increased with depolarization up to ~-30 mV (n=9) (Fig. 3*C*). Note that this reported peak amplitude value includes the CabPK-activated I_{MI} amplitude and, at the more depolarized steps, likely also includes the aforementioned voltage- and time-dependent outward current. The unusually shallow slope of the I-V curve between -40 mV and -10 mV likely results, at least partly, from the contribution of this outward current (Fig. 3*C*). The $I_{Trans\text{-}LTS}$ voltage threshold and time to peak suggested that this current was likely to be activated during the CabPK-gastric mill rhythm, during which time the LG membrane potential exhibits rhythmic oscillations between ~-70 mV and -40 mV (Saideman et al., 2007b). We could not measure the full time course of the $I_{Trans\text{-}LTS}$ decay to the baseline because it merged into the sustained inward current, which persisted for the remainder of each step (Figs. 3*B*, 4*A*). $I_{Trans\text{-}LTS}$ exhibited a reversal potential that was more depolarized than 0 mV (n=16 each) ($I_{Trans\text{-}LTS}$: Fig. 3*C*), suggesting that it is primarily carried by ions with positive equilibrium potentials (e.g. Ca^{2+} and/or Na^{+}). Both of the CabPK-activated transient currents were clearly distinct from

I_{MI}, because I_{MI} exhibits no time-dependent decrease in amplitude (e.g. Fig. 5) (Golowasch and Marder, 1992).

$I_{Trans\text{-}LTS}$ not only exhibited the property of inactivation, but it also exhibited deinactivation. This deinactivation was sensitive to the time and voltage range that occurs in LG during the CabPK-gastric mill rhythm. We therefore characterized this property by varying parameters of the voltage step protocol in voltage clamp experiments. To determine the time-dependence of this property, we maintained LG at a holding potential of -40 mV and systematically hyperpolarized it to -80 mV for a range of durations (1 s to 13 s), stepping the voltage back to -40 mV after each hyperpolarization. We then measured the maximum amplitude of the slow transient inward current after the return to -40 mV (Fig. 4). These data were then fit with a sigmoid curve (Igor Pro), from which two parameters were identified, including the midpoint and slope. There was a relatively long time-dependence for $I_{Trans\text{-}LTS}$ deinactivation (midpoint: 7.4 ± 0.4 s, slope: 2.4 ± 0.2 s^{-1}, n=3) (Fig. 4*B*).

We determined the voltage-dependence of the $I_{Trans\text{-}LTS}$ deinactivation by varying the pre-step voltage across a range (-75 to -50 mV) of membrane potentials, while maintaining the pre-step duration (8 s) and subsequent step potential (-45 mV) (midpoint: -60.9 ± 2 mV; slope: -5.3 ± 0.5 mV^{-1}, n=3). This midpoint value was well within the normal LG membrane potential range (-55 mV to -70 mV) during the gastric mill retraction phase (Saideman et al., 2007b). Thus, based on the time- and voltage dependence of this transient current in LG, and the LG membrane potential trajectories during the gastric mill rhythm

(Saideman et al., 2007a,b; this study), it likely exhibits considerable inactivation during the course of each gastric mill protraction phase and deinactivation during the retractor phase. These correlations support the hypothesis that the CabPK-activated slow transient inward current helps enable LG to generate a periodic burst during a pyloric-timed membrane potential depolarization produced by the combination of I_{MI} and the periodic (AB-mediated) removal of synaptic inhibition from Int1 (see below).

Both CabPK-activated transient inward currents were extracellular Ca^{2+}-dependent. Replacing most of the extracellular Ca^{2+} with Mn^{2+}, a Ca^{2+} channel antagonist (Turrigiano et al., 1995), consistently resulted in no measureable fast (n=4) or slow transient inward currents (peak $I_{Trans-LTS}$ at -50 mV: CabPK alone, -1.6 ± 0.1 nA; CabPK with 0.1 mM Ca^{2+}/10.9 mM Mn^{2+}, 0 ± 0 nA; CabPK post-reduced Ca^{2+}, -0.8 ± 0.02 nA; n=4) (Fig. 5*A*). This manipulation only had a moderate effect on I_{MI} (Fig. 5*A*), due to the divalent cation sensitivity of this current being approximately equivalent for Ca^{2+} and Mn^{2+} (Golowasch and Marder, 1992). In addition, replacing extracellular Na^{+} with a non-permeant ionic species ($NMDG^{+}$) also consistently resulted in no measureable $I_{Trans-LTS}$ (Max. amplitude: Control, -3.8 ± 0.9 nA; NMDG saline, 0 ± 0 nA, n=7) (Fig. 5*B*). In contrast, in all four of these $NMDG^{+}$ experiments where there was a discernible $I_{Trans-LTF}$ peak in the control recordings, this peak persisted in the $NMDG^{+}$ condition (data not shown). In the three experiments where there was no distinguishable $I_{Trans-LTF}$ peak in the control recording, it was not possible to determine whether it was influenced by the $NMDG^{+}$ substitution (e.g. Fig. 5*B*).

In sum, these results suggested that $I_{Trans\text{-}LTS}$ is either permeable to both Na^+ and Ca^{2+}, is a Ca^{2+}-sensitive I_{Na}, or is a Ca^{2+}-activated nonselective cation current (I_{CAN}), although we also did not rule out the possibility that $NMDG^+$ acts instead as an inhibitor of this current. I_{CAN} was identified previously in *C. borealis,* both in the stomatogastric nervous system and cardiac ganglion, where it exhibited a V_{rev} of ~-30 mV and was insensitive to changes in extracellular Na^+ but sensitive to caffeine application (10^{-2} M), which stimulates intracellular Ca^{2+} release, and the I_{CAN} antagonist flufenamic acid (FFA: 10^{-5} M) (Zhang et al., 1995; Kadiri et al., 2011; Ransdell et al., 2013). However, bath applied FFA did not alter any of the CabPK-activated currents (n=2). Insofar as $I_{Trans\text{-}LTS}$ exhibited a $V_{rev} > 0$ mV, sensitivity to extracellular Na^+ and insensitivity to FFA, it was not likely to be an I_{CAN}.

CabPK-activated transient inward currents enable post-inhibitory rebound in the LG neuron

To determine how the CabPK-activated currents might contribute to LG burst generation during the CabPK-gastric mill rhythm, we examined intrinsic properties in LG. Specifically, we found that brief hyperpolarizing current injections into LG were followed by passive responses during saline superfusion but elicited a post-inhibitory rebound (PIR) burst during CabPK superfusion. Under control conditions (saline), we depolarized LG to a membrane potential that was comparable to its CabPK-mediated baseline potential (~-50 mV) using

either direct depolarizing current injection or DClamp I_{MI} injection. Despite this depolarized baseline potential, following a period of hyperpolarization there was no evidence of PIR (n>10) (Fig. 6). In contrast to its passive response during saline superfusion, LG hyperpolarization from its CabPK-mediated depolarized resting potential was consistently followed by a PIR burst (Fig. 6). Specifically, during CabPK superfusion, injecting a modest hyperpolarizing current (-1 nA) into LG, which caused a 5 – 10 mV hyperpolarization, consistently elicited a PIR burst when the current injection was terminated (PIR burst: Duration, 5.14 ± 0.2 s; Number of Spikes: 8.22 ± 0.2, n=9). We used hyperpolarizing durations (5 s) and amplitudes that were similar to those experienced by LG during the gastric mill retraction phase. The trough of the subthreshold LG oscillations during retraction ranged from -55 mV to -65 mV across experiments (Saideman et al., 2007a,b).

LG also readily exhibited PIR bursts during CabPK application after an episode of synaptic inhibition from Int1 (n=5) (Fig. 6). To establish Int1-mediated PIR in LG, Int1 activity was suppressed via hyperpolarizing current injection and periodically released from this hyperpolarization to fire action potentials for 5 s, comparable to its active period during the gastric mill rhythm. The resulting inhibition in LG caused it to hyperpolarize by 10.2 ± 1.5 mV (n=5), comparable to its response to Int1 during gastric mill retraction (Saideman et al., 2007a,b). At the end of each inhibitory episode, LG generated a PIR burst comparable to those resulting from hyperpolarizing current injection (PIR Burst Duration: 5.3 ± 1 s; Number of Spikes: 8.2 ± 0.6, n=5; p>0.5 for both parameters).

PIR bursts are often driven at least partly by the hyperpolarization-

activated inward current (I_h) (McCormick and Bal, 1997; Sekirnjak and du Lac, 2002; Robinson and Siegelbaum, 2003; Sangrey and Jaeger, 2010; Engbers et al., 2011; Felix et al., 2011). However, I_h did not appear to contribute to the CabPK-enabled PIR bursts in LG insofar as neither hyperpolarizing current injection nor synaptic inhibition from Int1 revealed any evidence of a depolarizing sag potential during saline superfusion (n>10) or CabPK application (n=18/20) (Figs. 6,7). Similarly, there was no evidence in our voltage-clamp experiments for a sag current (n>10). However, the CabPK-activated $I_{Trans\text{-}LTS}$, with its voltage- and time-dependent properties of inactivation and deinactivation, was a candidate for the ionic current underlying PIR burst generation.

We first assessed the contribution of this CabPK-activated transient inward current to PIR in LG by simplifying the preparation with TTX (10^{-7} M) saline to silence all neurons. There was no evidence for a PIR response after LG was hyperpolarized in TTX saline either from its resting potential (-59.1 ± 1.1 mV) (n=18) or from a depolarized membrane potential (-47.4 ± 1 mV) (n=13) (Fig. 7*A*). In contrast, during CabPK (10^{-6} M) application under this condition, LG again exhibited a maintained depolarization (-48.4 ± 1.2 mV, n=18) from which it displayed PIR in response to hyperpolarizing pulses (-1 nA), albeit without associated action potentials (n=18) (Fig. 7*A*). Thus, this CabPK-mediated PIR did not require activation of TTX-sensitive I_{Na}. However, these PIR events were briefer than the PIR bursts that occurred during normal CabPK saline (2.0 ± 0.1 s, n=18; $p<0.01$), suggesting that a TTX-sensitive I_{Na} might prolong this response.

We tested the role in PIR generation played by the I_{MI}-associated depolarization in LG during CabPK application. To this end, during CabPK application in TTX saline, we injected constant amplitude hyperpolarizing current to return the LG membrane potential to its pre-CabPK resting potential. That is, we eliminated the effect of CabPK activated I_{MI}, which underlies the steady LG depolarization (see above). From that resting potential, we again injected hyperpolarizing current pulses as above. Doing so reduced the PIR amplitude to ~25% of the control amplitude (Control: V_m = -51.1 ± 2 mV, PIR Amplitude = 7.2 ± 0.4 mV; Hyperpolarized: V_m = -59.1 ± 2 mV, PIR Amplitude = 1.8 ± 0.7 mV; n=7; $p<0.01$), supporting the hypothesis that the I_{MI}-mediated depolarization in LG strengthens PIR generation mediated by activation of the transient inward current (see below).

We next assessed whether this CabPK-enabled PIR event in TTX saline was Ca^{2+}-sensitive by applying CabPK after replacing most of the Ca^{2+} (0.1X normal) in the saline with an equimolar concentration of Mn^{2+}. Under these conditions, the PIR amplitude was reversibly reduced (Pre-Control: 7.5 ± 0.7 mV; Reduced Ca^{2+}/Added Mn^{2+} saline: 0.4 ± 0.1 mV, n=6, $p<0.01$) (Fig. 7*A*). These results suggested that the CabPK-elicited PIR was mediated by activation of the CabPK-activated low threshold inward currents.

We tested the hypothesis that the CabPK-activated I_{MI} plus $I_{Trans\text{-}LTS}$ was sufficient to enable PIR in LG. To this end, in TTX saline, we injected into LG a dynamic clamp version of these two currents. This manipulation did indeed enable LG to express PIR in response to the same hyperpolarizing current

injections used in the presence of CabPK (PIR amplitude: 8.7 ± 1.5 mV; PIR duration: 4.5 ± 0.03 s, n=4) (Fig. 7*B*). Performing the same manipulation using only the DClamp version of I_{MI} or $I_{Trans\text{-}LTS}$ did not elicit PIR (n=4) (Fig. 7*B*). The absence of PIR during the latter manipulation likely resulted from the absence of a depolarized LG resting potential, which in turn limited the activation of the transient inward current after the hyperpolarizing current injection. Thus, the ability of CabPK to enable LG to generate PIR bursts apparently results from its coactivation of I_{MI}, to depolarize LG, and $I_{Trans\text{-}LTS}$, to provide the drive for the PIR burst.

CabPK-activated inward currents in the LG neuron are necessary for gastric mill rhythm generation

We tested the ability of the identified CabPK-activated inward currents in the LG neuron to enable gastric mill rhythm generation in a computational model, after which we tested the predictions of the model in the biological system. We developed a computational model of the CabPK-gastric mill rhythm generator (LG, Int1 and AB neurons) in which LG contained CabPK-activated I_{MI} plus $I_{Trans\text{-}LTS}$ (see Methods and Table 2). This model was based on one of three previously published models (PK Mechanism 1: I_{Plat}) that were focused on distinct candidate mechanisms for CabPK-mediated gastric mill rhythm generation (Kintos et al., 2008). As shown in Figure 8*A*, our model produced gastric mill rhythm-like alternating bursting in LG and Int1. The model rhythm exhibited a cycle period

(10.8 ± 2 x 10^{-4} s), LG burst duration (2.75 ± 1 x 10^{-4} s) and LG interburst duration (8.09 ± 1 x 10^{-4} s) similar to the biological CabPK-gastric mill rhythm (Cycle Period: 11.96 ± 1.1 s; LG burst duration: CabPK: 3.2 ± 0.3 s; LG interburst duration: 8.8 ± 1.1 s, n=12). Additionally, the average protraction and retraction duty cycles (DC: fraction of the cycle) were comparable (Prot. DC: model, 0.25; biol., 0.27; Ret. DC: model, 0.75; biol., 0.73). Note that, during the model rhythm, g_{MI} and $g_{Trans\text{-}LTS}$ followed the LG voltage trajectory (Fig. 8*A*), insofar as their activation was voltage-dependent. The deinactivation (h) state of $g_{Trans\text{-}LTS}$ also tracked the LG membrane potential, rising during the retractor phase when LG was rhythmically hyperpolarized by Int1 inhibition.

The model CabPK-gastric mill rhythm was also comparable to the biological rhythm in that it was suppressed by eliminating the AB inhibition of Int1 (Fig. 8*B*). In the biological system, this manipulation terminates the CabPK-gastric mill rhythm, but not the MCN1-gastric mill rhythm (Bartos et al., 1999; Saideman et al., 2007b). As discussed above, during the gastric mill rhythm each fast rhythmic depolarization (disinhibition) in LG results from the fast rhythmic AB inhibition of Int1 unmasking the depolarizing drive in LG due to CabPK-activated I_{MI} and $I_{Trans\text{-}LTS}$. When the AB inhibition of Int1 is suppressed, Int1 fires tonically (Bartos et al., 1999). Selectively silencing AB in the model CabPK-gastric mill rhythm generating circuit did cause Int1 to fire tonically and eliminated the rhythmic disinhibitions in LG that normally provide the trigger for each LG burst (Fig. 8*B*). Silencing AB also resulted in the Int1 inhibition dominating the LG membrane potential, keeping LG too hyperpolarized to

activate sufficient g_{MI} and $g_{Trans\text{-}LTS}$ (Fig. 8*B*).

Removing either I_{MI} or $I_{Trans\text{-}LTS}$ from the model LG neuron eliminated gastric mill rhythm generation, supporting the hypothesis that these currents are necessary for this process (Fig. 9*A,B*). When either the model g_{MI} or $g_{Trans\text{-}LTS}$ was removed (i.e. set to 0 nS), the pyloric-timed LG membrane potential oscillation peak amplitude was reduced, preventing LG from reaching action potential threshold and terminating the model gastric mill rhythm (Fig. 9*A,B*). The peak amplitude of these subthreshold oscillations in LG was larger after selectively removing $g_{Trans\text{-}LTS}$ (12.92 ± 3.4 mV; Fig. 9*B*) than after selectively removing g_{MI} (7.32 ± 1.6 mV; Fig. 9*A*). This result was not surprising given that with I_{MI} absent the subthreshold oscillations peaked at a membrane potential close to threshold for $I_{Trans\text{-}LTS}$ activation (Fig. 3).

We evaluated the predictions of the computational model in the biological system using dynamic clamp current injections into LG. We tested the necessity of I_{MI} and $I_{Trans\text{-}LTS}$ for CabPK-gastric mill rhythm generation by selectively nullifying each one during the CabPK-gastric mill rhythm. We performed each such manipulation by using the dynamic clamp to provide negative versions of each conductance, enabling injection of artificial I_{MI} or $I_{Trans\text{-}LTS}$ that was approximately equal in amplitude and opposite in sign to the CabPK-activated version of that same current (DeLong and Nusbaum, 2010).

As was the case during the comparable manipulations in our computational model (Fig. 9), moderate levels of negative conductance injection

(range: 50 – 200 pS) of either g_{MI} or $g_{Trans\text{-}LTS}$ caused only a modest reduction in the peak depolarization of the pyloric-timed oscillations in LG, but it was sufficient to arrest LG bursting and terminate the ongoing gastric mill rhythm for the duration of the manipulation (g_{MI}: n=7; $g_{Trans\text{-}LTS}$: n=5) (Fig. 10). In most experiments, we tested a 2-fold range of negative conductance values and found they all effectively suppressed the ongoing rhythm. These manipulations not only suppressed rhythmic bursting in LG but they eliminated the entire gastric mill rhythm. For example, the combined pyloric- and gastric mill-timed patterns of the IC and VD neurons were replaced by an exclusively pyloric rhythm-timed pattern (n=3 of 3 preparations) (Fig. 10). The gastric mill rhythm consistently resumed when the dynamic clamp injection was terminated (Fig. 10). Thus, both CabPK-activated I_{MI} and $I_{Trans\text{-}LTS}$ in the LG neuron were necessary for gastric mill rhythm generation.

CabPK-activated inward currents in the LG neuron are sufficient for gastric mill rhythm generation

To determine whether the CabPK-activated I_{MI} and $I_{Trans\text{-}LTS}$ in the LG neuron were sufficient for gastric mill rhythm generation, as was the case in the computational model, we first combined a dynamic clamp injection of $I_{Trans\text{-}LTS}$ into LG with bath-application of the muscarinic agonist oxotremorine (OXO: 10^{-5} M), an I_{MI} activator in pyloric circuit neurons (Swensen and Marder, 2000, 2001). We established via voltage clamp experiments that OXO consistently activated I_{MI} in

LG as well (n=5). In parallel current clamp experiments in which hyperpolarizing current steps were injected into LG during OXO superfusion, PIR was not elicited (n=5). The OXO-activated I_{MI} characteristics in LG were comparable to those resulting from CabPK and CCAP application (e.g. a relatively steady and small amplitude inward current at potentials more hyperpolarized than -60 mV [-0.3 ± 0.04 nA, n=5], and a similar V_m for peak amplitude [-7.6 ± 3.8 mV, n=5], although the peak amplitude was lower relative to these peptides [-1.2 ± 0.27 nA, n=5]) (DeLong et al., 2009a; this paper). OXO (10^{-5} M) superfusion consistently increased the amplitude of the subthreshold pyloric-timed oscillations in LG by 5 – 10 mV (n=10), by selectively increasing their depolarized peak V_m (Peak V_m: Control, -54.2 ± 1.7 mV; OXO, 45.8 ± 2 mV; n=10, $p<0.01$; Trough V_m: Control, -55.2 ± 1.8 mV; OXO, -55.7 ± 1.9; n=10, p=0.13), without activating LG bursting (Fig. 11*A*). This result was comparable to that occurring during CabPK applications with dynamic clamp nullification of $I_{Trans\text{-}LTS}$, when the only CabPK-activated inward current influencing the LG membrane potential was I_{MI} (Fig. 10*B*).

During OXO (10^{-5} M) superfusion, injecting $I_{dyn,Trans\text{-}LTS}$ (50 – 100 nS; peak current: 1 to 3 nA) enabled LG to generate gastric mill rhythm-like bursting (n=5) (Fig. 11*B*). This rhythmic bursting in LG exhibited characteristics that were similar to those occurring during the CabPK-gastric mill rhythm (n=12), such as its intraburst firing frequency (OXO/DClamp: 3.9 ± 0.6 Hz; CabPK: 2.7 ± 0.2 Hz, p=0.14), burst duration (OXO/DClamp: 2.3 ± 0.3 s; CabPK: 3.2 ± 0.3 s, p=0.17) and interburst duration (OXO/DClamp: 6.4 ± 0.8 s; CabPK: 8.8 ± 1.1 s, p=0.41).

These results were consistent across a 2-fold range of dynamic clamp conductances (e.g. 50 – 100 nS) within the same experiments.

In the above OXO experiments, it remained possible that rhythm generation resulted in part from additional OXO actions on other neurons (e.g. Int1, AB) necessary for gastric mill rhythm generation. Therefore, to determine whether the CabPK-activated inward currents in LG were likely to be truly sufficient to enable a gastric mill rhythm-like pattern in LG, we co-injected into the biological LG neuron dynamic clamp versions of I_{MI}, $I_{Trans\text{-}LTS}$ plus the Int1-mediated synaptic inhibition. These experiments were performed in PTX saline in order to isolate the LG neuron. These dynamic clamp co-injections consistently elicited gastric mill rhythm-like bursting in LG (n=4) (Fig. 12). The resulting cycle period (8.92 ± 1.7 s, $p>0.05$), LG burst duration (1.83 ± 0.2 s, $p>0.05$), interburst duration (7.09 ± 0.8 s, $p>0.05$), and number of spikes per burst (11.38 ± 0.9, $p>0.05$) were all similar to the above-reported values during the CabPK-gastric mill rhythm (Fig. 13). These experiments therefore supported the hypothesis that the CabPK-activated I_{MI} plus $I_{Trans\text{-}LTS}$ in the LG neuron were sufficient to enable gastric mill rhythm-equivalent alternating bursting in the core gastric mill rhythm generator neurons LG and Int1.

DISCUSSION

We have identified the cellular mechanisms underlying CabPK neuropeptide activation of a rhythmic motor pattern, thereby establishing that these mechanisms are distinct from those by which a previously studied modulatory pathway activates the same motor pattern. Specifically, bath applying CabPK or stimulating the projection neuron MCN1 configure different gastric mill circuits yet elicit the same gastric mill motor pattern (Fig. 1*B*) (Saideman et al., 2007b). Here we demonstrated that CabPK peptide-elicited gastric mill rhythm generation results from its persistent recruitment of at least two voltage-dependent inward currents (I_{MI}, $I_{Trans\text{-}LTS}$) in the rhythm generator neuron LG. These currents conjointly enable LG to rhythmically generate a PIR burst and thereby produce an alternating activity pattern with the rhythm generator neuron Int1, which they then impose on the other gastric mill motor neurons via their synaptic actions (Fig. 1*B*).

Our computational model and dynamic clamp manipulations support the hypothesis that the CabPK-elicited rhythmic LG bursting results from I_{MI} depolarizing LG closer to its spike threshold, enabling the voltage- and time-dependent properties of $I_{Trans\text{-}LTS}$ to periodically generate a PIR burst. The projection neuron MCN1 also activates the gastric mill rhythm generator via I_{MI} activation in LG (DeLong et al., 2009a). However, the MCN1-activated I_{MI} grows and decays during the gastric mill retractor and protractor phases, respectively, due to continual neuropeptide release from MCN1 during retraction and presynaptic feedback inhibition of that release during protraction. This MCN1-

mediated rhythmic buildup of I_{MI} is sufficiently strong to enable LG to periodically reach spike threshold and generate a self-terminating burst (Coleman et al., 1995; Bartos et al., 1999; DeLong et al., 2009a).

Different processes can potentially enable the same rhythmic motor pattern to be elicited by different modulatory inputs. These processes include convergent activation of the same direct input to a circuit (Viana di Prisco et al., 2000; Korn and Faber, 2005; Derjean et al., 2010), convergent modulation of the same properties in the same network neurons (Doi and Ramirez, 2010), divergent modulation in network neurons of multiple baseline intrinsic and synaptic conductances which functionally compensate for one another (MacLean et al., 2003; Prinz et al., 2004a; Goaillard et al., 2009; Grashow et al., 2010; Norris et al., 2011), or configuring different circuits by activating distinct conductances that enable different intrinsic properties in network neurons (Saideman et al., 2007b; this paper). The crab gastric mill system appears to provide the first example of the latter of these mechanisms.

Despite MCN1 and CabPK configuring different rhythm generating circuits, at their core both circuits include the reciprocally inhibitory neurons LG and Int1. These two neurons establish the protractor and retractor phases, respectively, and in each case the pivotal rhythm-generating event is LG activation, presumably because Int1 is spontaneously active (Bartos et al., 1999; Saideman et al., 2007b). However, despite these similarities and the fact that MCN1 and CabPK each recruit I_{MI}, they enable different active properties in LG. These different properties result from the distinct temporal dynamics of I_{MI} activation by

these two pathways, the likelihood that MCN1 activates more I_{MI} than CabPK (see below), and the fact that only CabPK appears to activate $I_{Trans\text{-}LTS}$ (Bartos et al., 1999; DeLong et al., 2009a; this paper).

PIR bursts often involve the complementary influence of multiple voltage-dependent inward currents, as during CabPK modulation of the LG neuron (McCormick and Bal, 1997; Sekirnjak and du Lac, 2002; Angstadt et al., 2005; Sangrey and Jaeger, 2010; Wang et al., 2010; Engbers et al., 2011; Felix et al., 2011; Zheng and Raman, 2011). One inward current that often contributes to the initial PIR depolarization is I_h (McCormick and Bal, 1997; Sekirnjak and du Lac, 2002; Robinson and Siegelbaum, 2003; Sangrey and Jaeger, 2010; Engbers et al., 2011; Felix et al., 2011). The I_h-mediated rebound depolarization facilitates activation of other voltage-dependent inward currents that elicit or strengthen the PIR burst. These latter currents often have time- and voltage-dependent properties similar to those of CabPK-activated $I_{Trans\text{-}LTS}$. In many neurons, the additional PIR-generating current is some type of I_{Ca} (McCormick and Bal, 1997; Angstadt et al., 2005; Sangrey and Jaeger, 2010; Wang et al., 2010; Engbers et al., 2011; Felix et al., 2011). The role of I_h in PIR bursts is similar to that of CabPK-activated I_{MI} in LG, which depolarizes LG after a period of inhibition and enables sufficient $I_{Trans\text{-}LTS}$ activation to generate the PIR burst. Also, similar to the CabPK comodulation of I_{MI} and $I_{Trans\text{-}LTS}$, the complementary PIR-generating currents in some other systems can be comodulated (Harris-Warrick et al., 1995; Angstadt et al., 2005; Wang et al., 2010).

MCN1- and CabPK activation of the gastric mill rhythm generator involves

both divergent actions of the same ionic current (I_{MI}) and a conserved function mediated by distinct ionic currents (I_{MI}, $I_{Trans\text{-}LTS}$) (Fig. 14). As discussed above, I_{MI} is the burst-generating conductance during MCN1-rhythm generation, whereas during CabPK-rhythm generation there is insufficient I_{MI} to directly enable LG bursting. In this latter condition, I_{MI} instead facilitates burst generation by $I_{Trans\text{-}LTS}$. The shared role of I_{MI} and $I_{Trans\text{-}LTS}$ during MCN1- and CabPK-rhythm generation, respectively, results from each current exhibiting a phase-dependent growth and decay process that is pivotal to determining the LG burst (protraction) and interburst (retraction) durations (Fig. 14) (Bartos et al., 1999; DeLong et al., 2009a; this paper). The growth and decay process for I_{MI} during MCN1 stimulation results from its synaptic regulation, as discussed above. In contrast, the availability of CabPK-activated $I_{Trans\text{-}LTS}$ grows and decays during gastric mill retraction and protraction, respectively, due to its voltage- and time-dependent properties. During retraction, when LG is hyperpolarized by rhythmic synaptic inhibition from Int1, $I_{Trans\text{-}LTS}$ exhibits a buildup of deinactivation which increases its availability, while during protraction it first enables and then limits the LG burst duration due to its depolarization- and time-dependent inactivation.

Despite these differences in the rhythm generating process, during both gastric mill rhythms the LG burst initiates during a pyloric rhythm-timed depolarization that results from AB inhibition of Int1 (Bartos et al., 1999; Saideman et al., 2007b). However, these pyloric-timed depolarizations are necessary only for CabPK-rhythm generation (Saideman et al., 2007b). This is because, when the pyloric rhythm is suppressed during MCN1 stimulation, the

MCN1-activated I_{MI} amplitude continues to grow during each prolonged retraction phase until it eventually becomes large enough to enable LG to escape from Int1 inhibition and generate a burst (Bartos et al., 1999). In contrast, CabPK-activated I_{MI} alone is insufficient to enable LG to depolarize and trigger $I_{Trans\text{-}LTS}$ activation in the presence of persistent Int1 inhibition.

The phase transitions occurring during rhythmic alternating bursting by reciprocally inhibitory neurons commonly result from the inhibited neuron either escaping from continuing inhibition ("escape" mode) or waiting until it is released from that inhibition ("release" mode) (Skinner et al., 1994; Marder and Calabrese, 1996; McCormick and Bal, 1997). Each mode can also mediate the same transition under different conditions (Bartos et al., 1999; Sorensen et al., 2004; Kristan et al., 2005). During the MCN1- and CabPK-gastric mill rhythms the protraction to retraction transition appears to occur via the release mechanism, as the LG burst self-terminates and releases Int1 from inhibition. In contrast, for reasons discussed above, during the retraction to protraction transition the CabPK-rhythm only operates via the release mode whereas the MCN1-rhythm can operate either in its normal "release" mode or, if the pyloric rhythm is very slow or suppressed, in the "escape" mode.

A neural network might have the ability to configure distinct circuits generating the same activity pattern because it needs to generate the same core behavior under different conditions. These differently configured circuits, however, might be differentially sensitive to particular inputs. This, for example, is evident for the pyloric pacemaker neuron AB influence on these two gastric mill

circuits (i.e. it is a necessary rhythm generating component only for the CabPK-gastric mill circuit). Such differential sensitivity likely also occurs in circuits that generate a consistent output pattern despite extensive, albeit compensatory, changes in the baseline intrinsic and synaptic conductances of circuit neurons (Prinz et al., 2004a; Grashow et al., 2009, 2010; Calabrese et al., 2011; Guttierrez et al., 2013). Two interesting tests of this hypothesis for the gastric mill circuit will be the influence of the gastro-pyloric receptor neuron, a muscle proprioceptor, and the peptide hormone CCAP (crustacean cardioactive peptide) on the CabPK-gastric mill rhythm. Both of these inputs regulate the MCN1-gastric mill rhythm via actions that involve MCN1, which does not participate in the CabPK-rhythm (Beenhakker et al., 2005; DeLong et al., 2009a,b).

This study highlights an alternative consequence to the well-established flexibility in neural circuit output imparted by their neuromodulatory inputs. Here, neuromodulation configures distinct circuits/mechanisms that generate a conserved output rather than generating distinct outputs. As part of this process, different modulatory pathways activate the same ionic current in the same neuron but use it in different ways, and they use different currents in the same neuron to perform the same function (Fig. 14). Whether the conserved output pattern resulting from these distinct mechanisms belies latent differences in responsiveness to the same perturbation remains to be determined.

REFERENCES

Angstadt JD, Grassmann JL, Theriault KM, Levasseur SM (2005) Mechanisms of postinhibitory rebound and its modulation by serotonin in excitatory swim motor neurons of the medicinal leech. J Comp Physiol A Neuroethol Sens Neural Behav Physiol 191:715 – 732.

Bal T, Nagy F, Moulins M (1994) Muscarinic modulation of a pattern-generating network: control of neuronal properties. J Neurosci 14:3019 – 3035.

Bartos M, Nusbaum MP (1997) Intercircuit control of motor pattern modulation by presynaptic inhibition. J Neurosci 17:2247 – 2256.

Bartos M, Manor Y, Nadim F, Marder E, Nusbaum MP (1999) Coordination of fast and slow rhythmic neuronal circuits. J Neurosci 19:6650 – 6660.

Beenhakker MP, Nusbaum MP (2004) Mechanosensory activation of a motor circuit by coactivation of two projection neurons. J Neurosci 24:6741 – 6750.

Beenhakker MP, Blitz DM, Nusbaum MP (2004) Long-lasting activation of rhythmic neuronal activity by a novel mechanosensory system in the crustacean stomatogastric nervous system. J Neurophysiol 91:78 – 91.

Beenhakker MP, DeLong ND, Saideman SR, Nadim F, Nusbaum MP (2005) Proprioceptor regulation of motor circuit activity by presynaptic inhibition of a modulatory projection neuron. J Neurosci 25:8794 – 8806.

Blitz DM, Christie AE, Coleman MJ, Norris BJ, Marder E, Nusbaum MP (1999) Different proctolin neurons elicit distinct motor patterns from a multifunctional neuronal network. J Neurosci 19:5449 – 5463.

Blitz DM, Beenhakker MP, Nusbaum MP (2004) Different sensory systems share projection neurons but elicit distinct motor patterns. J Neurosci 24:11381 – 11390.

Briggman KL, Kristan WB (2008) Multifunctional pattern-generating circuits. Annu Rev Neurosci 31:271 – 294.

Bucher D, Prinz AA, Marder E (2005) Animal-to-animal variability in motor pattern production in adults and during growth. J Neurosci 25:1611 – 1619.

Calabrese RL, Norris BJ, Wenning A, Wright TM (2011) Coping with variability in small neuronal networks. Integr Comp Biol 51:845 – 855.

Coleman MJ, Nusbaum MP (1994) Functional consequences of compartmentalization of synaptic input. J Neurosci 14:6544 – 6552.

Coleman MJ, Meyrand P, Nusbaum MP (1995) Presynaptic inhibition mediates a switch between two modes of synaptic transmission. Nature 378:502 – 505.

DeLong ND, Kirby MS, Blitz DM, Nusbaum MP (2009a) Parallel regulation of a modulator-activated current via distinct dynamics underlies comodulation of motor circuit output. J Neurosci 29:12355 – 12367.

DeLong ND, Beenhakker MP, Nusbaum MP (2009b) Presynaptic inhibition selectively weakens peptidergic cotransmission in a small motor system. J Neurophysiol 102:3492 – 3504.

DeLong ND, Nusbaum MP (2010) Hormonal modulation of sensorimotor integration. J Neurosci 30:2418 – 2427.

Derjean D, Moussaddy A, Atallah E, St-Pierre M, Auclair F, Chang S, Ren X, Zielinski B, Dubuc R (2010) A novel neural substrate for the transformation of olfactory inputs into motor output. PLoS Biol 8:e1000567.

Diehl F, White RS, Stein W, Nusbaum MP (2013) Motor circuit-specific burst patterns drive different muscle and movement patterns. J Neurosci 33: 12013 – 12029.

Doi A, Ramirez JM (2008) Neuromodulation and the orchestration of the respiratory rhythm. Respir Physiol Neurobiol 164:96 – 104.

Doi A, Ramirez JM (2010) State-dependent interactions between excitatory neuromodulators in the neuronal control of breathing. J Neurosci 30:8251 – 8262.

Engbers JD, Anderson D, Tadayonnejad R, Mehaffey WH, Molineux ML, Turner RW (2011) Distinct roles for I(T) and I(H) in controlling the frequency and timing of rebound spike responses. J Physiol 589:5391 – 5413.

Felix RA 2nd, Fridberger A, Leijon S, Berrebi AS, Magnusson AK (2011) Sound rhythms are encoded by postinhibitory rebound spiking in the superior paraolivary nucleus. J Neurosci 31:12566 – 12578.

Goaillard JM, Taylor AL, Schulz DJ, Marder E (2009) Functional consequences of animal-to-animal variation in circuit parameters. Nat Neurosci 12:1424 – 1430.

Golowasch J, Marder E (1992) Proctolin activates an inward current whose voltage dependence is modified by extracellular Ca^{2+}. J Neurosci 12:810 – 817.

Grashow R, Brookings T, Marder E (2009) Reliable neuromodulation from circuits with variable underlying structure. Proc Natl Acad Sci USA 106:11742 – 11746.

Grashow R, Brookings T, Marder E (2010) Compensation for variable intrinsic neuronal excitability by circuit-synaptic interactions. J Neurosci 30:9145 – 9156.

Gutierrez GJ, O'Leary T, Marder E (2013) Multiple mechanisms switch an electrically coupled, synaptically inhibited neuron between competing rhythmic oscillators. Neuron 77:845 – 858.

Harris-Warrick RM (2011) Neuromodulation and flexibility in central pattern generator networks. Curr Opin Neurobiol 21:685 – 692.

Harris-Warrick RM, Coniglio LM, Levini RM, Gueron S, Guckenheimer J (1995) Dopamine modulation of two subthreshold currents produces phase shifts in activity of an identified motoneuron. J Neurophysiol 74:1404 – 1420.

Kadiri LR, Kwan AC, Webb WW, Harris-Warrick RM (2011) Dopamine-induced oscillations of the pyloric pacemaker neuron rely on release of calcium from intracellular stores. J Neurophysiol 106:1288 – 1298.

Kintos N, Nusbaum MP, Nadim F (2008) A modeling comparison of projection neuron- and neuromodulator-elicited oscillations in a central pattern generating network. J Comput Neurosci 24:374 – 397.

Kirby MS, Nusbaum MP (2007) Peptide hormone modulation of a neuronally modulated motor circuit. J Neurophysiol 98: 3206 – 3220.

Korn H, Faber DS (2005) The Mauthner cell half a century later: a neurobiological model for decision-making? Neuron 47:13 – 28.

Kristan WB Jr, Calabrese RL, Friesen WO (2005) Neuronal control of leech behavior. Prog Neurobiol 76:279 – 327.

Li WC, Moult PR (2012) The control of locomotor frequency by excitation and inhibition. J Neurosci 32:6220 – 6230.

MacLean JN, Zhang Y, Johnson BR, Harris-Warrick RM (2003) Activity-independent homeostasis in rhythmically active neurons. Neuron 37:109 – 120.

Marder E (2012) Neuromodulation of neuronal circuits: back to the future. Neuron 76:1 – 11.

Marder E, Bucher D (2001) Central pattern generators and the control of rhythmic movements. Curr Biol 11: R986 – R996.

Marder E, Bucher D (2007) Understanding circuit dynamics using the stomatogastric nervous system of lobsters and crabs. Annu Rev Physiol 69:291 – 316.

Marder E, Calabrese RL (1996) Principles of rhythmic motor pattern generation. Physiol Rev 76:687 – 717.

Marder E, Eisen JS (1984) Transmitter identification of pyloric neurons: electrically coupled neurons use different transmitters. J Neurophysiol

51:1345 – 1361.

Marder E, Bucher D, Schulz DJ, Taylor AL (2005) Invertebrate central pattern generation moves along. Curr Biol 15:R685 – R699.

McCormick DA, Bal T (1997) Sleep and arousal: thalamocortical mechanisms. Annu Rev Neurosci 20:185 – 215.

Nadim F, Manor Y, Nusbaum MP, Marder E (1998) Frequency regulation of a slow rhythm by a fast periodic input. J Neurosci 18:5053 – 5067.

Norris BJ, Coleman MJ, Nusbaum MP (1994) Recruitment of a projection neuron determines gastric mill motor pattern selection in the stomatogastric nervous system of the crab, *Cancer borealis*. J Neurophys 72:1451 – 1463.

Norris BJ, Wenning A, Wright TM, Calabrese RL (2011) Constancy and variability in the output of a central pattern generator. J Neurosci 31:4663 – 4674.

Nusbaum MP, Marder E (1989a) A modulatory proctolin-containing neuron (MPN). I. Identification and characterization. J Neurosci 9:1591 – 1599.

Nusbaum MP, Marder E (1989b) A modulatory proctolin-containing neuron (MPN). II. State-dependent modulation of rhythmic motor activity. J Neurosci 9:1600 – 1607.

Nusbaum MP, Beenhakker MP (2002) A small systems approach to motor pattern generation. Nature 417:343 – 350.

Pirtle TJ, Willingham K, Satterlie RA (2010) A hyperpolarization-activated inward current alters swim frequency of the pteropod mollusk *Clione limacina*. Comp Biochem Physiol A Mol Integr Physiol 157:319 – 327.

Prinz AA, Abbott LF, Marder E (2004b) The dynamic clamp comes of age. Trends Neurosci 27:218 – 224.

Prinz AA, Bucher D, Marder E (2004a) Similar network activity from disparate circuit parameters. Nat Neurosci 7:1345 – 1352.

Ransdell JL, Temporal S, West NL, Leyrer ML, Schulz DJ (2013) Characterization of inward currents and channels underlying burst activity in motoneurons of crab cardiac ganglion. J Neurophysiol 110:42 – 54.

Rauscent A, Einum J, Le Ray D, Simmers J, Combes D (2009) Opposing aminergic modulation of distinct spinal locomotor circuits and their functional coupling during amphibian metamorphosis. J Neurosci 29:1163 – 1174.

Roberts A, Li WC, Soffe SR (2008) Roles for inhibition: studies on networks controlling swimming in young frog tadpoles. J Comp Physiol A Neuroethol Sens Neural Behav Physiol 194:185 – 193.

Saideman SR, Ma M, Kutz-Naber KK, Cook A, Torfs P, Schoofs L, Li L,

Nusbaum MP (2007a) Modulation of rhythmic motor activity by pyrokinin peptides. J Neurophysiol 97:579 – 595.

Saideman SR, Blitz DM, Nusbaum MP (2007b) Convergent motor patterns from divergent circuits. J Neurosci 27:6664 – 6674.

Sangrey T, Jaeger D (2010) Analysis of distinct short and prolonged components in rebound spiking of deep cerebellar nucleus neurons. Eur J Neurosci 32:1646 – 1657.

Satterlie RA (1985) Reciprocal inhibition and postinhibitory rebound produce reverberation in a locomotor pattern generator. Science 229:402 – 404.

Sekirnjak C, du Lac S (2002) Intrinsic firing dynamics of vestibular nucleus neurons. J Neurosci 22:2083 – 2095.

Sorensen M, DeWeerth S, Cymbalyuk G, Calabrese RL (2004) Using a hybrid neural system to reveal regulation of neuronal network activity by an intrinsic current. J Neurosci 24:5427 – 5438.

Sharp AA, O'Neil MB, Abbott LF, Marder E (1993) The dynamic clamp: artificial conductances in biological neurons. Trends Neurosci 16:389 – 394.

Skinner FK, Kopell N, Marder E (1994) Mechanisms for oscillation and frequency control in reciprocally inhibitory model neural networks. J Comput Neurosci 1:69 – 87.

Stein W (2009) Modulation of stomatogastric rhythms. J Comp Physiol A 195: 989 – 1009.

Viana di Prisco G, Pearlstein E, Le Ray D, Robitaille R, Dubuc R (2000) A cellular mechanism for the transformation of a sensory input into a motor command. J Neurosci 20:8169 – 8176.

Wang D, Grillner S, Wallén P (2011) 5-HT and dopamine modulates CaV1.3 calcium channels involved in postinhibitory rebound in the spinal network for locomotion in lamprey. J Neurophysiol 105:1212 – 1224.

Weimann JM, Meyrand P, Marder E (1991) Neurons that form multiple pattern generators: identification and multiple activity patterns of gastric/pyloric neurons in the crab stomatogastric system. J Neurophysiol 65:111 – 122.

Wood DE, Manor Y, Nadim F, Nusbaum MP (2004) Intercircuit control via rhythmic regulation of projection neuron activity. J Neurosci 24:7455 – 7463.

Zhang B, Harris-Warrick RM (1995) Calcium-dependent plateau potentials in a crab stomatogastric ganglion motor neuron. I. Calcium current and its modulation by serotonin. J Neurophysiol 74:1929 – 1937.

Zheng N, Raman IM (2011) Prolonged postinhibitory rebound firing in the

cerebellar nuclei mediated by group I metabotropic glutamate receptor potentiation of L-type calcium currents. J Neurosci 31:10283 – 10292.

Table 1: Dynamic Clamp Conductances

Neuron	**Conductances**		**$V_{1/2}$ [mV]**	**k [mV]**	**t_{lo} [ms]**	**t_{hi} [ms]**	**exp (p,q,r)**	**E_{rev}**	**G_{max}**
LG (Biological)	$I_{Trans-LTS}$	*m*	-50	-3	500	500	1	10	0.6
		h	-58	0.8	3500	1500	1		
	I_{MI}	*m*	-50	-5	5	5	1	10	0.1
Int1 (Model)	Na_v	*m*	-42	-5	1.5	0.45	3	45	7.5
		h	-52	9.2	10	2.4	1		
	K_V	*m*	-26	-9	27	3	4	-70	30
		h	-16	1.5	20	200	2		
	Leak							-60	0.012
Int1 -> LG	Synapse	*m*	-40	-1	200	200	1	-80	2
LG -> Int1	Synapse	*m*	-30	-0.1	200	200	1	-80	15

Table 2: CabPK Gastric Mill Network Model Parameters

Neuron	**Conductances**		**$V_{1/2}$ [mV]**	**k [mV]**	**t_{lo} [ms]**	**t_{hi} [ms]**	**exp (p,q,r)**	**E_{rev}**	**G_{max}**
LG	$I_{Trans-LTS}$	*m*	-55	-3	500	500	1		
		h	-63	0.8	3500	1500	1		
	I_{MI}	*m*	-60	-5	5	5	1		
Int1	Na_v	*m*	-42	-5	1.5	0.45	3	45	7.5
		h	-52	9.2	10	2.4	1		
	K_V	*m*	-26	-9	27	3	4	-70	30
		h	-16	1.5	20	200	2		
	Leak							-60	0.012
Int1 -> LG	Synapse	*m*	-40	-1	200	200	1	-80	2
LG -> Int1	Synapse	*m*	-30	-0.1	200	200	1	-80	15

FIGURES

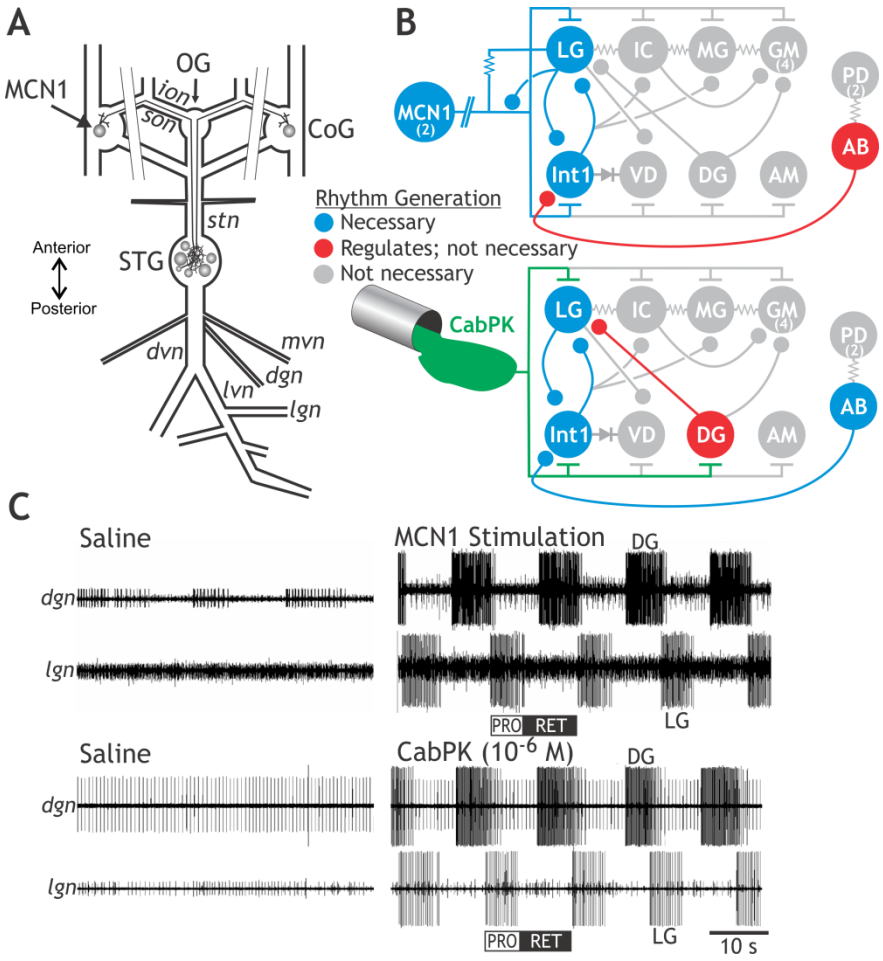

Figure 1. The projection neuron MCN1 and bath-applied CabPK peptide configure different gastric mill circuits but elicit the same gastric mill motor pattern. ***A,*** Schematic of the isolated stomatogastric nervous system (STNS), including its four ganglia (paired CoGs, OG, STG) plus their connecting nerves and a subset of the peripheral nerves. Paired parallel lines crossing the *sons* and *ions* represent their bisection, which occurred at the start of each experiment to separate the STG from the CoGs. Ganglia: CoG, commissural ganglion; OG,

oesophageal ganglion; STG, stomatogastric ganglion. Nerves: *dgn*, dorsal gastric nerve; *dvn*, dorsal ventricular nerve; *ion*, inferior oesophageal nerve; *lgn*, lateral gastric nerve; *lvn*, lateral ventricular nerve; *mvn*, medial ventricular nerve; *son*, superior oesophageal nerve; *stn,* stomatogastric nerve. Neuron: MCN1, modulatory commissural neuron 1. ***B,*** Schematic of the gastric mill circuit configured by (top) MCN1 stimulation and (bottom) CabPK peptide superfusion. Synapse symbols: t-bars, excitation; filled circles, inhibition; resistors, non-rectifying electrical coupling; diode, rectifying electrical coupling. Parallel lines crossing the MCN1 axon represent additional distance between the MCN1 soma in each CoG and its axon terminals in the STG. Numbers in parentheses indicate the copy number per STNS for each neuron type when it is present as more than 1 copy. Modified from: Saideman et al. (2007b). ***C,*** MCN1 stimulation and CabPK bath application elicit the same gastric mill motor pattern. These two manipulations were performed in different preparations. From: Saideman et al. (2007b).

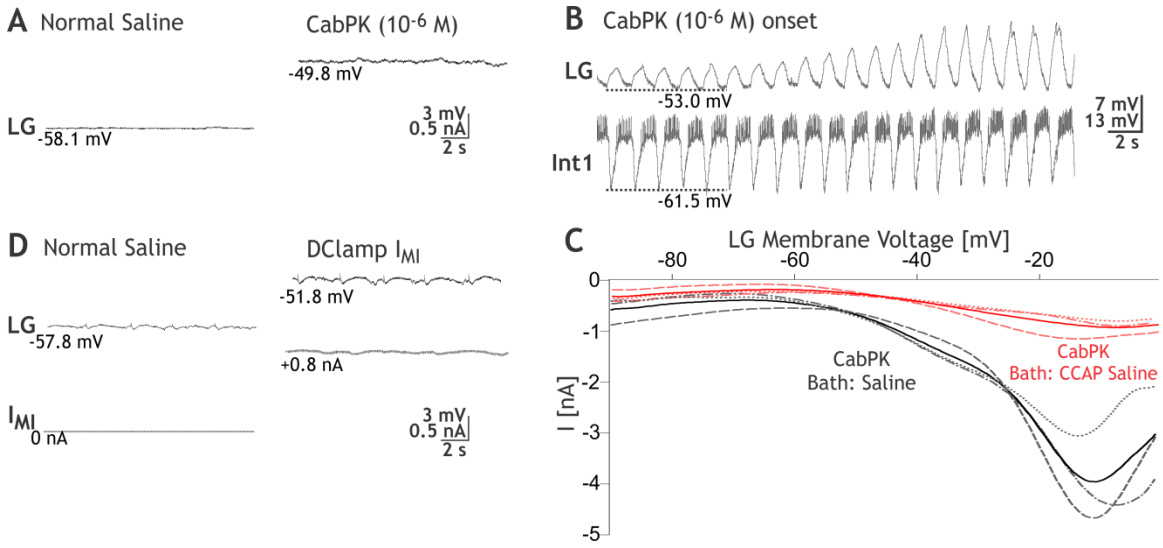

Figure 2. Bath applied CabPK peptide elicits a sustained, subthreshold depolarization in the isolated LG neuron by activating the voltage-dependent, modulator-activated inward current (I_{MI}). ***A,*** With Int1 activity suppressed by hyperpolarizing current injection, bath applied CabPK elicited a sustained, subthreshold depolarization in the LG neuron. ***B,*** With Int1 exhibiting its normal pyloric-timed burst pattern and thereby providing rhythmic inhibition to LG, bath applied CabPK initially caused a gradual increase in the amplitude of the subthreshold, pyloric-timed oscillations in LG. Note that the oscillation peaks became more depolarized, while the membrane potential of the trough was not changed. CabPK superfusion was begun immediately prior to the start of this trace. Subsequently, the gastric mill rhythm commenced. ***C,*** I-V plots of CabPK-influenced current in LG, obtained using TEVC and a voltage ramp protocol, during focal pressure application (5 psi, 1 s) of CabPK (10^{-4} M) under control conditions (black) and during CCAP (10^{-6} M) bath application (red). Each curve

represents the difference current (CabPK minus control or CCAP condition) as indicated. Solid curves represent the mean values for each condition; broken lines represent 3 individual experiments. ***D,*** Injection of artificial I_{MI} (g_{MI} = 100 nS) into LG, via the dynamic clamp, in a preparation where Int1 activity was weak (<5 Hz) caused a sustained depolarization comparable to that resulting from CabPK application.

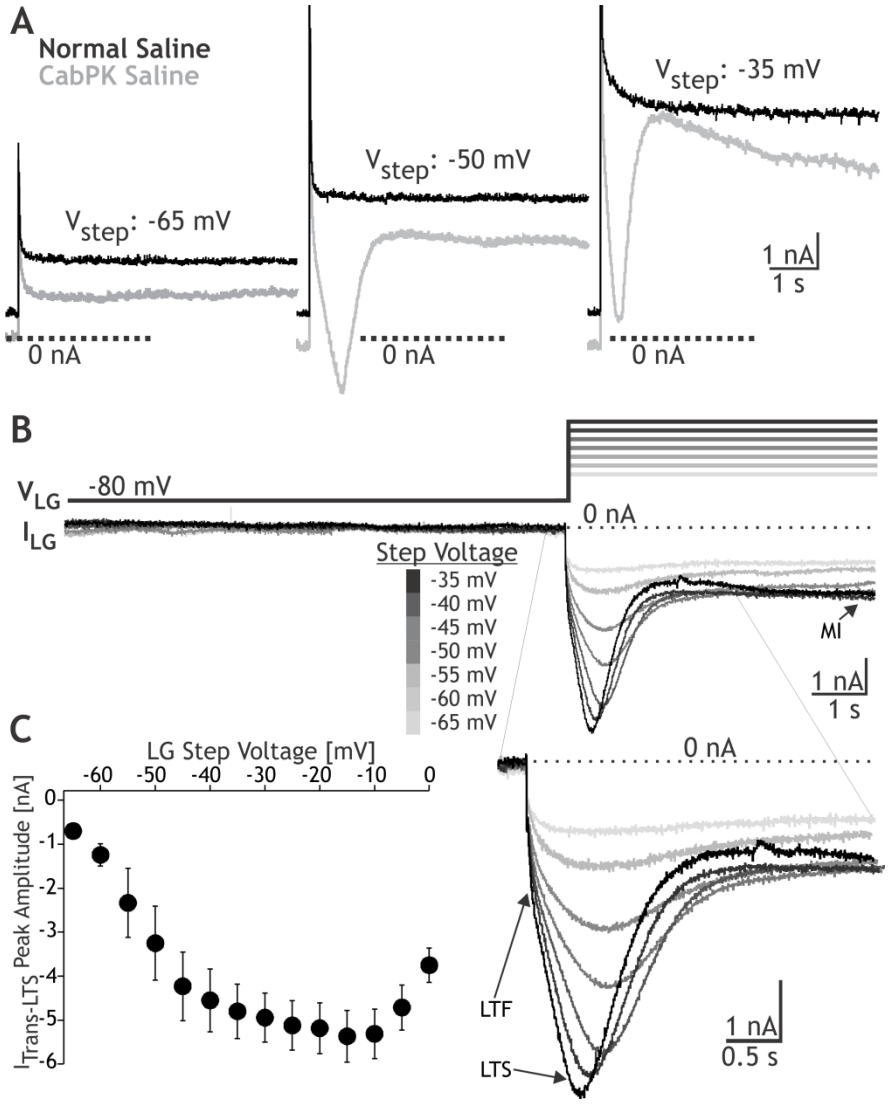

Figure 3. CabPK application influences both transient and sustained voltage-dependent inward currents in the LG neuron. ***A***, Example raw current traces recorded during TEVC using a voltage step protocol (V_{hold} = -80 mV) to the indicated step potentials, during superfusion with voltage clamp saline under control and CabPK conditions (see Methods). Note that, during the two more depolarized steps (-50 mV, -35 mV) in the presence of CabPK, there was a

relatively large amplitude transient inward current, while during all three steps there was a reduction in the amplitude of the sustained outward current relative to the control condition. ***B,*** (top) CabPK-influenced currents (CabPK condition minus control condition) resulting from a voltage step protocol during TEVC included a low threshold, fast transient current ($I_{Trans\text{-}LTF}$), low threshold, slow transient current ($I_{Trans\text{-}LTS}$) and sustained current (I_{MI}). $I_{Trans\text{-}LTS}$ was responsible for the transient current, while I_{MI} was predominantly responsible for the reduced outward current in Panel A. $I_{Trans\text{-}LTF}$ did not exhibit a distinct, separate peak in this experiment (see Figs. 4*A*, 5*A*), but is evident as an initial steep inward slope prior to the shallower rising slope representing $I_{Trans\text{-}LTS}$. Entire voltage step protocol (hold at -80 mV: 10s; step to test voltage: 6s) is shown. (bottom) Expansion of the current traces to highlight the events occurring during each voltage step. ***C,*** I-V plot of the current (mean ± SE) at the peak of $I_{Trans\text{-}LTS}$ for the step protocol used in experiments such as that in Panel B (n=9).

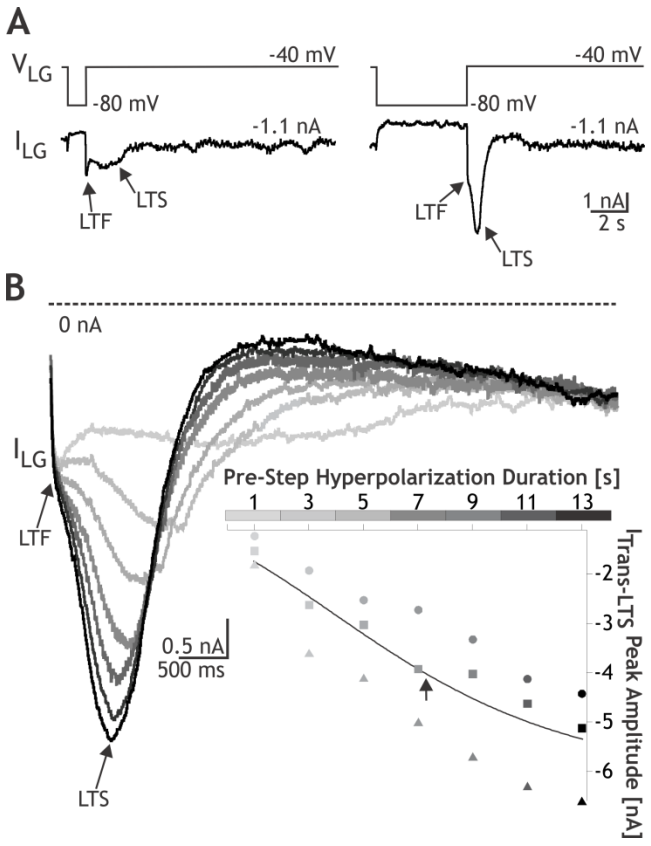

Figure 4. CabPK-activated $I_{Trans-LTS}$ in the LG neuron exhibits a time-dependent deinactivation. ***A,*** Using TEVC, hyperpolarizing voltage steps to -80 mV were injected into LG for relatively (left) brief and (right) long durations, and then returned to -40 mV. A larger peak $I_{Trans-LTS}$ amplitude resulted upon the return to -40 mV after the longer duration hyperpolarization. In contrast, there was little change in the peak amplitude of $I_{Trans-LTF}$ for both step durations. ***B,*** Superimposed series of current responses in LG, aligned to the return to -40 mV after hyperpolarizing steps of different durations to -80 mV (see the gray scale, representing the different step durations, aligned with the x-axis of the inset scatter plot). Inset: Plot of $I_{Trans-LTS}$ peak amplitude as a function of

hyperpolarizing step duration from 3 experiments. Each symbol represents a different experiment. The line represents the sigmoid fit to the data (Igor Pro), and the arrow represents the calculated midpoint.

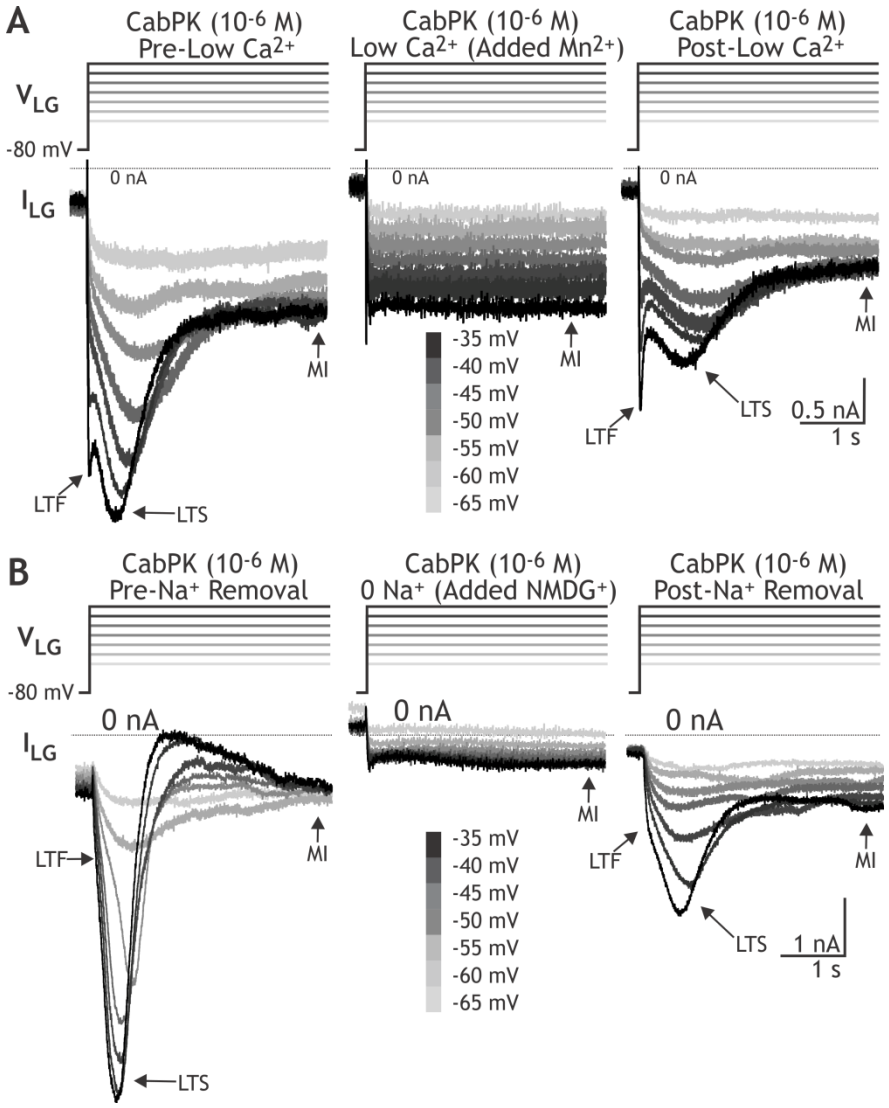

Figure 5. CabPK-activated $I_{Trans\text{-}LTS}$ is sensitive to changes in extracellular Ca^{2+} and extracellular Na^{+}. ***A,*** Superimposed sweeps of current recordings from LG, recorded in TEVC with TEACl/CsCl-filled electrodes, during depolarizing steps to different membrane potentials (-65 mV to -35 mV) from a holding voltage of -80 mV, during CabPK application in control-, reduced Ca^{2+} (0.1X normal)- and post-reduced Ca^{2+} solutions. Note that in the reduced Ca^{2+} condition $I_{Trans\text{-}LTS}$ is not evident, nor is $I_{Trans\text{-}LTF}$. ***B,*** Same protocol as in panel A, except that in the experimental condition (middle trace) extracellular Na^{+} was

replaced with an equimolar concentration of $NMDG^+$. Note the absence of $I_{Trans-LTS}$ in the presence of $NMDG^+$.

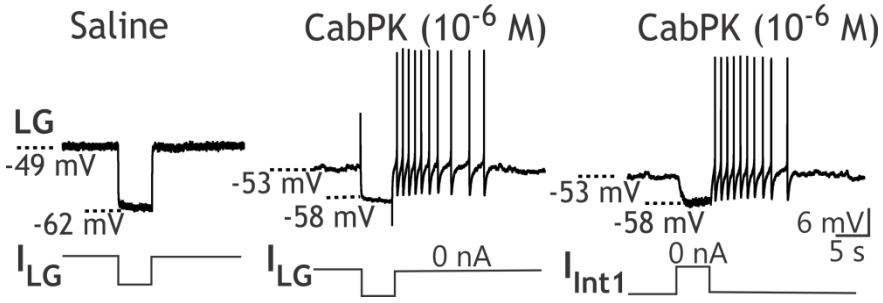

Figure 6. CabPK enables the LG neuron to generate post-inhibitory rebound (PIR) bursts. (Left) During saline superfusion, the LG neuron membrane potential was held depolarized by constant depolarizing current injection, during which it was hyperpolarized for 5 s by current injection (-1 nA). After the hyperpolarization, the LG membrane potential returned directly to its original, depolarized baseline. (Middle) In the same LG recording, during CabPK superfusion, a hyperpolarizing current injection (amplitude: -1 nA, duration: 5 s) from the CabPK-mediated depolarized baseline was followed by a PIR burst (duration: 8.5 s). Note that the last two spikes were excluded from the PIR duration due to their large interspike intervals. (Right) In the same preparation, during CabPK application, Int1 activity was suppressed by constant hyperpolarizing current injection and then released from hyperpolarization to fire action potentials for 5 s. This Int1 activity inhibited LG, causing a hyperpolarization comparable to that in the middle trace. When Int1 activity was again suppressed, LG generated a PIR burst (duration: 8.9 s). The last spike was excluded from the PIR burst duration due to the large interspike interval.

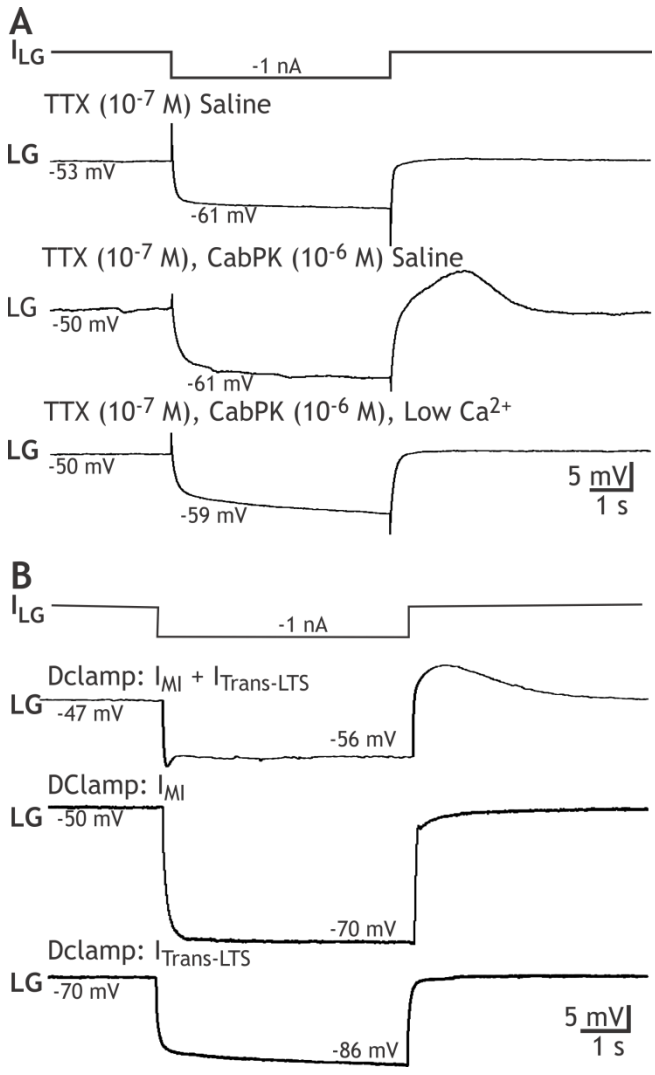

Figure 7. PIR in the LG neuron persists in the presence of TTX during either CabPK application or dynamic clamp co-injection of artificial I_M plus $I_{Trans-LTS}$. ***A,*** (top) In the presence of TTX saline, a 5 s hyperpolarization in LG from a depolarized baseline was followed by a direct return to the depolarized baseline. (middle) During CabPK superfusion in TTX saline, a comparable 5 s

hyperpolarization in LG was followed by PIR, albeit without action potentials. Here, the depolarized baseline resulted from the influence of CabPK. (bottom) CabPK superfusion in TTX saline containing 0.1 X normal Ca^{2+}, substituted with equimolar Mn^{2+}, did not enable PIR after the same hyperpolarizing step as above. All recordings were from the same LG neuron. ***B,*** (top) Dynamic clamp injection of artificial I_{MI} (g_{MI}: 80 nS) plus $I_{Trans\text{-}LTS}$ ($g_{Trans\text{-}LTS}$: 100 nS) in TTX saline enabled PIR in LG after a hyperpolarizing step. The initial dip in the LG membrane potential occurred in all (n=4) of these responses to hyperpolarizing current injection during the dynamic clamp co-injections but not during the individual injections (e.g. see below). (middle, bottom) In contrast, separate dynamic clamp injection of (middle) I_{MI} or (bottom) $I_{Trans\text{-}LTS}$ in TTX saline did not enable PIR in LG. Note that, in the bottom recording without artificial I_{MI}, the LG resting potential is not depolarized.

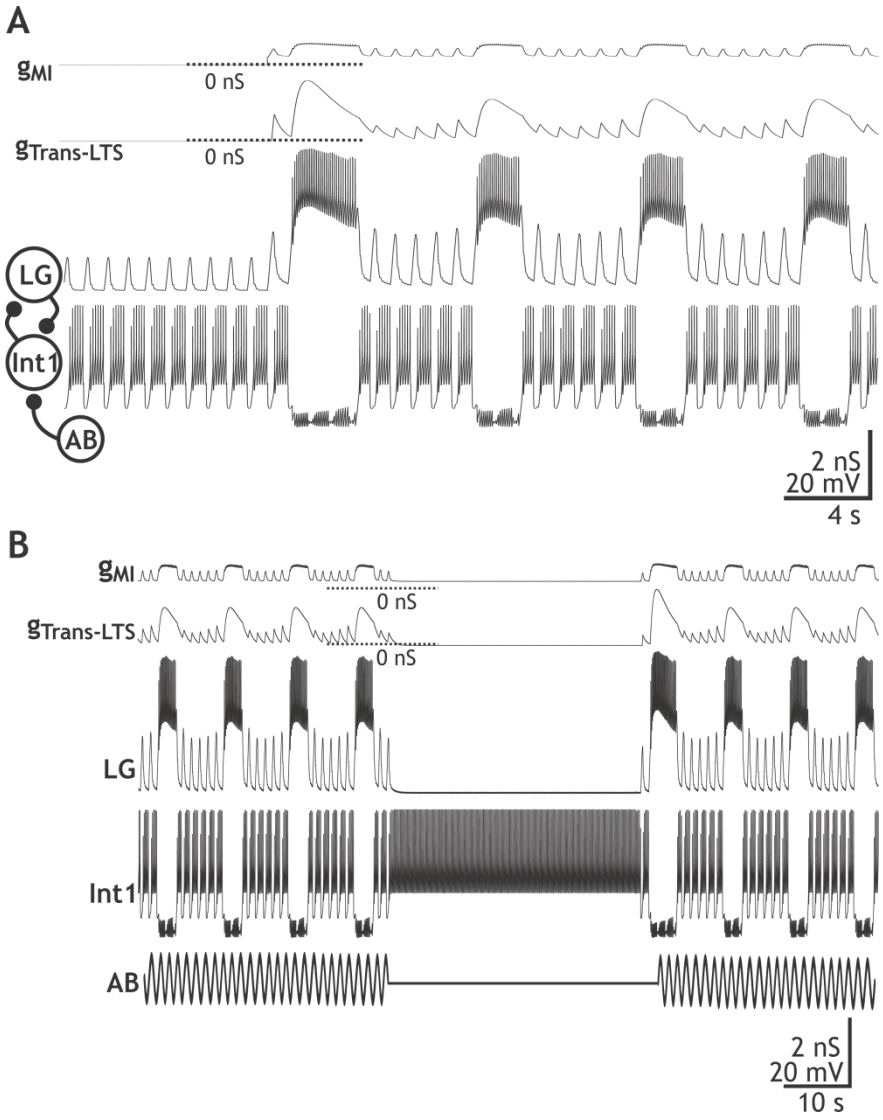

Figure 8. CabPK-like gastric mill rhythm generation output from a computational model that includes models of the LG, Int1 and AB neurons. ***A,*** Output of the computational model showing the rhythmic alternating bursting in LG and Int1 that commences upon activating the CabPK-activated conductances ($g_{Trans\text{-}LTS}$; g_{MI}). The AB neuron influence is evident in the fast

rhythmic Int1 hyperpolarizations and the associated subthreshold depolarizations (removal of Int1 inhibition) in LG. Note that the CabPK-activated conductances all track the membrane potential changes in LG, while $g_{Trans\text{-}LTS}$ also exhibits time-dependent processes, including inactivation during the LG burst and an increasing level of activation (due to deinactivation) during the LG interburst. Most hyperpolarized membrane potentials: Int1, -60.5 mV; LG, -58.4 mV. Synaptic symbol: filled circle, inhibition. ***B,*** Suppressing the AB inhibition of Int1 terminates the ongoing gastric mill rhythm in the computational model of the CabPK-gastric mill rhythm generator, as occurs in the biological system (Bartos et al., 1999). When the AB activity was temporarily terminated (horizontal line, middle of the AB trace), Int1 activity changed from a fast rhythmic pattern to tonic firing, while the LG membrane potential exhibited a steady hyperpolarized potential. Note that, due to the hyperpolarized LG membrane potential, $g_{Trans\text{-}LTS}$ was at 0 nS while g_{MI} was maintained at a reduced level. Most hyperpolarized membrane potentials: Int1, -47.7 mV; LG, -58.4 mV.

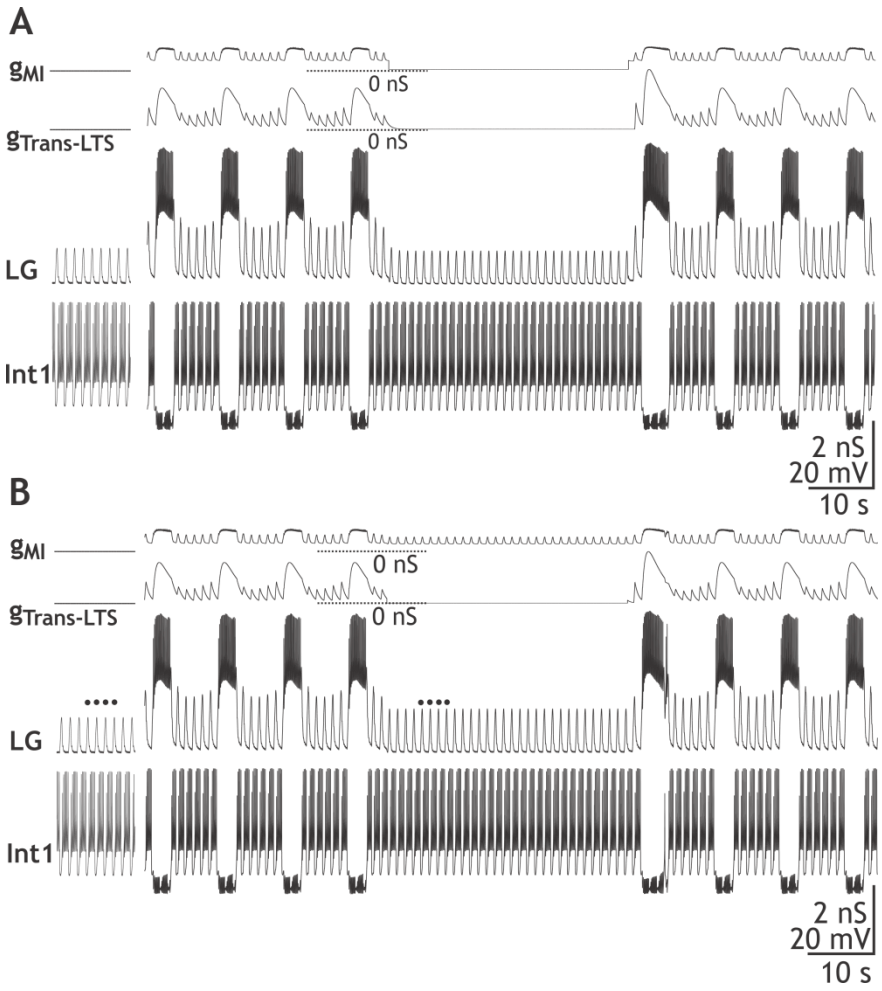

Figure 9. Selective elimination of either g_{MI} or $g_{Trans\text{-}LTS}$ is sufficient to suppress the gastric mill rhythm in a computational model of the CabPK-gastric mill rhythm generator. ***A,*** Eliminating g_{MI} in the middle of an episode of the model CabPK-gastric mill rhythm terminated that rhythm, until g_{MI} was reinstated. Note that, when g_{MI} was eliminated, $g_{Trans\text{-}LTS}$ was also reduced to nearly 0 nS due to the less depolarized peak of the subthreshold oscillations in LG. ***B,*** Eliminating $g_{Trans\text{-}LTS}$ terminated the ongoing model gastric mill rhythm until this conductance was re-activated. It did not, however, eliminate g_{MI}. As a

result, the peaks of the subthreshold oscillations remained larger than prior to the onset of the CabPK influence (black dots). However, g_{MI} alone was not sufficient to enable LG to fire a burst.

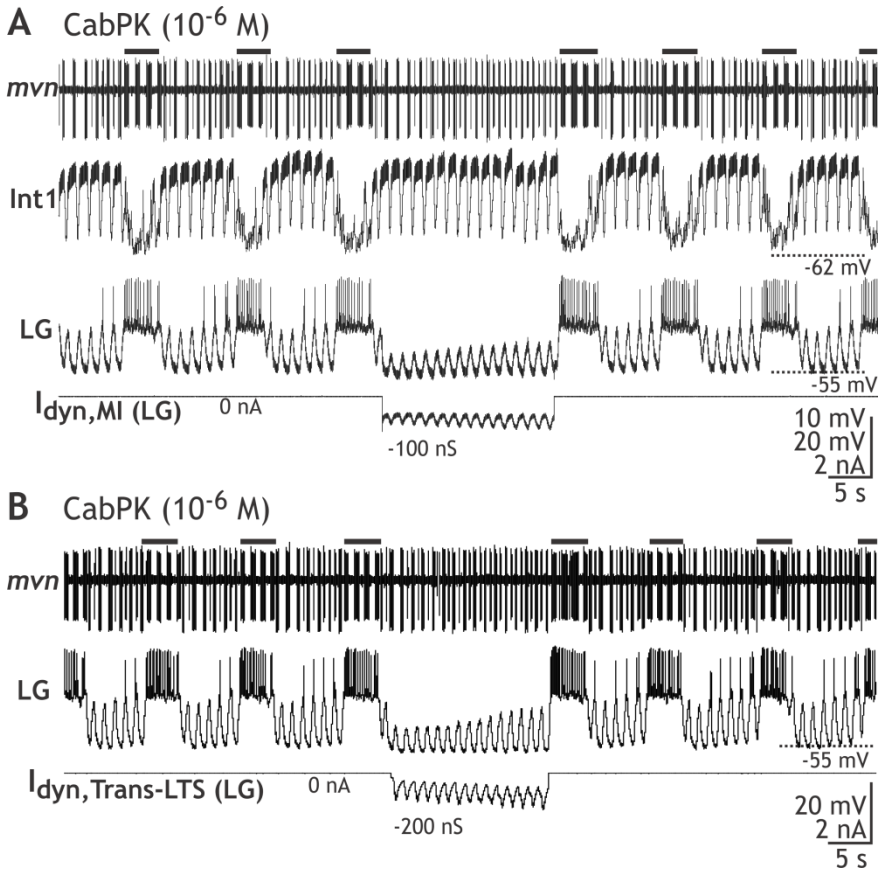

Figure 10. Selectively nullifying CabPK-activated g_{MI} or $g_{Trans\text{-}LTS}$ via dynamic clamp injection of a negative version of that conductance suppressed an ongoing CabPK-gastric mill rhythm. ***A,B:*** Injecting into LG a negative version of (A) g_{MI} [$I_{dyn,MI\ (LG)}$] or (B) $g_{Trans\text{-}LTS}$ [$I_{Trans\text{-}LTS\ (LG)}$] reduced the amplitude of the LG subthreshold oscillations and prevented its bursting. During this time, Int1 activity remained pyloric-timed, while the IC (*mvn*: small unit) and VD (*mvn*: large unit) neuron activity switched from exhibiting gastric mill- and pyloric-timed bursting to exclusively pyloric-timed activity. Black bars: gastric mill protraction phase-timed IC neuron bursting. Both panels are from the same preparation.

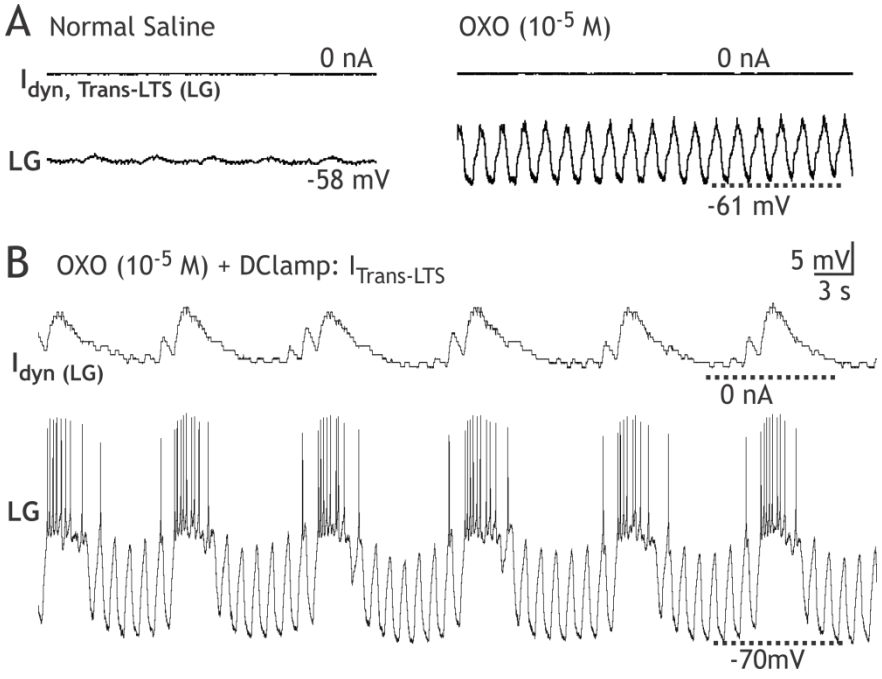

Figure 11. Gastric mill rhythm-equivalent bursting in the LG neuron during application of the I_{MI} activator OXO plus dynamic clamp injection of $I_{Trans-LTS}$. ***A,*** (left) During saline superfusion and no dynamic clamp injection, the LG neuron membrane potential exhibited small amplitude pyloric-timed oscillations. (right) OXO application increased the amplitude of these oscillations, but they remained subthreshold. These subthreshold oscillations exhibited a more depolarized peak, presumably due to OXO-activated I_{MI}, and a more hyperpolarized trough, presumably due to OXO excitation of Int1 (Norris et al., 1994). The oscillation frequency also increased, because OXO also excites the pyloric CPG (Bal et al., 1994). ***B,*** Dynamic clamp injection of $I_{Trans-LTS}$ ($g_{Trans-LTS}$: 100 nS) during OXO superfusion elicited gastric mill-equivalent bursting in the LG neuron.

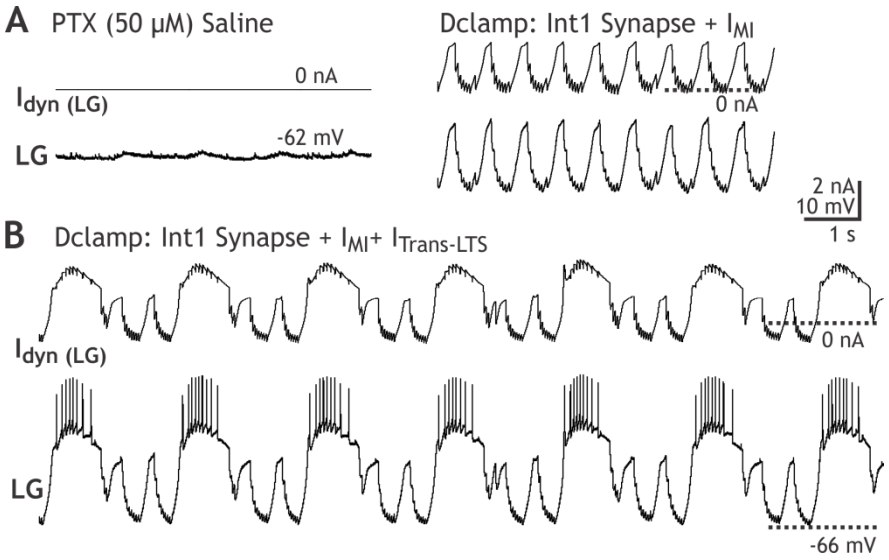

Figure 12. Dynamic clamp injection of all CabPK-gastric mill rhythm generator conductances into the LG neuron elicits gastric mill rhythm-like bursting in LG. ***A,*** (left) In PTX saline with no dynamic clamp injection, LG maintained a steady resting potential of -62 mV. (right) Dynamic clamp co-injection of the inhibitory synapse from Int1 (200 nS) plus CabPK-activated I_{MI} (80 nS) in PTX saline elicited subthreshold, pyloric rhythm-like oscillations in LG. ***B***, Dynamic clamp co-injection into LG of the rhythmic inhibitory synapse from Int1 (200 nS), CabPK-activated I_{MI} (80 nS) plus CabPK-activated $I_{Trans-LTS}$ (100 nS) in PTX saline elicited gastric mill rhythm-like bursting in LG.

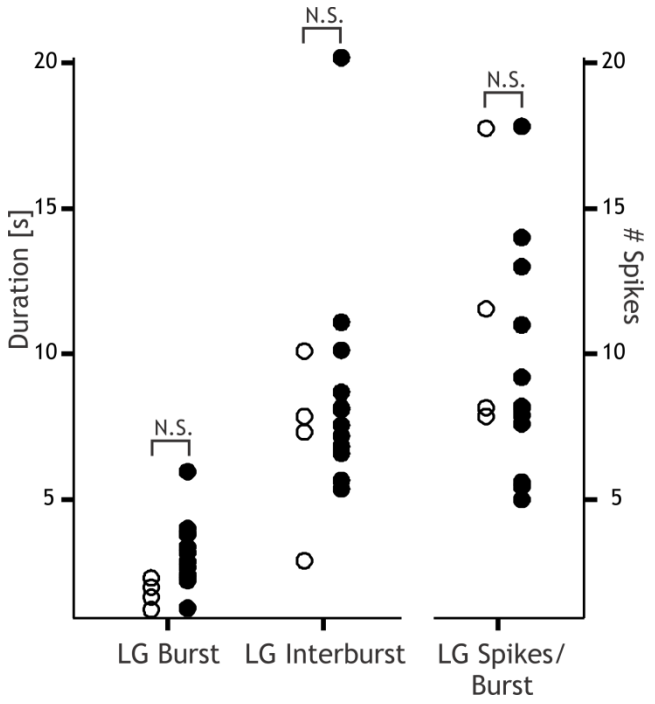

Figure 13. The range of the gastric mill rhythm-related parameters in LG are comparable during the biological CabPK-gastric mill rhythm and when artificial versions of synaptic inhibition plus the CabPK-activated conductances are co-injected into LG. Distribution of mean values is shown for the LG burst duration, interburst duration and number of spikes per burst during CabPK-gastric mill rhythms (filled circles: n=11) and dynamic clamp-elicited gastric mill rhythm-like bursting in LG (n=4). All error bars (SEM) are smaller than the associated circles. N.S., not significantly different ($p>0.05$).

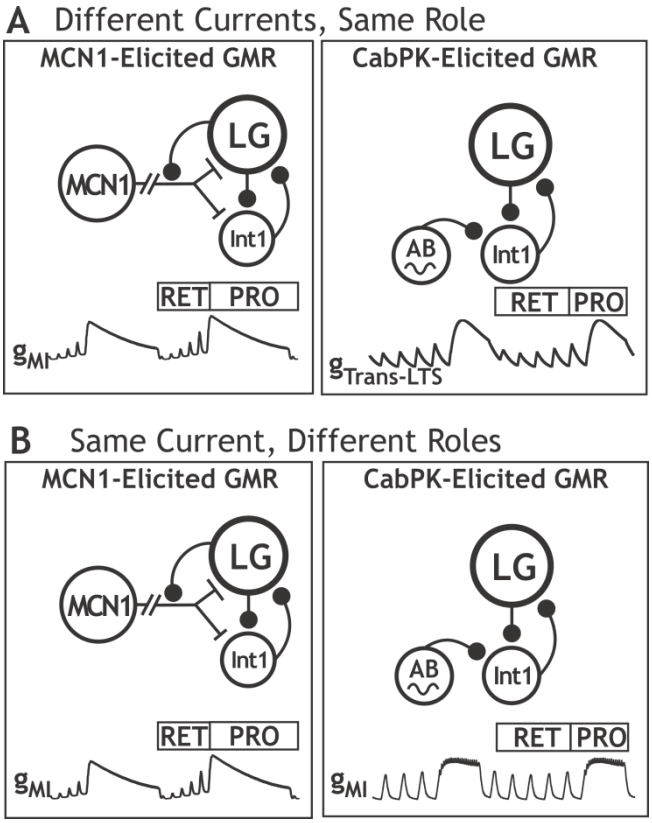

Figure 14. MCN1 stimulation and CabPK superfusion activate different conductances to perform the same function, and activate the same conductance to perform different functions, during gastric mill rhythm generation. ***A,*** Rhythmic LG neuron burst generation results from the rhythmic build-up and decay of (left) MCN1-activated g_{MI}, and (right) CabPK-activated $g_{Trans-LTS}$. During MCN1 stimulation, the build-up occurs during retraction and results from continual MCN1 activation of g_{MI}, while the decay during protraction results from LG presynaptic inhibition of MCN1 transmitter release. During CabPK application, the build-up during retraction results from the accumulation of a deinactivation-like state in $g_{Trans-LTS}$, while the decay during protraction results

from the time-dependent inactivation of this conductance. ***B,*** The g_{MI} in LG is the burst generating conductance during the MCN1-gastric mill rhythm, whereas it provides a sustained but subthreshold depolarizing drive that facilitates PIR burst generation by $I_{Trans\text{-}LTS}$ during the CabPK-gastric mill rhythm. Note that the different g_{MI} trajectories during protraction result from g_{MI} being both voltage- and synaptic inhibition-dependent during the MCN1-gastric mill rhythm whereas during the CabPK-gastric mill rhythm it is only voltage-dependent.

CHAPTER 3

Differential Sensitivity to Modulatory Input of Different Circuits Generating the Same Motor Pattern

Jason C. Rodriguez

Nicholas D. DeLong

Matthew S. Kirby

Michael P. Nusbaum*

Dept. of Neuroscience, 215 Stemmler Hall, Perelman School of Medicine, Univ. of Pennsylvania, Philadelphia, PA 19104-6074

Running Header: State-dependent responses of a conserved motor pattern

Abstract: 247/250 Words

Introduction: 500/500 Words

Discussion: 771/1500 Words

Pages: 39

Figures: 13

*Corresponding Author:

Dr. Michael P. Nusbaum

Dept. of Neuroscience

215 Stemmler Hall

Perelman School of Medicine

Univ. of Pennsylvania

Philadelphia, PA 19104-6074

Phone: 215-898-1585

FAX: 215-573-9050

Email: nusbaum@upenn.edu

Acknowledgments: This work was supported by National Institute of Neurological Diseases and Stroke Grant No. R37-NS029436 (M.P.N.).

ABSTRACT

Different modulatory inputs can elicit the same output pattern from a central pattern generator (CPG) despite configuring different circuits. We are assessing the functional consequences of this organization by determining whether such circuits are differentially sensitive to additional input. We use the gastric mill (chewing) CPG, which generates the biphasic (tooth protraction, retraction) gastric mill motor pattern in the crab stomatogastric ganglion. Specifically, stimulating the projection neuron MCN1 or superfusing the neuropeptide CabPK elicits the same gastric mill motor pattern via distinct cellular and synaptic mechanisms. The MCN1-driven gastric mill rhythm is regulated by sensory feedback and circulating hormones. For example, the muscle stretch-sensitive GPR neurons slow this rhythm by prolonging tooth retraction, while the peptide hormone CCAP slows it by prolonging protraction. We show here that, relative to the MCN1-gastric mill rhythm, the CabPK-rhythm exhibits a similar response to GPR stimulation but responds differently to CCAP application. First, GPR slows the MCN1-rhythm via presynaptic inhibition of MCN1, whereas it slows the CabPK-rhythm by its synaptic action on one or more gastric mill rhythm generator neurons. Second, the response threshold to CCAP is higher for CabPK (~10^{-7} M) than for MCN1 (10^{-10} M). Third, CCAP decreases the CabPK-rhythm cycle period by reducing retraction duration, while it increases the MCN1-rhythm cycle period by increasing protraction duration. These results demonstrate that different network states that produce the same steady-state

output can be differentially sensitive to some inputs while maintaining responsiveness to others, albeit via different cellular and synaptic mechanisms.

INTRODUCTION

Different modulatory inputs commonly elicit distinct outputs from a central pattern generator (CPG) network (Getting, 1989; Stein, 2009; Marder, 2012; Nusbaum and Blitz, 2012). In some cases, however, distinct modulators configure different CPG circuit states but elicit the same output pattern (Saideman et al., 2007b; Goaillard et al., 2009; Grashow et al., 2009; Rodriguez et al., 2013). This latter condition suggests the need for caution when interpreting the consequences of CPG activation by different pathways in systems where the CPG is not accessible to a cellular-level analysis. Additionally, different CPG circuit states generating the same motor pattern could exhibit distinct responses to particular inputs, such as those from sensory feedback and circulating hormones.

We are assessing this latter issue using the gastric mill (chewing) circuit in the crab (*Cancer borealis*) stomatogastric ganglion (STG). Specifically, selectively stimulating the projection neuron MCN1 (modulatory commissural neuron 1) and superfusing the neuropeptide CabPK (*C. borealis* pyrokinin) elicit the same gastric mill motor pattern, despite MCN1 not containing CabPK and the CabPK-gastric mill rhythm occurring without MCN1 activity (Saideman et al., 2007b). MCN1 and CabPK provide distinct modulatory influences to the same gastric mill rhythm generator neuron (LG, lateral gastric), which results in different gastric mill circuits and rhythm-generating mechanisms (Saideman et al., 2007b; Rodriguez et al., 2013).

The MCN1-driven gastric mill rhythm is influenced by the muscle stretch-sensitive GPR (gastropyloric receptor) sensory neuron and the peptide hormone

CCAP (crustacean cardioactive peptide) (Beenhakker et al., 2005; Kirby and Nusbaum, 2007; DeLong et al., 2009ab; DeLong and Nusbaum, 2010). In brief, GPR stimulation slows this rhythm by selectively prolonging the retractor phase. This effect results from GPR presynaptic inhibition of the STG terminals of MCN1 ($MCN1_{STG}$), which inhibits MCN1 neuropeptide release but not GABA corelease. CCAP also slows this gastric mill rhythm, but by selectively prolonging protraction. This effect results from convergent activation of the same ionic current (I_{MI}, modulator-activated inward current) in the LG neuron by CCAP and the MCN1-released neuropeptide CabTRP Ia (*C. borealis* tachykinin-related peptide Ia).

Here, we determine the influence of GPR and CCAP on the CabPK-gastric mill rhythm. GPR stimulation slowed this rhythm by selectively prolonging retraction, as during the MCN1-rhythm, albeit via a distinct synaptic pathway. Interestingly, despite operating via distinct synapses, during both rhythms the GPR action was mimicked by focal application of the GPR cotransmitter serotonin (5HT) (DeLong et al., 2009a). 5HT causes a slow inhibition of LG but has no direct effect on the gastric mill rhythm generator neuron Int1 (DeLong et al., 2009a). CCAP superfusion did not influence the CabPK-gastric mill rhythm unless it was applied at ≥ 10^{-7} M. In contrast, the threshold CCAP action on the MCN1-rhythm is ~10^{-10} M. Furthermore, in contrast to the MCN1-rhythm, when CCAP was applied at effective concentrations the CabPK-rhythm cycled faster, due to a reduced retraction duration. Thus, the same motor pattern driven by

distinct circuit states can be equally sensitive to a particular input, albeit via different synaptic mechanisms, and can also respond differently to other inputs.

MATERIALS AND METHODS

Animals. Male Jonah crabs (*Cancer borealis*) were purchased from commercial suppliers (Fresh Lobster; Marine Biological Laboratory) and maintained in aerated, filtered artificial seawater at 10 – 12° C. Animals were cold anesthetized by packing in ice for at least 30 min before dissection, after which the foregut was removed, in physiological saline at ~4° C, and the STNS isolated.

Solutions. C. borealis physiological saline contained (in mM): 440 NaCl, 26 $MgCl_2$, 13 $CaCl_2$, 11 KCl, 10 Trisma base, 5 maleic acid, 5 glucose, pH 7.4 – 7.6. All preparations were superfused continuously with *C. borealis* saline (8 – 12° C). CabPK-I, CabPK-II (Saideman et al., 2007a) (Biotechnology Center, Univ. of Wisconsin, Madison, WI), and CCAP (DeLong and Nusbaum, 2010) (Bachem) were each diluted from a stock solution (10^{-3} M) into physiological saline immediately before use. Bottles containing *C. borealis* saline, CabPK saline, CCAP saline, and CabPK/CCAP saline were connected to the same switching manifold for rapid solution changes.

Electrophysiology. Electrophysiology experiments were performed using standard techniques for this system (Beenhakker and Nusbaum, 2004). In brief, the isolated STNS (Fig. 1*A*) was pinned into a silicone elastomer (Sylgard 184, KR Anderson)-lined Petri dish. Extracellular nerve recordings were obtained using pairs of stainless steel wire electrodes (reference and recording) whose ends were pressed into the Sylgard-coated dish. A differential AC amplifier

(Model 1700: AM Systems) amplified the voltage difference between the reference wire, in the main bath compartment, and the recording wire, isolated with a section of an individual nerve from the main bath compartment by petroleum jelly (Vaseline, Lab Safety Supply). This signal was then further amplified and filtered (Model 410 Amplifier: Brownlee Precision). For extracellular nerve stimulation, the pair of wires used to record nerve activity was placed into a stimulus isolation unit (Model SIU 5: Astromed/Grass Instruments) connected to a stimulator (Model S88: Astromed/Grass Instruments).

For current clamp experiments, intrasomatic recordings of STG neurons were made with sharp glass microelectrodes (15 – 30 MΩ) filled with either K_2SO_4 (0.6 M) plus KCl (10 mM) or KCl (1 M). All intracellular recordings were amplified using Axoclamp 900A amplifiers (Molecular Devices) in bridge mode or discontinuous current clamp mode (2 – 5 kHz sampling rate) and digitized at 5 kHz using a Micro 1401 data acquisition interface and Spike2 software (Cambridge Electronic Design). To facilitate intracellular recording, the desheathed STG was viewed with light transmitted through a dark-field condenser (Nikon). In all experiments, the STG was isolated from the commissural ganglia (CoGs) by bisecting the inferior (*ions*)- and superior oesophageal nerves (*sons*) (Fig. 1*A*). Individual STNS neurons were identified by their axonal pathways, activity patterns and interactions with other neurons (Weimann et al., 1991; Beenhakker and Nusbaum, 2004).

During the gastric mill rhythm, the LG burst defines the protractor phase while its interburst duration, which is equivalent to the duration of Int1 activity,

defines the retractor phase (Coleman et al., 1995; Bartos et al., 1999; Diehl et al., 2013).

Data analysis. Data were collected onto a computer, with later playback onto a chart recorder (Astro-Med Everest). Acquisition onto computer (sampling rate 5 kHz) used the Spike2 data acquisition and analysis system (Cambridge Electronic Design). Analysis of CabPK-gastric mill rhythm parameters was conducted on the digitized data using a custom-written Spike2 program (The Crab Analyzer: freely available at http://www.uni-ulm.de/~wstein/spike2/index.html).

For gastric mill rhythm analyses, unless otherwise stated, each data point in a data set was derived by determining the mean for the analyzed parameter from 10 consecutive gastric mill cycles. One gastric mill cycle was defined as extending from the onset of consecutive LG neuron action potential bursts (Beenhakker et al., 2004; Wood et al., 2004) . Thus, the gastric mill cycle period was measured as the duration (s) between the onset of two successive LG neuron bursts. The protractor phase was measured as the LG burst duration, while the retractor phase was measured as the LG interburst duration. The gastric mill rhythm-timed LG burst duration was defined as the duration (s) between the onset of the first and last action potential within an impulse burst, during which no inter-spike interval was longer than 1.5 s (a duration that is ~one pyloric cycle period during the CabPK-gastric mill rhythm, and briefer than the duration of each gastric mill phase; Saideman et al., 2007a). The intraburst firing rate of LG was defined as the number of action potentials minus one, divided by the burst duration.

Data were plotted with Igor Pro (version 6.10A). Figures were produced using CorelDraw (version 16.0 for Windows). Statistical analyses were performed with Microsoft Excel (Microsoft) and SigmaStat 3.0 (SPSS). Comparisons were made to determine statistical significance using the paired Student's *t*-. In all experiments, the effect of each manipulation was reversible, and there was no significant difference between the pre- and post-manipulation groups. Data are expressed as the mean ± standard error (SE).

Gastric Mill Model. We modified an existing computational model of the CabPK-gastric mill rhythm generator (Nadim et al., 1998; Beenhakker et al., 2005; Rodriguez et al., 2013). The previously published version modeled the LG and Int1 neurons as having multiple compartments separated by an axial resistance, with each compartment possessing intrinsic and/or synaptic conductances. The parameters of the CabPK-gastric mill rhythm generator model were based on both previously published voltage clamp analyses in STG neurons (including LG) and on the LG neuron voltage clamp results obtained with CabPK modulation (Golowasch and Marder, 1992; Swensen and Marder, 2000, 2001; DeLong et al., 2009b; Rodriguez et al., 2013). To mimic in the computational model the effects of CCAP bath application to the biological system, we added CCAP-activated I_{MI} to the LG neuron and/or Int1 neuron dendrite compartment as an intrinsic (non-synaptically activated) current (Table 1). To mimic the effects of GPR, we imported the GPR neuron and synapses from a published model (Beenhakker et al., 2005). To assess the impact of the model GPR neuron activation on the

CabPK-GMR, we either stimulated GPR during protraction (10 Hz; 2 s) or during retraction (10 Hz; 15 s).

Simulations were performed on a PC with the freely available Ubuntu Linux operating system (www.ubuntu.com). We used the Network simulation software developed in the Nadim laboratory (http://stg.rutgers.edu/software/network.htm). This included using a fourth-order Runge–Kutta numerical integration method with time steps of 0.05 and 0.01 ms. Results were visualized by plotting outputted data points using the freely available Gnuplot software package (www.gnuplot.info). In most figures showing the model output, we present conductance (g) instead of the associated current (I) to more clearly display the trajectory during the gastric mill retractor and protractor phases. The main difference between “g” and “I” is that the former lacks the fast transient changes that occur in the latter during each LG action potential (DeLong et al., 2009a). In particular, the relatively slow kinetics of the CabPK-activated conductances make them insensitive to these fast transient changes in voltage.

RESULTS

The gastric mill rhythm is an episodic motor pattern, in vivo and in vitro, which is driven by modulatory inputs that are not spontaneously active (Nusbaum and Beenhakker, 2002; Beenhakker et al., 2004; White and Nusbaum, 2011; Nusbaum and Blitz, 2012; Diehl et al., 2013; Rodriguez et al., 2013). There are at least several distinct gastric mill motor patterns, driven by different pathways, but in all cases the core rhythm generator appears to include the reciprocally inhibitory protractor motor neuron LG and retractor interneuron Int1 (interneuron 1) (Saideman et al., 2007; White and Nusbaum, 2011). When the gastric mill rhythm is not occurring, Int1 is spontaneously active while LG is silent. Consequently, a pivotal action of any gastric mill rhythm-activating pathway is to enable LG to become active and burst in alternation with Int1.

In contrast to the ability of most gastric mill-activating pathways to drive different gastric mill motor patterns, tonic MCN1 stimulation and bath applied CabPK (10^{-6} M) elicit the same gastric mill motor pattern (Fig. 1*B*) (Saideman et al., 2007b). However, despite the ability of MCN1 and CabPK to each drive the gastric mill rhythm primarily by enabling rhythmic bursting in the LG neuron, the associated cellular and synaptic mechanisms for gastric mill rhythm generation are distinct (Fig. 1*C*) (Rodriguez et al., 2013). In brief, MCN1 provides the LG neuron with metabotropic excitation (during retraction) that culminates in a LG burst (during protraction), with the transition from retraction to protraction including LG presynaptic inhibition of $MCN1_{STG}$ (Coleman et al., 1995; Bartos et al., 1999; DeLong et al., 2009a). During retraction, MCN1-released CabTRP Ia

elicits a continual build-up of I_{MI} in LG until there is sufficient depolarizing drive to trigger a LG burst. During protraction, LG presynaptically inhibits MCN1 transmitter release, causing a slow decay of I_{MI}. During this time, however, LG also receives relatively large amplitude electrical EPSPs (eEPSPs) from MCN1 which strengthens LG activity until the LG membrane potential repolarizes and self-terminates, due to I_{MI} decay.

Unlike the MCN1 influence on the LG neuron, CabPK enables LG to periodically generate a post-inhibitory rebound (PIR) burst after a sufficient duration of inhibitory input from Int1 (Rodriguez et al., 2013). These PIR bursts result from CabPK activation of I_{MI} plus a transient, low threshold slow inward current ($I_{Trans\text{-}LTS}$). I_{MI}, which is the burst-generating current during the MCN1-rhythm, instead enables a subthreshold depolarization in LG during the CabPK-rhythm which facilitates each PIR burst generated by $I_{Trans\text{-}LTS}$. Thus, MCN1 and CabPK configure different gastric mill network states. We therefore tested the hypothesis that these different states would enable the same gastric mill motor pattern to be altered differently by additional input, such as that provided by circulating hormones or sensory input.

CCAP distinctly influences the CabPK- and MCN1-gastric mill rhythms

CCAP (Pro-Phe-Cys-Asn-Ala-Phe-Thr-Gly-Cys_{NH2}) is a highly conserved neuropeptide transmitter and hormone localized in neurons and neurohemal structures of many arthropods, including *C. borealis* (Trube et al., 1994). Simulating hormonal CCAP release by bath application modulates the MCN1-

gastric mill rhythm (Kirby and Nusbaum, 2007; DeLong et al., 2009a; DeLong and Nusbaum, 2010). Specifically, CCAP slows the MCN1-gastric mill rhythm by selectively prolonging protraction. This action results from CCAP activation of I_{MI} in the LG neuron (DeLong et al., 2009a). Insofar as the CabPK-gastric mill rhythm is also driven primarily through actions on the LG neuron, we anticipated that CCAP would also influence this motor pattern.

Bath-application of a likely hormonal CCAP concentration (10^{-8} M) did not consistently change the CabPK-elicited gastric mill cycle period (Control: 14.04 ± 2.1 s; CCAP: 12.57 ± 1.6 s, n=7, p=0.13), protraction duration (Control: 3.54 ± 0.4 s; CCAP: 3.62 ± 0.4 s, n=7, p=0.70) or retraction duration (Control: 10.50 ± 2.0 s; CCAP: 8.95 ± 1.6 s, n=7, p=0.12). Furthermore, despite the ability of CCAP to activate I_{MI} in LG, there was no change in the LG firing frequency (Control: 4.11 ± 0.3 Hz; CCAP: 4.29 ± 0.2 Hz, n=7, p=0.39). Insofar as the CCAP influence on the MCN1-gastric mill rhythm has a considerably lower threshold (10^{-10} M), the CabPK-gastric mill rhythm was relatively insensitive to CCAP modulation.

Applying a relatively high CCAP concentration (10^{-6} M) did consistently influence the CabPK-gastric mill rhythm (Fig. 2). Specifically, its presence decreased the CabPK-gastric mill cycle period (Control: 16.45 ± 2.8 s; CCAP: 12.93 ± 2.2 s, n=4, p<0.05). This action was accompanied by a briefer retraction phase (Control: 11.38 ± 1.9 s; CCAP: 8.06 ± 1.5 s, n=4, p<0.05), with no change in protraction duration (Control: 5.07 ± 0.8 s; CCAP: 4.87 ± 0.7 s, n=4, p=0.68). In parallel with the unchanged LG burst duration, the presence of CCAP did not

alter the LG intraburst firing frequency (Control: 3.37 ± 0.3 Hz; CCAP: 3.65 ± 0.4, n=4, p=0.48).

The gastric mill rhythm generator neurons (LG, Int1) are each directly excited by CCAP (Kirby and Nusbaum, 2007). Therefore, we determined whether the gastric mill rhythm response to 10^{-6} M CCAP likely resulted from peptide modulation of LG and/or Int1, by importing these actions into our previously developed computational model of the CabPK-gastric mill rhythm generator (Rodriguez et al., 2013). The computational model was adapted to simulate CCAP peptide modulation by its activation of I_{MI} in LG and/or Int1. Previous work established that CCAP activates I_{MI} in LG, and we made the assumption that its excitatory action on Int1 also results from I_{MI} activation because CCAP exclusively activates I_{MI} in several pyloric circuit neurons as well as LG (Swensen and Marder, 2000, 2001; DeLong et al., 2009b). To assess its effectiveness and robustness, we added CCAP-activated I_{MI} to LG or Int1 across a range of g_{MI} values (0 – 20 pS).

Adding g_{MI} (range: 0 – 10 pS) to Int1 modestly but consistently increased the Int1 intraburst firing frequency (Control: 5.9 ± 0.0 Hz; Added I_{MI}: 6.1 ± 0.0 Hz; n=3; $p<0.01$). This effect was accompanied by an increased retraction duration (Control: 9.5 ± 0.08 s; Added I_{MI}: 12.2 ± 0.0004 s; n=3; $p<0.01$) with no change in protraction duration (Control: 2.7 ± 0.09 s; Added I_{MI}: 2.7 ± 0.0004 s; n=3; p=0.23) (Fig. 3). This result was opposite to the biological CabPK-gastric mill rhythm response to CCAP, where the cycle period was decreased due to a selective decrease in retraction duration (Fig. 2). This result suggested that

CCAP excitation of Int1 was not the dominant CCAP action during the CabPK-rhythm.

Adding g_{MI} to the LG neuron in the CabPK-gastric mill model selectively decreased the retractor phase duration (Control: 12.2 ± 0.0004 s; Added I_{MI}: 10.8 ± 0.0005 s; n=3; $p<0.01$) over a range of conductance values (0-5 pS), without changing the LG firing frequency or burst duration. Therefore, I_{MI} activation by CCAP in the LG neuron was sufficient to replicate the effect of bath-applied CCAP on the biological CabPK-gastric mill rhythm suggesting that, as for the MCN1-gastric mill rhythm, LG is the primary target by which CCAP regulates this rhythm.

Comparable regulation of the CabPK- and MC1-gastric mill rhythms

The GPR neuron dendrites arborize in specific lateral tooth protractor muscles (Katz et al., 1989). As a result, stretch of these muscles during the gastric mill retraction phase activates GPR (Katz et al., 1989; Birmingham et al., 1999). Selectively stimulating GPR during the retraction phase of the MCN1-gastric mill rhythm in the isolated STNS, by electrically stimulating the nerve (*gpn*) through which its axon projects towards the STG, consistently prolongs retraction without altering the subsequent protraction phase (Beenhakker et al., 2005, 2007).

GPR is a multi-transmitter neuron which contains serotonin (5HT), acetylcholine (ACh) and an allatostatin (AST) peptide (Katz et al., 1989; Skiebe and Schneider, 1994). It also directly inhibits $MCN1_{STG}$ and LG, and directly

excites Int1 (Beenhakker et al., 2005; DeLong et al., 2009b). However, the GPR action on the MCN1-gastric mill rhythm results exclusively from its slow, serotonergic inhibition of $MCN1_{STG}$, which selectively inhibits neuropeptide release from $MCN1_{STG}$ and thereby reduces the rate of I_{MI} build-up in LG (DeLong et al., 2009a). Insofar as MCN1 does not participate in the CabPK-gastric mill rhythm, we anticipated that GPR stimulation would influence this latter motor pattern differently.

Stimulating GPR during the CabPK-gastric mill rhythm, using the same stimulation parameters as during the MCN1-rhythm (5 Hz tonic stimulation during each retraction phase), had a comparable effect to that occurring during the MCN1-rhythm. Specifically, GPR stimulation prolonged the CaPK-gastric mill cycle period (Control: 15.9 ± 3.3 s; GPR: 35.8 ± 8.9 s; n=6; $p<0.05$) by prolonging the retraction phase (Control: 11.6 ± 2.8 s; GPR: 31.4 ± 8.8 s; n=6; $p<0.05$) without altering protraction phase duration (Control: 4.4 ± 0.7 s; GPR: 4.4 ± 0.8 s; n=6; $p=0.49$) (Fig. 4). Insofar as MCN1 activity is not necessary for the CabPK-gastric mill rhythm, it was unlikely that the comparable GPR action during these two gastric mill rhythms occurred via the same synaptic mechanism (i.e. presynaptic inhibition of $MCN1_{STG}$).

Although GPR regulates the MCN1-gastric mill rhythm exclusively by its presynaptic inhibition of $MCN1_{STG}$, as noted above GPR has additional synapses onto the gastric mill rhythm generator which are functionally ineffective during the MCN1-rhythm (Fig. 5). These additional GPR synapses include a slow serotonergic inhibition of LG and a fast, non-serotonergic ionotropic excitation of

Int1 (DeLong et al., 2009b). The transmitter(s) responsible for GPR excitation of Int1 is not known, but it is not likely serotonin because Int1 is not responsive to 5HT application (DeLong et al., 2009b). GPR also has a strong, serotonergic excitatory action on the DG neuron (Katz and Harris-Warrick, 1989; Kiehn and Harris-Warrick, 1992; Zhang and Harris-Warrick, 1995). DG does not influence the MCN1-gastric mill rhythm generator, but it does influence the rhythm generator during the CabPK-gastric mill rhythm (Saideman et al., 2007b).

Any or all of the aforementioned GPR actions could contribute to the selective GPR prolongation of the CabPK-retraction phase. For example, its direct inhibition of LG could impede the LG ability to depolarize sufficiently during retraction to generate its PIR burst and transition the rhythm to the protraction phase. Additionally, insofar as both Int1 and DG are active during the CabPK-gastric mill retraction phase and inhibit LG at this time, GPR excitation of either (or both) of these neurons could strengthen their inhibition of LG and slow the onset of the LG PIR burst.

Suppressing DG activity with hyperpolarizing current injection during the CabPK-rhythm did not alter the ability of GPR to prolong the retraction phase (Control: 5.1 ± 1.3 s; GPR: 16.3 ± 3.4 s; n=5; $p<0.05$) (Fig. 6). Thus, DG activity was not necessary for the GPR action on the CabPK-gastric mill rhythm.

It was not feasible to assess the relative contribution of the GPR actions on LG and Int1 to its influence on the CabPK-gastric mill rhythm by selectively suppressing each ones activity, as we did for the DG neuron, because suppressing LG or Int1 activity terminates the CabPK-gastric mill rhythm

(Saideman et al., 2007b). Therefore, we first assessed the consequences of these GPR synaptic actions in our computational model of the CabPK-gastric mill rhythm generator. To this end, we incorporated into this model the previously developed model GPR synapses that were used to evaluate the likely site of GPR action during the MCN1-gastric mill rhythm (Delong et al., 2009b). Using this approach, we obtained the output from three different versions of the model CabPK-rhythm generator, including ones containing only GPR excitation of Int1 or inhibition of LG, and one in which both synapses were active.

The computational model output that occurred with either GPR excitation of Int1 or GPR inhibition of LG were equally effective at prolonging the CabPK-gastric mill retractor phase (Control: 9.5 ± 0.1 s; GPR to Int1 synapse active: 29.0 ± 0.8 s, n=3, $p<0.01$; GPR to LG synapse active: 29.0 ± 0.8 s; n=3, $p<0.01$) (Fig. 7,8). Additionally, there was no change in protraction duration when either GPR synapse was activated (Control: 2.7 ± 0.1 s; GPR to Int1 synapse active: 2.8 ± 0.01 s; GPR to LG synapse active: 2.8 ± 0.01 s; $p=0.1$). For both GPR synapses we implemented a 5-fold range of conductance values and found they had similar effectiveness and potency for prolonging the LG interburst. Interestingly, when either GPR synapse was activated during protraction, instead of retraction, it prematurely terminated the LG burst (LG burst duration: Control, 2.7 ± 0.10 s; GPR to Int1 synapse, 1.5 ± 0.08 s; GPR to LG synapse 1.4 ± 0.10 s; n=3, $p<0.01$), even when implemented at a relatively low conductance level (e.g. 0.3 nS) (Fig. 9). In contrast, GPR stimulation during MCN1-protraction did not influence either protraction or the subsequent retraction phase (DeLong et al.,

2009b). These results suggested that the GPR synapses onto both LG and Int1 are candidates for mediating the GPR influence on the CabPK-gastric mill rhythm.

To test whether coactivation of both GPR synapses (i.e. excitation of Int1, inhibition of LG) might also selectively prolong the CabPK-gastric mill retraction phase, we ran the model with both synapses active. This model output did indeed produce comparable results to the separate GPR actions on LG and Int1 (Fig. 10), producing a prolonged retractor phase (Control: 9.5 ± 0.09 s; GPR synapses active: 33.4 ± 6.49 s; n=3, $p<0.5$), without any change in protraction (Control: 2.7 ± 0.10 s; GPR synapses active: 2.8 ± 0.01 s; n=3, p=0.1). We next determined the impact of these synapse on the CabPK-rhythm in the biological preparation.

We examined the Int1 response to GPR stimulation during CabPK-GMR indirectly, by determining the frequency of Int1-mediated IPSPs in LG when DG was hyperpolarized, to eliminate the confound of DG-mediated IPSPs in LG. Under these conditions, Int1 is the sole source of IPSPs in LG. The presence of CabPK did not alter the frequency of these IPSPs in LG (Control: 14.5 ± 1.2 Hz; CabPK: 17.0 ± 1.7 Hz; n=3; p=0.1). It should be noted that, because CabPK also directly excites Int1 (Saideman et al., 2007a), the apparent lack of GPR excitation of Int1 might result from a ceiling effect due to the CabPK excitation of Int1.

Although GPR stimulation did not alter the frequency of Int1-mediated IPSPs in LG during the CabPK-gastric mill rhythm, it might have nevertheless

strengthened the Int1 synaptic action (e.g. by an activity-independent increase in Int1 transmitter release). Therefore, we determined whether a strengthened Int1 inhibition of LG during the CabPK-elicited gastric mill rhythm reproduced the result of GPR stimulation. To this end, we injected depolarizing current into the VD neuron, which is electrically-coupled to Int1 but has no direct synaptic action on LG. During these manipulations, the Int1 firing frequency was moderately but consistently increased (Control vs. VD dep.: 5.7 to 6.1 Hz; 8.3 to 9.6 Hz; n=2). When Int1 activity was increased, there was an increased LG hyperpolarization (Control vs. VD dep.: -57 to -61 mV; -65 to -67 mV; n=2). Despite the strengthened inhibitory response in LG, this manipulation did not dramatically increase CabPK-retraction phase duration (Control vs. VD dep.: 5.7 to 6.8 s; 16.4s to 19.5 s; n=2) and, hence, did not mimic the GPR action on the CabPK-gastric mill rhythm. Insofar as the GPR influence on neither DG nor Int1 appeared necessary for the GPR-mediated prolongation of the gastric mill retractor phase, we determined whether GPR inhibition of LG prolonged gastric mill retraction by substituting focal 5HT application for GPR stimulation with DG hyperpolarized.

Focal application of 5HT (10^{-4} M: 5 psi, 1 s) onto the desheathed STG neuropil selectively prolongs the MCN1-gastric mill retractor phase (DeLong et al., 2009b). This 5HT action results from its selective inhibition of MCN1 neuropeptide release (DeLong et al., 2009b). In our initial experiments focally applying 5HT (10^{-4} M) during the CabPK-gastric mill rhythm again prolonged the retractor phase (Control vs. 5HT: 4.2 to 69.5 s; 3.6 to 25.0 s) (Fig. 11). This 5HT

action was similar to the GPR action on the CabPK-retractor phase (Control: 11.6 ± 2.8 s; GPR: 31.4 ± 8.8 s, n=6). This response was likely a direct action of 5-HT, insofar as 5-HT directly inhibits LG and has no influence on Int1 (DeLong et al., 2009b). These data support the hypothesis that GPR selectively prolongs the CabPK-elicited gastric mill retractor phase by its serotonergic inhibition of LG.

DISCUSSION

In this paper we have shown that distinct circuit states generating the same motor pattern are differentially sensitive to some, but not all modulatory inputs. Specifically, the comparable gastric mill rhythms elicited by the projection neuron MCN1 and bath applied CabPK peptide respond differently to the peptide hormone CCAP but exhibit the same response to the modulatory action of the GPR proprioceptor neuron.

CCAP application increases the MCN1-gastric mill cycle period by selectively prolonging protraction, via a low threshold (10^{-10} M) action (Kirby and Nusbaum, 2007). In contrast, it decreases the CabPK-gastric mill cycle period by selectively shortening retraction, via a high threshold (10^{-7} M) action (this paper). The CCAP action on the MCN1-rhythm results from the convergent activation of I_{MI} in the LG neuron by CCAP and MCN1-released CabTRP Ia, which not only prolongs protraction but prevents prolongation of retraction (DeLong et al., 2009b). The mechanism underlying CCAP modulation of the CabPK-rhythm remains to be determined, although the results of our computational modeling suggest that CCAP activation of I_{MI} in LG is again the pivotal event. Presumably the consequences for the CabPK-rhythm involve the impact of increased I_{MI} availability on the influence of $I_{Trans\text{-}LTS}$, the CabPK-activated current that enables LG to generate the periodic PIR bursts that define the CabPK-protraction phase (Rodriguez et al., 2013).

Surprisingly, sensory feedback mediated by the GPR neuron selectively prolonged retraction during both of these gastric mill rhythms, despite the fact

that GPR acted via different synapses under each condition. GPR also selectively prolongs retraction during a distinct gastric mill motor pattern triggered by the VCN (ventral cardiac neurons) mechanosensory neurons (Beenhakker et al., 2007). As is the case during the MCN1- and CabPK-gastric mill rhythms, an overlapping but distinct subset of GPR synapses is functionally ineffective during the VCN-rhythm (Beenhakker et al., 2007).

Degeneracy increases robustness and/or degrees of freedom?

This invariant GPR action is an example of degeneracy at the network level. Degeneracy is a concept wherein different elements of a circuit perform the same function (Marder and Taylor, 2011). In this case, GPR seemingly exhibits degeneracy in that it can perform the same network function with any of its multiple points of influence on the same circuit. This allows GPR to provide an input that is both state-specific and consequence-invariant. The state[s] where the GPR excitation of Int1 and DG is pivotal is not yet known, but, given the model prediction, it could be a state similar to that produced by CabPK modulation. There are at least several additional versions of the gastric mill rhythm, during which GPR may act via these additional synapses (Blitz et al., 2004, 2008; Christie et al., 2004).

As suggested above, CCAP likely influences the CabPK- and MCN1-elicited circuit states by activating I_{MI} in the LG neuron, but the consequences for the motor pattern are clearly state-dependent. If true, CCAP would be activating the same conductance in the same neuron (LG) during these two circuit states

yet having opposite actions on the resulting motor patterns. Such an outcome has been predicted in computational modeling and computational-biological hybrid systems, but no study has verified this prediction using a purely biological system (Grashow et al., 2009; Kispersky et al., 2012; Britton et al., 2013). This result would provide evidence against the notion that the convergent MCN1- and CabPK-gastric mill motor patterns are an example of degeneracy and support the idea that these are different states with distinct stimulus-response relationships. The fact that these network states have overlapping outputs could simply be an artifact of sampling a limited region of the input space. It is, therefore, possible that degeneracy is itself an artifact of a small input sample size and that subtle differences between states are important for adequate function. Regardless of the function of degeneracy, this work provides guidance for systems, like the feeding circuits found in the mammalian brain, where many neuromodulators are identified (e.g. various peptide transmitters systems) yet the interaction between these modulators is still unknown (Jobst et al., 2004).

The present study also highlights a prevalent limitation in neural circuit research. First, it supports previous modeling and experimental work demonstrating that it is inappropriate to use network output as a proxy for network state (Prinz et al., 2004; Marder and Goaillard, 2006; Grashow et al., 2009; Norris et al., 2011). Second, it exemplifies the consequences of such an assumption by demonstrating that, even in a small system with relatively few inputs, the circuit-level details are critical for the circuit state response to a given input. These results, therefore, represent a cautionary note to investigators

working in less well-defined systems without adequate access to cellular-level events.

REFERENCES

Bartos M, Manor Y, Nadim F, Marder E, Nusbaum MP (1999) Coordination of fast and slow rhythmic neuronal circuits. J Neurosci 19:6650–6660.

Beenhakker MP, Blitz DM, Nusbaum MP (2004) Long-lasting activation of rhythmic neuronal activity by a novel mechanosensory system in the crustacean stomatogastric nervous system. J Neurophysiol 91:78–91.

Beenhakker MP, DeLong ND, Saideman SR, Nadim F, Nusbaum MP (2005) Proprioceptor regulation of motor circuit activity by presynaptic inhibition of a modulatory projection neuron. J Neurosci 25:8794–8806.

Beenhakker MP, Kirby MS, Nusbaum MP (2007) Mechanosensory gating of proprioceptor input to modulatory projection neurons. J Neurosci 27:14308–14316.

Beenhakker MP, Nusbaum MP (2004) Mechanosensory activation of a motor circuit by coactivation of two projection neurons. J Neurosci 24:6741–6750.

Birmingham JT, Szuts ZB, Abbott LF, Marder E (1999) Encoding of muscle movement on two time scales by a sensory neuron that switches between spiking and bursting modes. J Neurophysiol 82:2786–2797.

Blitz DM, Beenhakker MP, Nusbaum MP (2004) Different sensory systems share projection neurons but elicit distinct motor patterns. J Neurosci 24:11381–11390.

Blitz DM, White RS, Saideman SR, Cook A, Christie AE, Nadim F, Nusbaum MP (2008) A newly identified extrinsic input triggers a distinct gastric mill rhythm via activation of modulatory projection neurons. J Exp Biol 211:1000–1011.

Britton OJ, Bueno-Orovio A, Van Ammel K, Lu HR, Towart R, Gallacher DJ, Rodriguez B (2013) Experimentally calibrated population of models predicts and explains intersubject variability in cardiac cellular electrophysiology. Proc Natl Acad Sci U S A 110:E2098–105.

Christie AE, Stein W, Quinlan JE, Beenhakker MP, Marder E, Nusbaum MP (2004) Actions of a histaminergic/peptidergic projection neuron on rhythmic motor patterns in the stomatogastric nervous system of the crab *Cancer borealis*. J Comp Neurol 469:153–169.

Coleman MJ, Meyrand P, Nusbaum MP (1995) A switch between two modes of synaptic transmission mediated by presynaptic inhibition. Nature 378:502–505.

DeLong ND, Kirby MS, Blitz DM, Nusbaum MP (2009a) Parallel regulation of a modulator-activated current via distinct dynamics underlies comodulation of motor circuit output. J Neurosci 29:12355–12367.

DeLong ND, Beenhakker MP, Nusbaum MP (2009b) Presynaptic inhibition selectively weakens peptidergic cotransmission in a small motor system. J Neurophysiol 102:3492–3504.

DeLong ND, Nusbaum MP (2010) Hormonal modulation of sensorimotor integration. J Neurosci 30:2418–2427.

Diehl F, White RS, Stein W, Nusbaum MP (2013) Motor circuit-specific burst patterns drive different muscle and behavior patterns. J Neurosci 33:12013–12029.

Getting PA (1989) Emerging principles governing the operation of neural networks. Annu Rev Neurosci 12:185–204.

Goaillard J-M, Taylor AL, Schulz DJ, Marder E (2009) Functional consequences of animal-to-animal variation in circuit parameters. Nat Neurosci 12:1424–1430.

Golowasch J, Marder E (1992) Proctolin activates an inward current whose voltage dependence is modified by extracellular Ca2+. J Neurosci 12:810–817.

Grashow R, Brookings T, Marder E (2009) Reliable neuromodulation from circuits with variable underlying structure. Proc Natl Acad Sci U S A 106:11742–11746.

Jobst EE, Enriori PJ, Cowley M a (2004) The electrophysiology of feeding circuits. Trends Endocrinol Metab 15:488–499.

Katz PS, Eigg MH, Harris-Warrick RM (1989) Serotonergic/cholinergic muscle receptor cells in the crab stomatogastric nervous system. I. Identification and characterization of the gastropyloric receptor cells. J Neurophysiol 62:558–570.

Katz PS, Harris-Warrick RM (1989) Serotonergic/cholinergic muscle receptor cells in the crab stomatogastric nervous system. II. Rapid nicotinic and prolonged modulatory effects on neurons in the stomatogastric ganglion. J Neurophysiol 62:571–581.

Kiehn O, Harris-Warrick RM (1992) Serotonergic stretch receptors induce plateau properties in a crustacean motor neuron by a dual-conductance mechanism. J Neurophysiol 68:485–495.

Kirby MS, Nusbaum MP (2007) Peptide hormone modulation of a neuronally modulated motor circuit. J Neurophysiol 98:3206–3220.

Kispersky TJ, Caplan JS, Marder E (2012) Increase in sodium conductance decreases firing rate and gain in model neurons. J Neurosci 32:10995–11004.

Marder E (2012) Neuromodulation of neuronal circuits: back to the future. Neuron 76:1–11.

Marder E, Goaillard J-MM (2006) Variability, compensation and homeostasis in neuron and network function. Nat Rev Neurosci 7:563–574.

Marder E, Taylor AL (2011) Multiple models to capture the variability in biological neurons and networks. Nat Neurosci 14:133–138.

Nadim F, Manor Y, Nusbaum MP, Marder E (1998) Frequency regulation of a slow rhythm by a fast periodic input. J Neurosci 18:5053–5067.

Norris BJ, Wenning A, Wright TM, Calabrese RL (2011) Constancy and variability in the output of a central pattern generator. J Neurosci 31:4663–4674.

Nusbaum MP, Beenhakker MP (2002) A small-systems approach to motor pattern generation. Nature 417:343–350.

Nusbaum MP, Blitz DM (2012) Neuropeptide modulation of microcircuits. Curr Opin Neurobiol 22:592–601.

Prinz AA, Bucher D, Marder E (2004) Similar network activity from disparate circuit parameters. Nat Neurosci 7:1345–1352.

Rodriguez JC, Blitz DM, Nusbaum MP (2013) Convergent Rhythm Generation from Divergent Cellular Mechanisms. J Neurosci 33:18047–18064.

Saideman SR, Ma M, Kutz-Naber KK, Cook A, Torfs P, Schoofs L, Li L, Nusbaum MP (2007a) Modulation of rhythmic motor activity by pyrokinin peptides. J Neurophysiol 97:579–595.

Saideman SR, Blitz DM, Nusbaum MP (2007b) Convergent motor patterns from divergent circuits. J Neurosci 27:6664–6674.

Skiebe P, Schneider H (1994) Allatostatin peptides in the crab stomatogastric nervous system: inhibition of the pyloric motor pattern and distribution of allatostatin-like immunoreactivity. J Exp Biol 194:195–208.

Stein W (2009) Modulation of stomatogastric rhythms. J Comp Physiol A Neuroethol Sens Neural Behav Physiol 195:989–1009.

Swensen AM, Marder E (2000) Multiple peptides converge to activate the same voltage-dependent current in a central pattern-generating circuit. J Neurosci 20:6752–6759.

Swensen AM, Marder E (2001) Modulators with convergent cellular actions elicit distinct circuit outputs. J Neurosci 21:4050–4058.

Trube A, Audehm U, Dircksen H (1994) Crustacean cardioactive peptide-immunoreactive neurons in the ventral nervous system of crayfish. J Comp Neurol 348:80–93.

Weimann JM, Meyrand P, Marder E (1991) Neurons that form multiple pattern generators: identification and multiple activity patterns of gastric/pyloric neurons in the crab stomatogastric system. J Neurophysiol 65:111–122.

White RS, Nusbaum MP (2011) The same core rhythm generator underlies different rhythmic motor patterns. J Neurosci 31:11484–11494.

Wood DE, Manor Y, Nadim F, Nusbaum MP (2004) Intercircuit control via rhythmic regulation of projection neuron activity. J Neurosci 24:7455–7463.

Zhang B, Harris-Warrick RM (1995) Calcium-dependent plateau potentials in a crab stomatogastric ganglion motor neuron. I. Calcium current and its modulation by serotonin. J Neurophysiol 74:1929–1937.

Table 1: CabPK Gastric Mill Network Model Parameters

Neuron	**Conductances**		**$V_{1/2}$ [mV]**	**k [mV]**	**t_{lo} [ms]**	**t_{hi} [ms]**	**exp (p,q,r)**	**E_{rev} [mV]**	**G_{max} [nS]**
LG	$I_{Trans-LTS}$	*m*	-55	-3	500	500	1	10	0.4
		h	-63	0.8	3500	1500	1		
	I_{MI}	*m*	-60	-5	5	5	1	10	0.11
LG/Int1	CCAP- I_{MI}	*m*	-60	-5	5	5	1	10	0- 20 pS
Int1	Na_v	*m*	-42	-5	1.5	0.45	3	45	7.5
		h	-52	9.2	10	2.4	1		
	K_V	*m*	-26	-9	27	3	4	-70	18
		h	-16	1.5	20	200	2		
	Leak							-60	0.012
Int1 -> LG	Synapse	*m*	-40	-1	200	200	1	-80	2
LG -> Int1	Synapse	*m*	-30	-0.1	200	200	1	-80	15
GPR -> Int1/LG	Synapse	*m*	-60	1	1000	2000	1	0 (Int1) -80 (LG)	0-0.5

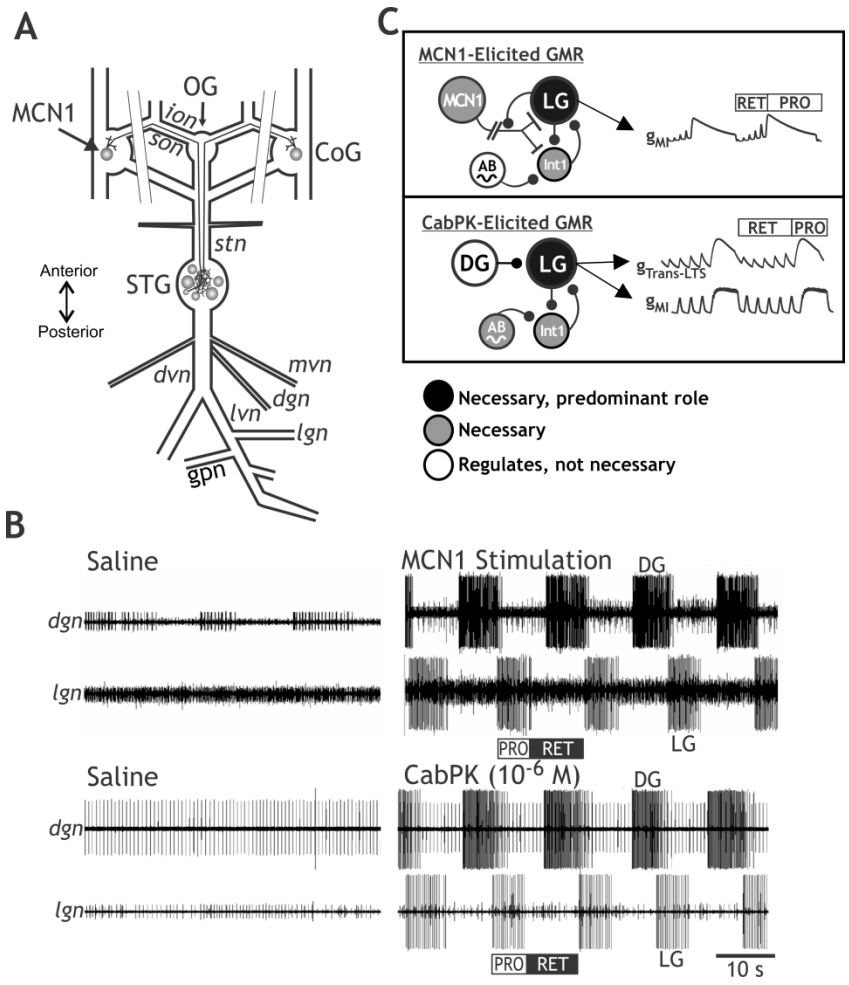

Figure 1. MCN1 projection neuron stimulation and bath-applied CabPK produce the same gastric mill pattern by configuring distinct rhythm-generators. A, Schematic of the STNS, including its four ganglia (paired CoGs, OG, and STG), interconnecting nerves, and a selection of peripheral nerves. The parallel lines that disrupt the continuity in the *ions* and *sons* represent locations where these nerves were bisected before each experiment to prevent projection neuron activity in the CoGs from influencing STG neurons. **B,** Bath-

applied CabPK and MCN1 neuron stimulation use distinct rhythm generators to produce the same output patterns. Extracellular nerve recordings (*dgn, lgn)* monitor the gastric mill motor pattern (from: Saideman et al. 2007b) . Top, Tonic MCN1 stimulation produces a gastric mill rhythm. Bottom, Bath-applied CabPK produces a comparable gastric mill rhythm. In both experiments, there was no gastric mill activity prior to modulation. **C,** The MCN1 and CabPK-elicited rhythm generators employ a distinct yet overlapping set of neurons and properties. In both rhythm generators, the LG neuron is not only necessary, but it is the pivotal target for rhythm generation. In the MCN1-rhythm, the periodic growth and decay of the LG burst-generating current I_{MI} (g_{MI} when expressed as conductance) results from MCN1-mediated I_{MI} activation being phasically interrupted by presynaptic inhibition. The CabPK-elicited rhythm is caused by the coactivation of I_{MI} and $I_{Trans\text{-}LTS}$, which enable the LG neuron to rhythmically express PIR after a period of Int1-mediated inhibition.

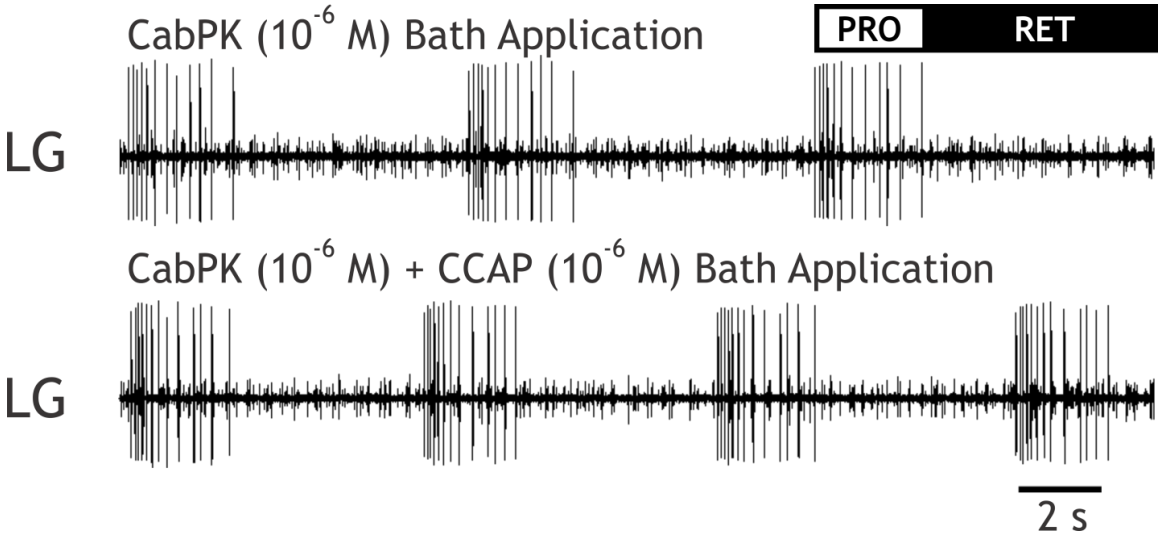

Figure 2. The peptide hormone CCAP reduces the CabPK-elicited gastric mill cycle period. Top, Bath-applied CabPK elicited a gastric mill rhythm, monitored by exctracellular recording (*lgn*) of LG neuron activity (large amplitude action potentials). Bottom, Coapplied CCAP and CabPK elicited a gastric mill rhythm with a briefer cycle period than CabPK alone (top). This reduced cycle period resulted from a selective reduction in the retractor phase.

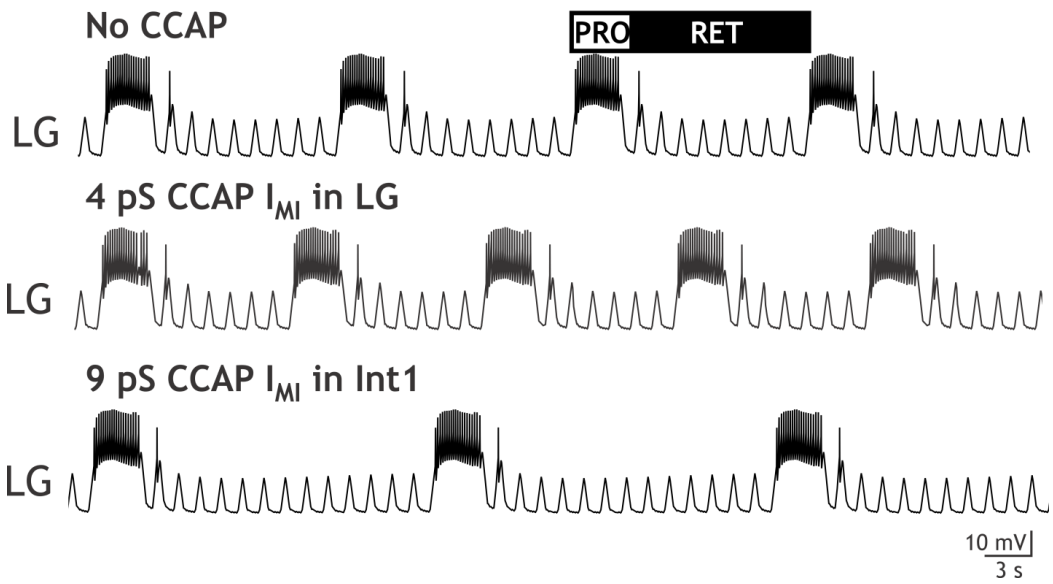

Figure 3. A computational model of the CabPK-rhythm generator response to CCAP modulation. Top, The control (no CCAP modulation) CabPK-gastric mill rhythm model output, represented by rhythmic LG neuron bursting. Middle, CCAP-activated I_{MI} added to the LG neuron decreased the gastric mill cycle period (duration between consecutive LG burst onsets) by selectively shortening retraction (LG interburst duration). Bottom, Addition of CCAP-activated I_{MI} to Int1 increased the gastric mill cycle period by prolonging retraction.

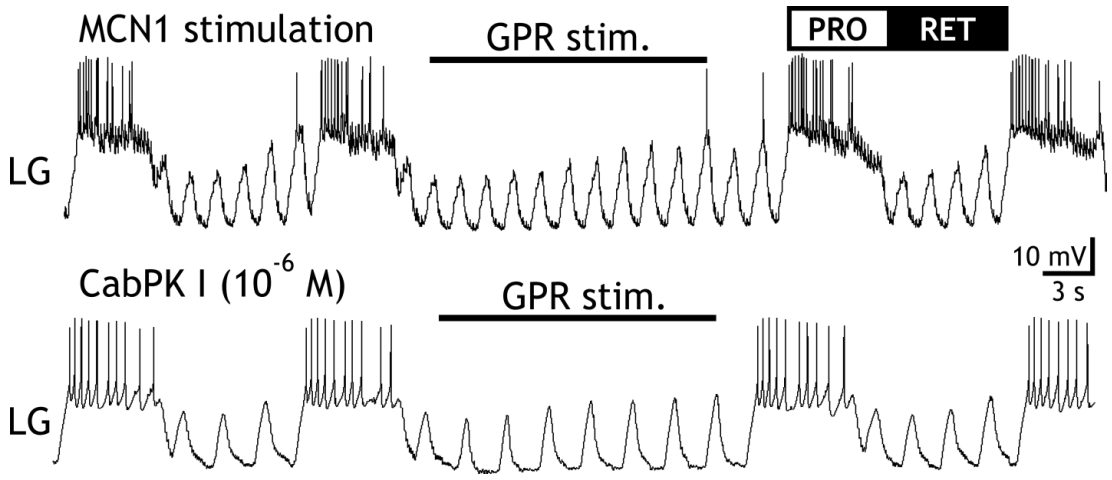

Figure 4. The GPR feedback action is conserved between the CabPK and MCN1-elicited gastric mill rhythms. Top, GPR stimulation (5 Hz) during the MCN1-gastric mill rhythm prolonged retraction (LG interburst interval). Bottom, GPR stimulation (5 Hz) also prolonged retraction during CabPK-gastric mill rhythm. Panels are from different experiments.

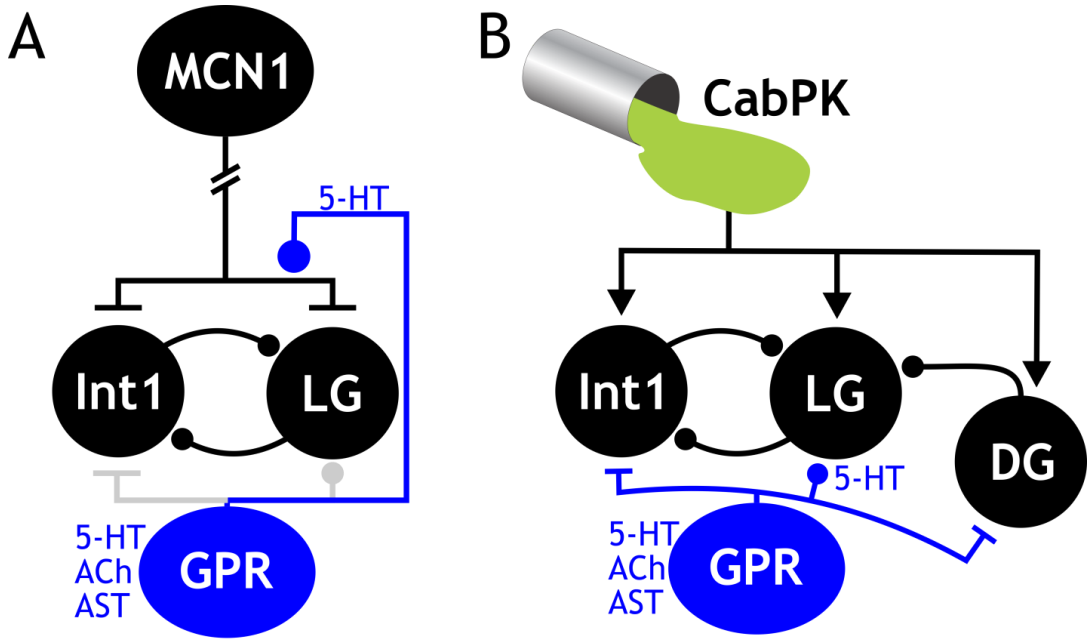

Figure 5. Schematic of GPR synapses on the MCN1- and CabPK-gastric mill rhythm generators. GPR contains three cotransmitters (5HT, ACh, AST) and has several known synaptic actions on the gastric mill rhythm generator neurons. **A,** When stimulated during MCN1-gastric mill retraction, GPR uses 5HT to presynaptically inhibit $MCN1_{STG}$ (DeLong et al., 2009b). The GPR synapses onto LG and Int1 (gray) are not effective in this circuit state. Symbols: filled circles, inhibition; t-bars, excitation; arrowheads, targets of bath-applied CabPK. **B,** GPR has three synaptic actions through which it could be regulating the CabPK-gastric mill rhythm. GPR uses 5HT to inhibit LG and excite DG, and an unknown transmitter to excite Int1.

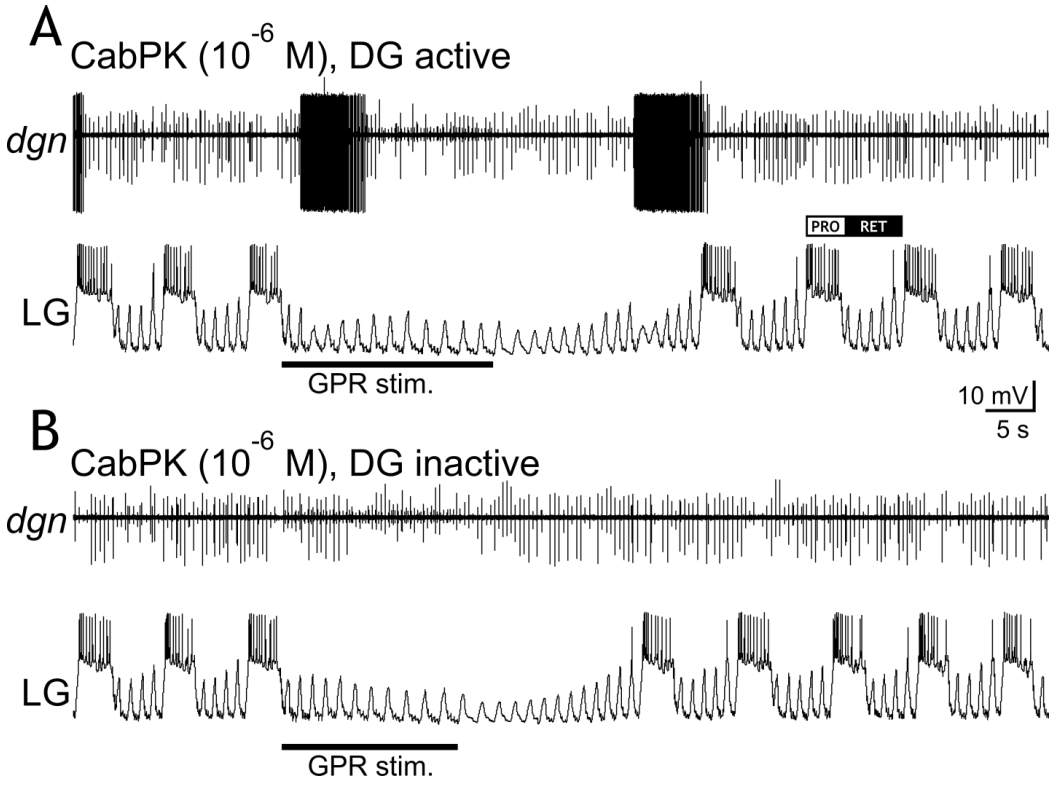

Figure 6. DG activity is not necessary for the GPR action on the CabPK-gastric mill rhythm. A, During the CabPK-gastric mill rhythm, GPR stimulation (8 Hz) prolongs the retraction phase (LG interburst). **B,** GPR stimulation still prolongs CabPK-retraction after DG activity was suppressed by continuous hyperpolarizing current injection. Both panels are from the same preparation.

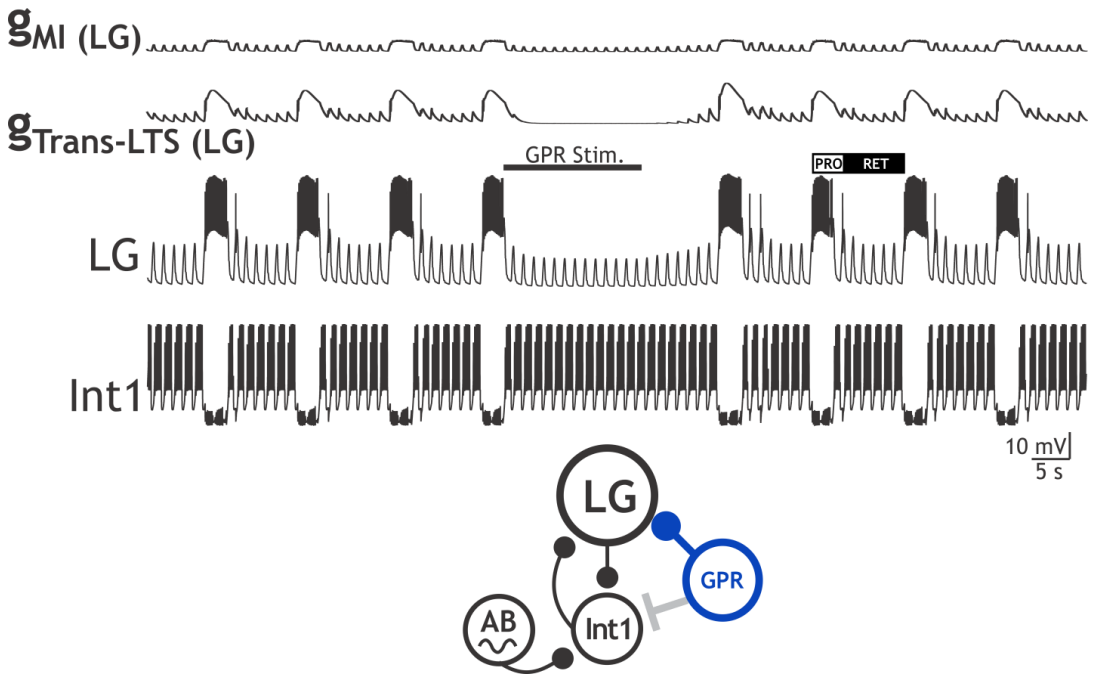

Figure 7. GPR inhibition of LG selectively prolongs CabPK-retraction in a computational model of the CabPK-gastric mill rhythm generator. This version of the CabPK-gastric mill rhythm generator model included only GPR inhibition of LG. Activating the model GPR inhibition of LG (10 Hz, 15 s) during retraction prolonged that retractor phase, as occurs when GPR is stimulated in the biological system (Figs. 4,6). Note that GPR stimulation reduced the amplitude of the subthreshold pyloric-timed oscillations in LG, resulting in a reduced amplitude of the CabPK-activated voltage-dependent conductances (g_{MI}, $g_{Trans\text{-}LTS}$) relative to their amplitude during the non-stimulated retraction phases. Symbols: Blue, active synapse; grey, inactive synapse.

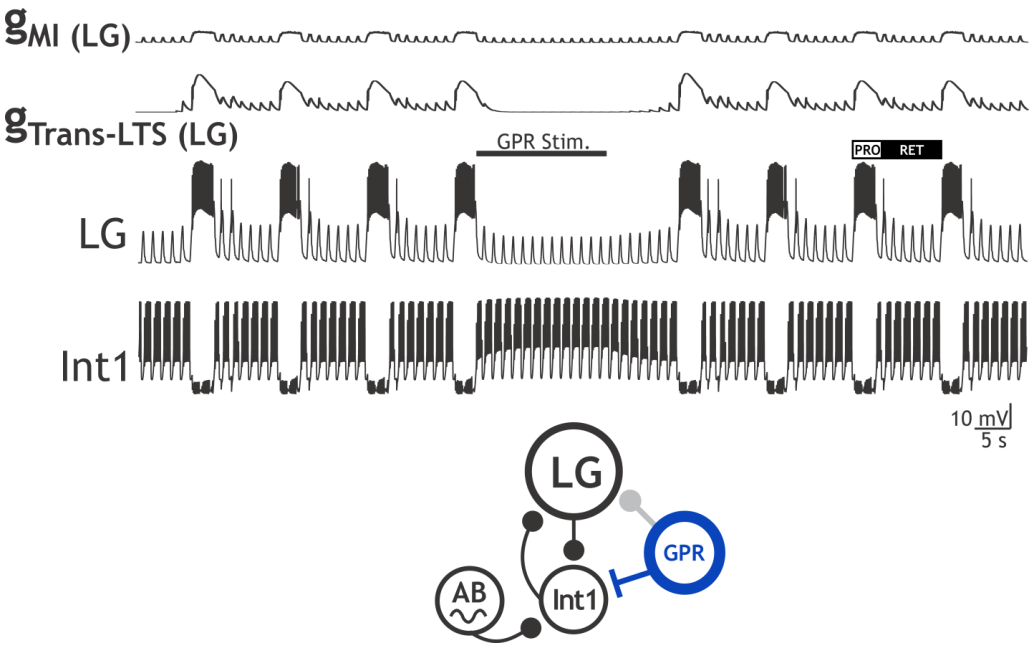

Figure 8. GPR excitation of Int1 selectively prolongs CabPK-retraction in a computational model of the CabPK-gastric mill rhythm generator. This version of the CabPK-gastric mill rhythm generator model included only GPR excitation of Int1. Activating GPR stimulation (10 Hz, 15 s) during retraction prolonged that retractor phase, as occurs when GPR is stimulated in the biological system (Figs. 4,6). As in Fig. 7, note the reduced amplitude of the CabPK-activated conductances (g_{MI}, $g_{Trans\text{-}LTS}$) relative to their amplitude during the non-stimulated retraction phases. Symbols: Blue, active synapse; grey, inactive synapse.

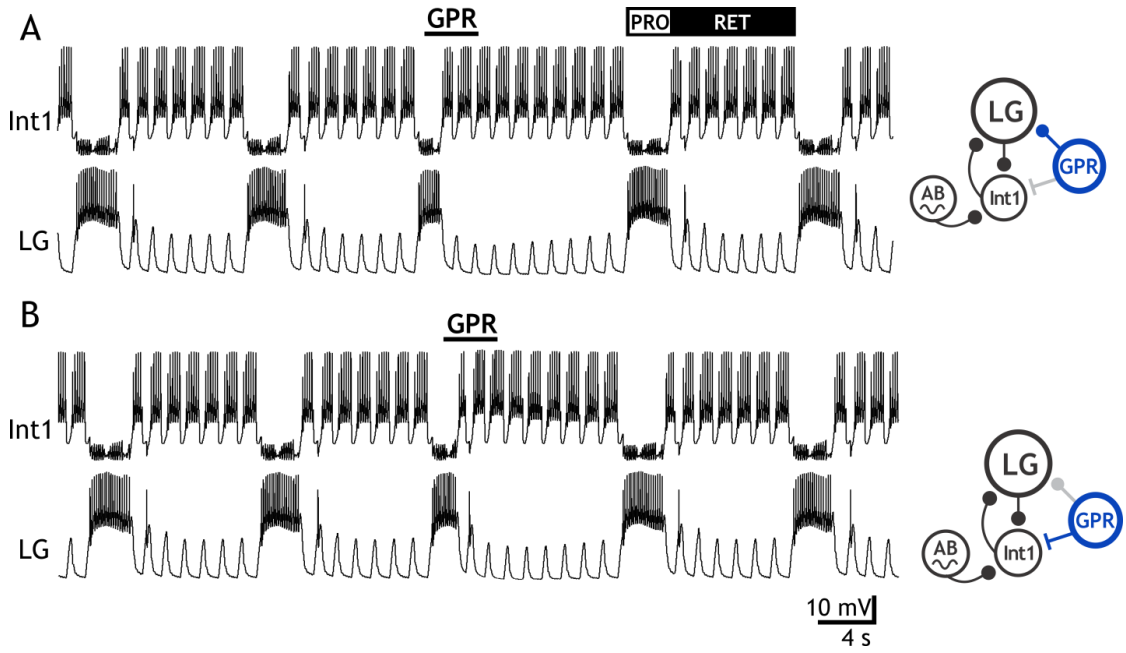

Figure 9. GPR stimulation during CabPK-protraction reduces the duration of that protraction phase in a computational model of the CabPK-gastric mill rhythm generator. Activating GPR stimulation (10 Hz, 15 s) during protraction reduces the duration of that protractor phase when exclusively activating its **(A)** inhibition of LG or **(B)** excitation of Int1. Symbols: Blue, active synapse; grey, inactive synapse.

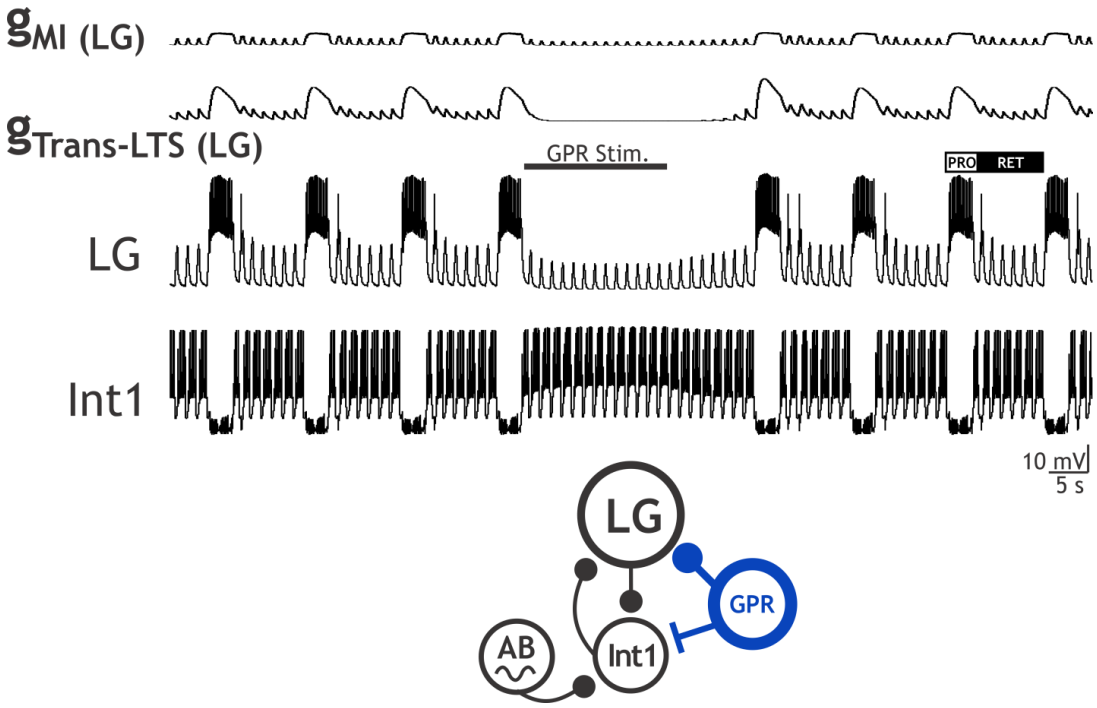

Figure 10. Coactivation of the GPR synapses on the CabPK-gastric mill rhythm generator neurons LG and Int1 selectively prolongs CabPK-retraction in a computational model of the CabPK-gastric mill rhythm generator. Activating GPR stimulation (10 Hz, 15 s) during retraction prolonged that retractor phase, as occurs when either GPR synapse was selectively activated in the model (Figs. 7,8) and when GPR is stimulated in the biological system (Figs. 4,6). As in Figures 7 and 8, note the reduced amplitude of the CabPK-activated conductances (g_{MI}, $g_{Trans\text{-}LTS}$) relative to their amplitude during the non-stimulated retraction phases. Symbols: Blue, active synapse; grey, inactive synapse.

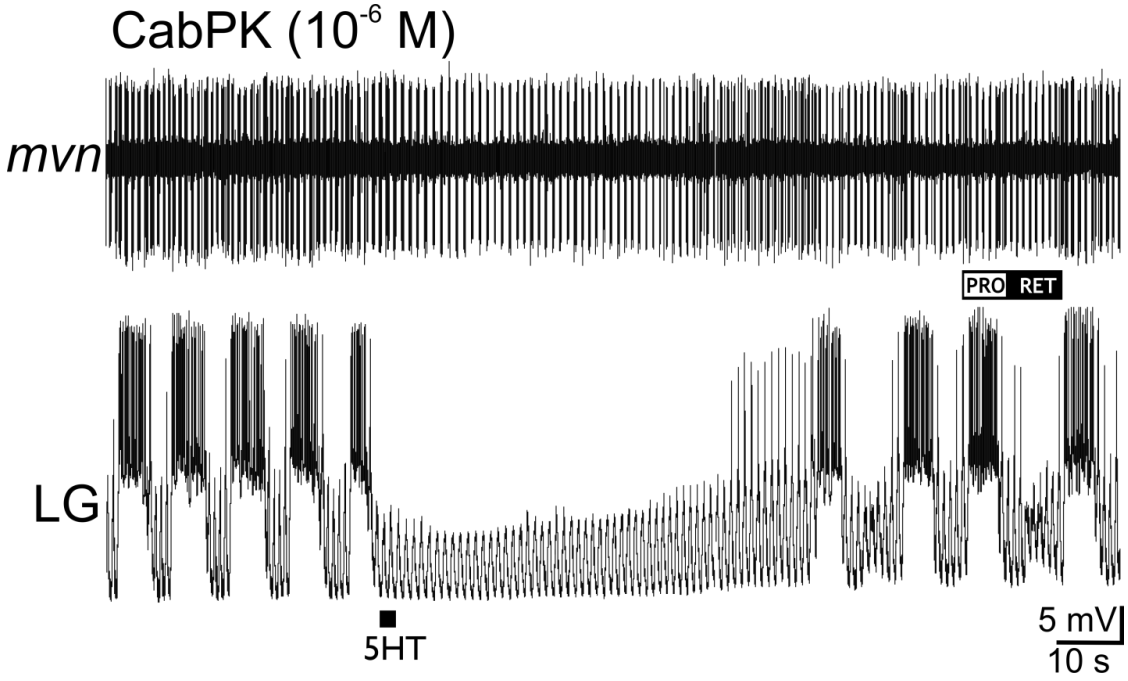

Figure 11. Focally applied 5HT selectively prolongs retraction during the CabPK-gastric mill rhythm. Prior to 5HT application, there was an ongoing gastric mill rhythm (LG) and pyloric rhythm (*mvn*). Pressure ejecting 5HT onto the desheathed STG neuropil (10^{-4} M; 4 psi; 2 s) prolonged the LG interburst duration (gastric mill retraction) without compromising the pyloric rhythm.

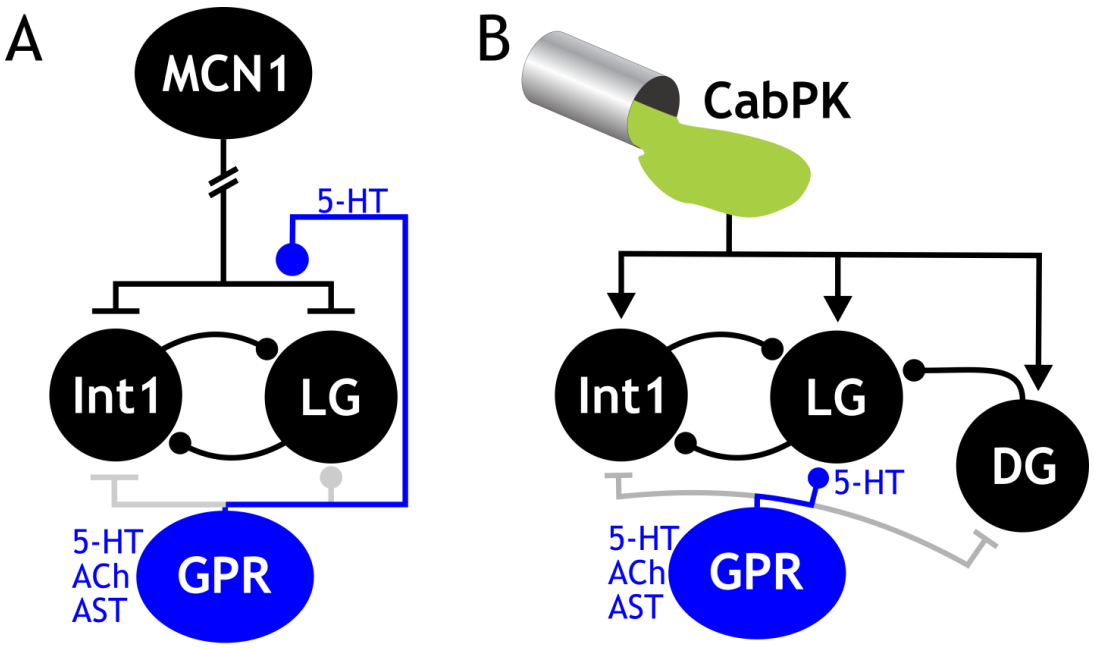

Figure 12. Circuit schematics showing that GPR uses different, state-dependent synapses to regulate the MCN1- and CabPK-gastric mill rhythm generators. A, GPR selectively prolongs MCN1-retraction via its presynaptic (5HT) inhibition of $MCN1_{STG}$ (DeLong et al., 2009b). The GPR synapses onto LG and Int1 (gray) are not effective during this circuit state. Symbols: filled circles, inhibition; t-bars, excitation; arrowheads, targets of bath-applied CabPK. **B,** GPR has three synaptic actions on the CabPK-gastric mill rhythm generator neurons, but it appears to selectively prolong CabPK-retraction via its 5HT-mediated inhibition of LG.

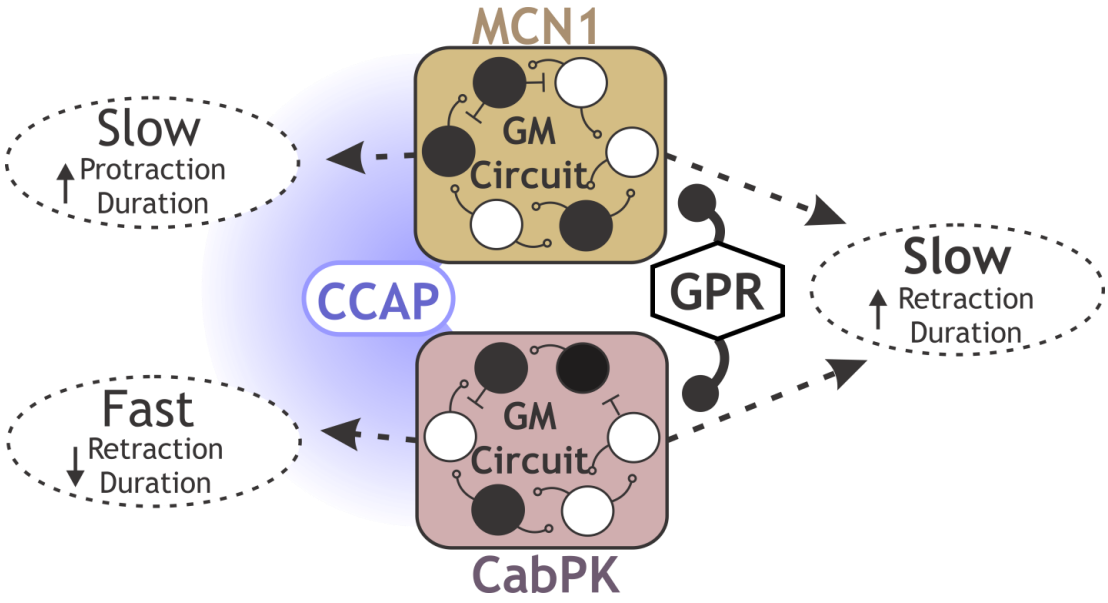

Figure 13. Different circuit states generating the same neural activity pattern exhibit divergent or convergent responses to modulatory input. The MCN1- and CabPK-configured circuit states respond **(left)** differently to the peptide hormone CCAP (Kirby and Nusbaum, 2007; this Chapter) but **(right)** comparably to metabotropic sensory feedback from the GPR neuron (Beenhakker et al., 2005; DeLong et al., 2009b; this Chapter). The blue cloud to the left of the MCN1- and CabPK-circuit schematics represents bath application of CCAP.

CHAPTER 4

CONCLUSIONS

In Chapter 2, I used electrophysiological (i.e. voltage clamp) methods to characterize the CabPK-activated ionic currents that underlie rhythmic LG neuron bursting during the CabPK-gastric mill rhythm. These currents ($I_{Trans\text{-}LTS}$, I_{MI}) were then injected into the LG neuron using the dynamic clamp and imported into a computational model of the CabPK-gastric mill rhythm, to demonstrate that they are necessary and sufficient for enabling post-inhibitory rebound bursting in LG and, as a consequence, producing this version of the gastric mill rhythm.

Insofar as the CabPK-gastric mill rhythm was shown previously to be nearly identical to the MCN1-gastric mill rhythm, and distinct from all other characterized gastric mill rhythms, elucidating the cellular mechanisms by which CabPK elicits this rhythm enabled me to compare and contrast rhythm generating mechanisms during CabPK application and MCN1 stimulation. This comparison revealed that different burst-generating currents [I_{MI} (MCN1), $I_{Trans\text{-}LTS}$ (CabPK)] were activated in LG under these two conditions, but their time course during gastric mill protraction and retraction were remarkably similar. This was the case despite being regulated by different mechanisms [inhibitory synaptic feedback (during MCN1) vs. intrinsic voltage-dependent properties (during CabPK)]. Additionally, the same current (I_{MI}), activated by both pathways, played different roles during each gastric mill rhythm. These observations provide novel insight into the degrees of freedom, and cellular mechanisms, available to distinct modulatory pathways that influence the same neural circuit. Additionally, it is the first detailed characterization of distinct inputs eliciting the same motor output by configuring different circuits. As such, it highlights the need for caution when interpreting the results of

comparable manipulations performed on systems where there is not sufficient access to the cellular-level operation of the studied circuit.

In Chapter 3, I explored the consequences of having divergent circuit states that produce convergent output patterns by assaying their response to extrinsic inputs. Specifically, I tested the hypothesis that the divergent circuit states would be differentially sensitive to a given input. The inputs used included sensory feedback from the muscle stretch-sensitive GPR neurons, and hormonal modulation by CCAP. The results stress the importance of knowing circuit level details, because there was no consistent pattern to how these circuits responded to extrinsic inputs. First, consistent with the hypothesis, CCAP had distinct actions on the MCN1- and CabPK-gastric mill rhythms. It prolonged the MCN1-gastric mill cycle period (via a low threshold [10^{-10} M] action), and shortened the CabPK-gastric mill cycle period (via a high threshold [10^{-7} M] action). This was the case despite it being likely that under both conditions the primary CCAP action was to activate I_{MI} in the LG neuron. Second, in contrast to the hypothesis, GPR had the same action on the MCN1- and CabPK-gastric mill rhythms, selectively prolonging retraction. This was the case despite GPR influencing each rhythm via a different synapse. Presumably, the behavioral function of the GPR feedback is sufficiently important under different versions of the gastric mill rhythm that the system has ensured its persistence. It is perhaps not surprising that there could be regions within the dynamic operating range of distinct circuit states where a particular influence would evoke a similar change in both circuits, but we had not anticipated that a shared response from the same input (GPR neuron) could be achieved with different synapses. This novel outcome provides additional flexibility to the state-dependent responses of neural circuits.

FUTURE DIRECTIONS

The primary goals for my thesis research were to determine the cellular and synaptic mechanisms by which different modulatory inputs configure different circuit states to generate the same neural activity pattern, and to assess the relative sensitivity of these circuit states to additional modulatory inputs. As a result of achieving these goals, additional interesting issues were revealed. With respect to the relative influence of MCN1 and CabPK on the gastric mill circuit, it is noteworthy that CabPK is not only neurally-released but is also a circulating hormone released by the pericardial organs into the hemolymph. Whereas hormonal levels (e.g. $<10^{-7}$ M) do not activate the gastric mill rhythm, they may well still activate I_{MI} and/or $I_{Trans\text{-}LTS}$ in LG. As a result, it would be interesting to determine the influence of hormonal CabPK levels on the MCN1-gastric mill rhythm, and to compare that influence to the previously determined CCAP influence on that rhythm (Kirby and Nusbaum, 2007; DeLong and Nusbaum, 2010). If there is indeed a hormonal-type of CabPK action on the MCN1-rhythm, then it would be worthwhile to determine whether I_{MI} and/or $I_{Trans\text{-}LTS}$ is activated at those lower concentrations and, if so, then to what amplitude. Additionally, the balance of I_{MI} to $I_{Trans\text{-}LTS}$ might be concentration-dependent, which could in turn underlie a concentration-dependent action on the MCN1-gastric mill rhythm. In contrast, the CCAP influence on the MCN1-gastric mill rhythm is qualitatively the same, but quantitatively distinct, at different concentrations (10^{-10} M to 10^{-7} M) (Kirby and Nusbaum, 2007).

The MCN1- and CabPK-gastric mill motor patterns involve more than just rhythm generation (the focus of this work). There is also the associated issue of how pattern generation is achieved under these two conditions. Pattern generation involves both the rhythm generator neuron synapses on the other gastric mill neurons, as well as synapses between these other neurons. Both MCN1 and CabPK have direct actions on

most or all of these other gastric mill neurons (Saideman et al., 2007a; Stein et al., 2007). Their contributions to the convergent pattern generation during these two gastric mill rhythms remains to be determined. The MCN1 influence likely involves I_{MI} activation, insofar as its two peptide cotransmitters (CabTRP Ia, proctolin) are known to activate I_{MI} in some pyloric circuit neurons and the gastro-pyloric neurons IC and VD, but whether additional currents are activated is not yet known. Similarly, the influence of CabPK on the gastric mill pattern generator neurons is currently unknown. Determining the mechanisms underlying convergent pattern generation will be a more extensive project than the one for determining rhythm generation insofar as the number of gastric mill neurons involved (6 vs. 2) is larger.

Another potential fruitful direction to pursue pertains to the mechanism underlying CCAP modulation of the CabPK-gastric mill rhythm. My work thus far suggests that CCAP influences this rhythm by activating I_{MI} in LG, as it does during the MCN1-rhythm. However, this has yet to be established, and CCAP does influence additional gastric mill neurons, including Int1 (Kirby and Nusbaum, 2007). Moreover, previous voltage clamp analysis of the CCAP action on LG (and other STG neurons) was performed using only a ramp protocol (Swensen and Marder, 2000; DeLong et al., 2009). As my voltage clamp analysis of the CabPK-influenced currents in LG has established, while only I_{MI} was identified using the voltage ramp protocol, additional transient (due to time-dependent inactivation) currents were identified using a voltage step protocol. Therefore, one logical next step is to fully characterize the CCAP modulation of the CabPK circuit by using the voltage step protocol to assess whether additional currents are influenced by CabPK in LG and/or in other relevant gastric mill neurons. Any measured changes imparted by CCAP modulation could be modeled and injected back into LG with the dynamic clamp in order to test sufficiency.

With respect to the GPR influence on the CabPK-gastric mill rhythm, in the short-term the mechanism underlying this action remains to be determined. My preliminary data support the hypothesis that this action is due to serotonergic inhibition of LG by GPR. However, this hypothesis remains to be tested. One potentially fruitful approach to testing it is to use voltage clamp to identify the current(s) influenced in LG by 5HT, and then import them into the computational model of the CabPK-gastric mill rhythm and into the dynamic clamp software. Using the dynamic clamp, we can test whether the CabPK-influenced current(s) is necessary (nullify the GPR-activated current with dynamic clamp negative conductance injections) and sufficient (use positive conductance injections in place of GPR stimulation) to mimic the GPR action on this gastric mill rhythm. If these manipulations are not sufficient to explain this GPR action, then we would proceed to determine the role of GPR excitation of Int1 in this process.

GPR has two modes of activity, including spontaneous bursting and stretch/tension-related activity, in semi-intact preparations (Katz et al., 1989; Birmingham et al., 1999). In this study, I focused on the stretch-related bursting by stimulating GPR during the retractor phase, which as indicated above had the same effect on the CabPK- and MCN1-gastric mill rhythms. It is possible that the influence of GPR on these distinct circuit states when it is expressing spontaneous bursting might differentially influence these circuit states. If so, then one possible mechanism underlying such a changed influence results from GPR containing three cotransmitters, including 5HT, ACh, and the peptide AST (allatostatin) (Katz and Harris-Warrick, 1989; Skiebe and Schneider, 1994). In at least some instances, cotransmitter-containing neurons can alter the relative amount of released cotransmitters during different firing rates and/or patterns.

My thesis work extends the concept known as degeneracy to the level of neural circuit operation. In this context, degeneracy pertains to the ability of a neural network to

use different mechanisms to reach the same endpoint, such as the ability of the distinct MCN1- and CabPK-circuit states to elicit the same gastric mill rhythm. This concept also extends to the shared response of these two circuit states to sensory (GPR) feedback. There are some points where degeneracy breaks down (e.g. CCAP modulation) after only sampling a relatively small proportion of modulatory inputs into these two networks. There are many influences on neural circuits, even small ones such as the gastric mill CPG (Blitz and Nusbaum, 2011; Marder, 2012). The concept of degeneracy is often couched in terms of a limited context, such as the aforementioned two gastric mill rhythms in the isolated STG. In most systems, it remains to be determined whether degeneracy in circuit operation is a mechanism to ensure resilience of circuit function or whether it is an artifact of working with reduced systems receiving only a limited set of their full behaviorally-relevant repertoire of inputs. The crab STNS is one system that is sufficiently accessible and well-defined to it may well be possible to address this issue in some detail.